



INVESTIGATION OF HIGH FREQUENCY OSCILLATIONS IN EPILEPSY  
USING COMPUTATIONAL INTELLIGENCE

A Dissertation

Presented to

The Faculty of the Department of Biomedical Engineering

University of Houston

In Partial Fulfillment

Of the Requirements for the Degree of

Doctor of Philosophy

in Biomedical Engineering

By

Su Liu

August 2017

INVESTIGATION OF HIGH FREQUENCY OSCILLATIONS IN EPILEPSY  
USING COMPUTATIONAL INTELLIGENCE

---

Su Liu

Approved:

---

Chair of the Committee  
Nuri Ince, Assistant Professor,  
Department of Biomedical  
Engineering

Committee Members:

---

Yingchun Zhang, Assistant Professor,  
Department of Biomedical  
Engineering

---

Ahmet Omurtag, Associate Professor,  
Department of Biomedical  
Engineering

---

Vallabh Das, Professor,  
Department of Optometry

---

Michael Quach, Assistant Professor,  
Department of Neurology, Baylor  
College of Medicine

---

Suresh K. Khator, Associate Dean  
Cullen College of Engineering

---

Metin Akay, Professor and Chair  
Department of Biomedical  
Engineering

© Copyright by Su Liu 2017

All Right Reserved

## ACKNOWLEDGEMENTS

First and foremost, I am taking this opportunity to express my sincerest gratitude to my advisor Dr. Nuri Ince for igniting my interest in biomedical signal processing, and for his continuous support during my PhD program. His ideas, vision, patience and support have helped me throughout my PhD research, leading to a rapid development of skills and experiences. I will always be grateful to him, for accepting me into the Clinical Neural Engineering Lab and giving me guidance towards the field of computational neuroscience. His energy and spiritual dedication also enhanced my enthusiasm and passion for neural engineering and will certainly leave a permanent impact in my future career.

I would like to thank my committee members, Dr. Yingchun Zhang, Dr. Ahmet Omurtag, Dr. Vallabh Das and Dr. Michael Quach, for the insightful discussions and feedback they have given.

My special thanks goes to Dr. Zhiyi Sha for his advices and unconditional support since the beginning of this journey, as well as his graciousness as host on my visit to University of Minnesota. I also express my thankfulness to Dr. Dan Curry, for the many hours he and Dr. Quach had devoted into the collaborative work, and for their assistance in data collection and interpretation.

My deepest appreciation is extended to Dr. Candan Gurses for the tremendous amount of data she kindly provided, and for endorsing my joyful summer visit in Istanbul. I would like to thank Dr. Thomas Henry for all the fruitful discussion we had. His in-depth knowledge in neurophysiology and epilepsy helped me gained insight into

the meaning of my research. Besides, I express my sense of gratitude to Dr. Nerses Bebek, Dr. Altay Sencer, and many other collaborators for giving me the opportunity to execute the algorithm on some of the most interesting and challenging datasets that they are willing to share.

My appreciation would be incomplete without giving credits to my dearest friends and lab mates, Ilknur, Tianxiao and Musa: I cherish every moment spent with you throughout the past few years. Many thanks to my friends who left ahead of us a little bit — Shruti and Hasan — with whom we've shared so many wonderful memories.

Most heartfelt thanks to my mom, Lian, for being there always. Thanks are also owed to my grandparents, for raising me the way they did. I would like to send special thanks to my aunt, uncle and her families, including my cousin, Georgia, for always being kind and supportive.

Finally, I would like to dedicate this work to all the patients, especially those kids who have suffered from the disease and who have contributed to this research. I wish my journey after here could provide practical implications for the betterment of diagnosis and treatment in epilepsy.

INVESTIGATION OF HIGH FREQUENCY OSCILLATIONS IN EPILEPSY  
USING COMPUTATIONAL INTELLIGENCE

An Abstract

Of a

Dissertation

Presented to

The Faculty of the Department of Biomedical Engineering

University of Houston

In Partial Fulfillment

Of the Requirements for the Degree of

Doctor of Philosophy

in Biomedical Engineering

By

Su Liu

August 2017

## **ABSTRACT**

Epilepsy is affecting over 1% of the population worldwide, wherein 1/3 of the patients remain refractory to medication. Successful surgical treatment for patients with intractable epilepsy depends critically on the accurate delineation of the seizure onset zone (SOZ). High frequency oscillations (HFOs, 80 – 500 Hz) are proposed as putative biomarkers in epilepsy with their potentials of identifying the SOZ, either by augmenting or replacing the current preoperative evaluation modality which requires detailed visual examination of long-term intracranial EEG recordings. The clinical utility of HFOs has been hampered due to the challenges associated with the quantitative identification of HFOs in massive-volume iEEG datasets. The lack of established criteria for distinguishing pathological HFOs from physiological oscillations also adds to the complexity of the problem.

This dissertation aims at the computational analysis of HFOs with specific concerns over its practical application for the localization and prediction of SOZ. We proposed novel algorithms and tools for the auto-detection of HFO in prolonged clinical data based on advanced signal processing and unsupervised machine learning techniques, and investigated the correlation of possible HFO clusters and clinician-determined SOZ in different states. The algorithm achieved significant improvement compared to existing SOZ approximation techniques, indicating that unsupervised clustering methods exploring the time-frequency content of HFOs in the available full-band can efficiently be used to localize the epileptogenic zone in clinical practice. We further investigated the spatial and temporal dynamics of HFO in long-term iEEG recordings, verified the spatial

correlation of HFO and SOZ, and assessed the feasibility using automatically detected HFOs to identify SOZ in challenging cases where the ictal pattern was unclear. Finally, for the first time, we introduced SOZ-specific HFO waveform patterns, which are barely observed in the functional cortex introducing physiological HFOs.

The outcomes of this work add to our understanding of the electrophysiological basis of HFOs as well as the epileptogenic networks, and provide new possibilities for the interpretation of HFOs that can be efficiently applied to distinguish SOZ from eloquent cortical areas, which is a critical step towards the translation of HFOs to valid clinical biomarkers.

# TABLE OF CONTENTS

ACKNOWLEDGEMENTS .....	v
ABSTRACT .....	viii
TABLE OF CONTENTS .....	x
LIST OF FIGURES .....	xiv
LIST OF TABLES .....	xix
CHAPTER 1 INTRODUCTION AND BACKGROUND .....	1
1.1 Research Background .....	1
1.2 Aims and Contributions .....	9
CHAPTER 2 REVIEW OF PRIOR WORK .....	11
2.1 Definition of High Frequency Oscillations .....	11
2.2 HFOs in Clinical Epilepsy .....	13
2.3 Identification of HFO in Human Intracranial EEG.....	15
CHAPTER 3 UNSUPERVISED HFO DETECTION USING MULTICHANNEL IIEG RECORDINGS IN PATIENTS WITH EPILEPSY .....	24
3.1 Introduction.....	24
3.2 Data Acquisition .....	26
3.3 Proposed Algorithm .....	29
3.3.1. Initial Detection .....	29
3.3.2. Time-Frequency Analysis and “Denoising”.....	31
3.3.3. Feature Extraction.....	33
3.3.4. Unsupervised Clustering.....	36
3.3.5. Validation .....	39
3.4 Results.....	41
3.4.1. Feature Distribution of Detected Events.....	41
3.4.2. Localization of the Seizure Onset Zone.....	43
3.4.3. Spatial Distribution of sHFO, fHFO, and Spikes .....	46
3.4.4. Comparing with existing techniques.....	47

3.5 Discussion .....	49
3.5.1. Main Contributions .....	49
3.5.2. Identifying SOZ in Different States .....	51
3.5.3. The Prognostic Value of HFOs .....	52
3.5.4. Towards the Clinical Application.....	55
CHAPTER 4 HFO AUTO-DETECTION FOR THE LOCALIZATION OF SEIZURE	
ONSET ZONE: CASE STUDIES .....	57
4.1 Introduction.....	57
4.2 Data Acquisition and Analysis .....	58
4.3 Case 1: HFOs in Epilepsy Associated with Cavernous Malformation .....	62
4.3.1. Case Presentation .....	63
4.3.2. Results.....	65
4.4 Case 2: HFOs in Extra-Temporal Lobe Epilepsy .....	69
4.4.1. Case Presentation .....	70
4.4.2. Results.....	70
4.5 Case 3: the Influence of Contact Size on HFO Detection .....	74
4.5.1. Case Presentation .....	75
4.5.2. Results.....	77
4.6 Discussion.....	81
CHAPTER 5 DISCRIMINATION OF SEIZURE ONSET ZONES AND CRITICAL	
FUNCTIONAL REGIONS.....	88
5.1 Introduction.....	88
5.2 Materials and Methods.....	91
5.2.1. Patient Population .....	91
5.2.2. Electrode Placement and Intracranial EEG Recording.....	91
5.2.3. Delineation of SOZ and Functional Regions .....	92
5.2.4. Data Selection and HFO Detection.....	93
5.2.5 Detection of Stereotyped HFOs .....	95
5.2.6. Identification of SOZ Using Stereotyped HFOs .....	97

5.2.7. Statistical Analysis .....	98
5.3 Results.....	98
5.3.1. SOZ Identification and Functional Mapping Results .....	98
5.3.2. Unsupervised HFO detection .....	101
5.3.3. Comparison of HFOs Originating From Different Locations.....	102
5.3.4. Stereotyped HFO Waveform Patterns.....	104
5.3.5. Comparison of HFOs in Epilepsy Patients and the Control Group .....	108
5.3.6. Spatial Correlation of HFO Waveform Patterns with SOZ and Eloquent Cortex.....	110
5.3.7. Localizing the SOZ Using Stereotyped HFO Waveforms.....	112
5.3.8. Stereotyped Ripple and Fast Ripple Oscillations.....	115
5.4 Discussion.....	116
CHAPTER 6 TEMPORAL CHARACTERIZATION OF HFO AND EARLY PREDICTION OF THE SEIZURE ONSET ZONE IN TEMPORAL LOBE EPILEPSY ....	
123	
6.1 Introduction.....	123
6.2 Materials and Methods.....	125
6.2.1. Data Description .....	125
6.2.2 Delineation of the Seizure Onset Zone .....	126
6.2.3 HFO Detection.....	127
6.2.4. Temporal Characterization of HFO.....	128
6.2.5. Early Prediction of the SOZ.....	129
6.2.6. Statistical Analysis .....	130
6.3 Results.....	131
6.3.1. Automatic Detection of HFO and Spike .....	131
6.3.2. Spatial Characterization of Detected Events.....	132
6.3.3. Comparing the Event Rates In Different States .....	132
6.3.4. Temporal Dynamics of Events In Different States .....	134
6.3.5. Early Prediction of the SOZ.....	138

6.4 Discussion.....	142
CHAPTER 7 SIGNIFICANCE AND CONCLUSION .....	149
7.1 Major Contributions .....	149
7.2 Future Directions .....	152
REFERENCES .....	154

## LIST OF FIGURES

Figure 1-1. (A) Scheme showing the pathway of partial seizure originates from temporal lobe (left) and primary generalized seizure (right). (B) Forty seconds of intracranial EEG recording segment.....	2
Figure 1-2. Three seconds of raw iEEG data (top) and its time-frequency representation (bottom). A fast ripple occurs at the center with its primary high-band energy peak extending beyond 200 Hz.....	7
Figure 2-1. Examples of ripple (left) from 10-second window (a) and fast ripple (right) from window (b). For both events, the raw and filtered signals above 80 Hz and 200 Hz are shown.....	12
Figure 2-2. (A) Previous study demonstrating the pitfalls associated with straight-forward filtering. (B) The distinctions between HFOs and “pseudo” events are clearer by inspecting the time-frequency characteristics.....	16
Figure 3-1. Data collection protocol with sample bipolar raw and 80 – 500 Hz band-pass filtered iEEG data. Only 5 seconds of SB/WB, and 15 seconds before and after the seizure onset are shown.....	27
Figure 3-2. (A) Schematic diagram of the algorithm. (B) Interface of the customized HFO investigation tool.....	30
Figure 3-3. HFO sieving and denoising step. Appropriate denoising would reveal the high frequency component of an HFO. The spectrum was derived from the original and denoised time-frequency map.....	32
Figure 3-4. Frequency corresponding to maximum peak to notch ratio.....	34
Figure 3-5. Number of cluster (left) and HFOs detected per 10-minute segment (right) in different states. There is no significant difference in cluster numbers or HFO	

numbers.....	42
Figure 3-6. (A) Feature distribution and the curvature of log-likelihood with respect to K values of GMM in 2 patients. (B) Time-frequency maps averaged from randomly selected 20 events in each cluster.....	43
Figure 3-7. (A) HFO spatial distribution in SB, WB and PI. (B) For each Engel class I patient, all channels are sorted according to their HFO numbers (up to 20 channels are shown).....	45
Figure 3-8. (A) Feature distribution for spikes and HFOs in P3. (B) Spatial distribution for sHFO, fHFO and spikes in 3 patients. (C) Proportion of events inside the SOZ. (D) Spatial distribution for sHFO.....	48
Figure 4-1. Scheme and photos showing the data collection setup.....	59
Figure 4-2. Schematic diagram of the three-stage automatic HFO detection method.....	60
Figure 4-3. Workflow for the coregistration of pre-op MRI and post-op CT images. A customized software is developed for the visualization of electrodes.....	61
Figure 4-4. (A) Structural MRI. (B) Postoperative CT image. (C) PET image showing hypometabolism. (D) Magnetic source imaging. (E) A schematic of grid channel orders. (F) Three-dimensional rendering of the individual brain with electrode model. ....	64
Figure 4-5. Twenty seconds of ECoG recording in bipolar montage, with seizure onset represented by the red vertical line. Thirty-two channel pairs are shown. ....	65
Figure 4-6. Feature distribution of the three clusters calculated from the first 10 min of recording.....	66
Figure 4-7 (A) 3D rendering of the MRI with spatial distribution maps, with red representing the locations with most of the captured events. (B) Spatial	

distribution of HFOs and spikes in bar plot.....	68
Figure 4-8. (A) Twenty-seconds of iEEG data in bipolar montage showing the seizure onset. (B) Co-registration of pre-operative MRI and post-operative CT with SOZ information and functional zone. ....	71
Figure 4-9. (A) Feature distribution in 3D space. (B) Averaged time-frequency maps across 20 random samples in type 1 and type 2 HFO groups. (C) Spatial distribution of type 1 (left) and 2 HFO (right).....	73
Figure 4-10. (A) Preoperative image (upper) and postoperative MRI (lower). (B) Coregistration of the preoperative MRI and the intraoperative photos of the cortex. (C) The sketch of the hybrid electrode grid.....	76
Figure 4-11. (A) Thirty-second of raw ECoG data in monopolar montage. (B) Feature distribution and clustering result using 1 hour of data, 8 random samples are shown with their averaged time-frequency maps. ....	78
Figure 4-12. Spatial distribution of HFO (left) and spike (right) projected to the individual MRI data, with the resection border given (yellow line).....	79
Figure 4-13. Comparison of the event count between small and large contact groups for HFO and spike. For each group, three sample events are presented. ....	80
Figure 4-14. Spatial maps of HFOs captured by small contacts (left) and large contacts (right).....	81
Figure 5-1. Data analysis workflow. The HFO clusters were first categorized by their spatial origins for a group-wise comparison. Next, the detection of stereotyped HFOs was blindly performed in the entire HFO pool.....	94
Figure 5-2. DBSCAN clustering algorithm. A core point has neighboring points more than a specified number ( <i>MinPts</i> ) within distance $\epsilon$ , a noise point is any point that is not a core point or a border point.....	96

Figure 5-3. Three-dimensional distribution of HFO and spikes identified by GMM clustering in 2 patients. In P9, the HFOs were generated from both SOZ (red line) and functional area (blue line)..... 102

Figure 5-4. Group comparison of sHFO, oHFO and fHFO. The mean frequency for sHFO was higher than oHFO and fHFO events. The rate for sHFO was higher compared to oHFO but not to fHFO events..... 103

Figure 5-5. Examples of HFO subclusters and their spatial locations in five patients. For each pattern, 4 sample events and the pile plot of the events in the same subcluster are shown with the averaged t-f map..... 105

Figure 5-6. (A) Circular network visualizing the distance matrix in 13 HFO samples. (B) Network plots in 3 groups, each being composed of 30 HFOs inside the SOZ, outside SOZ, and inside the motor area in P9. .... 107

Figure 5-7. (A) Clustering ratio curves for three representative patients. (B) The average clustering ratio plots. (C) The curves in fHFOs of epilepsy patients and controls. (D) Group differences in the AUC and minimum  $\epsilon$  to generate sub-clusters. .... 109

Figure 5-8. Spatial projection of repetitive and non-repetitive HFOs in four patients. Using a  $\epsilon \leq 0.5$ , the remaining un-clustered HFOs are spatially localized at functional cortex or brain regions distinct from the SOZ. .... 111

Figure 5-9. Spatial association of “cloned” HFO waveforms and the SOZ. As the intra-cluster similarity decreases, the clustered HFO provides a larger spatial expansion that extends beyond the SOZ..... 113

Figure 5-10. SOZ identification performance using HFOs clustered by using radius ( $\epsilon$ ) ranging from 0.05 to 1. As the radius increases to 1, the overall specificity and accuracy decrease considerably..... 114

Figure 5-11. Proportion of stereotyped FR versus ripple clustered by different radius. FRs were recorded in four patients, and consistently presented a higher degree of signal similarity compared to ripples.....	115
Figure 6-1. Schematic diagram of the HFO detection algorithm.....	128
Figure 6-2. Spatial distribution of FR, ripples and spikes. Compared to ripples and spikes, Majority of the FRs were detected inside of the SOZ. ....	132
Figure 6-3. Event rates for FR, ripple and spike in different states. FR rates were significantly lower in pre- and postictal periods compared to IB and SB . .	133
Figure 6-4. (A) The number of FR, ripple and spike captured during IB and SB states in P4. (B) The FR and ripple temporal variation in each 10-min window in baseline segments for 6 patients. ....	135
Figure 6-5. Pre- and postictal HFO temporal distribution results in 3 seizures derived from P6 where three preictal patterns were observed for FR. ....	137
Figure 6-6. (A) Event count of FRs and (B) ripples inside the SOZ in each 10-min bin, computed from each seizure in each patient.....	139
Figure 6-7. Left: spatiotemporal distribution for FRs in 1-min discrete windows throughout the 2-hour IB recording in P3. Middle: cumulative FRs distribution. Right: spatiotemporal distribution for ripples. ....	141
Figure 6-8. Cumulative prediction results for FR, ripple and spikes.....	143

## **LIST OF TABLES**

Table 1-1 (A) Review of HFO characterization studies.....	22
Table 1-1 (B) Review of HFO auto-detection techniques .....	23
Table 3-1. Patient demographics.....	28
Table 3-2. Cluster number and average event number per data segment .....	42
Table 3-3. SOZ detection results.....	46
Table 5-1 Patient demographic data.....	99
Table 6-1. Patient demographic data.....	126

# CHAPTER 1 INTRODUCTION AND BACKGROUND

## 1.1 Research Background

Epilepsy is a neurological disorder characterized by an enduring predisposition to generate recurrent, unprovoked seizures (Fisher et al., 2005). It is one of the most common neurological diseases, affecting over 65 million people all over the world (Moshé et al., 2015). The overall incidence of the disease reaches a percentage between 0.5% – 2% (England et al., 2012; Holden et al., 2005). Seizures, which are caused by disorganized and sudden electrical activities of the brain, could be extremely hazard due to its unpredictability. According to the definition given by International League against Epilepsy (ILAE), the epileptic seizure is defined as “a transient occurrence of signs and/or symptoms due to abnormal excessive or synchronous neuronal activity in the brain” (Fisher et al., 2005).

During the past 30 years, the revolution in molecular cell biology and genetics, together with the development of human genomic technologies, have brought better insight into the mechanisms and pathophysiology of epilepsy. In 2017, ILAE has released a revised basic and expanded classification clarifying the seizure types, with initial categorization into “focal” versus “generalized” onset or unknown onset seizures. A scheme showing the pathway of focal and generalized seizures is provided in figure 1-1 (A). In ILAE’s recommended terminology and concepts, the original generalized seizures, known as “originating at some point within and rapidly engaging bilaterally distributed networks”, were optionally sub-grouped into motor and nonmotor (absence) seizures. Focal seizures, which are formerly known as partial seizures, are defined as

“originating at some point with networks limited to one hemisphere”, and were further classified as focal seizure by level of awareness of the patients. The status of awareness is defined as “knowledge of self and environment”, which specifically refers to the status during a seizure, instead of the awareness of “whether a seizure has occurred” (Fisher et al., 2017). Unlike it was sub-classified to complex and simple partial types before, there is no specific artificial categories defined according to the new concept. Seizures should be described by their semiologic features only (Berg and Scheffer, 2011).

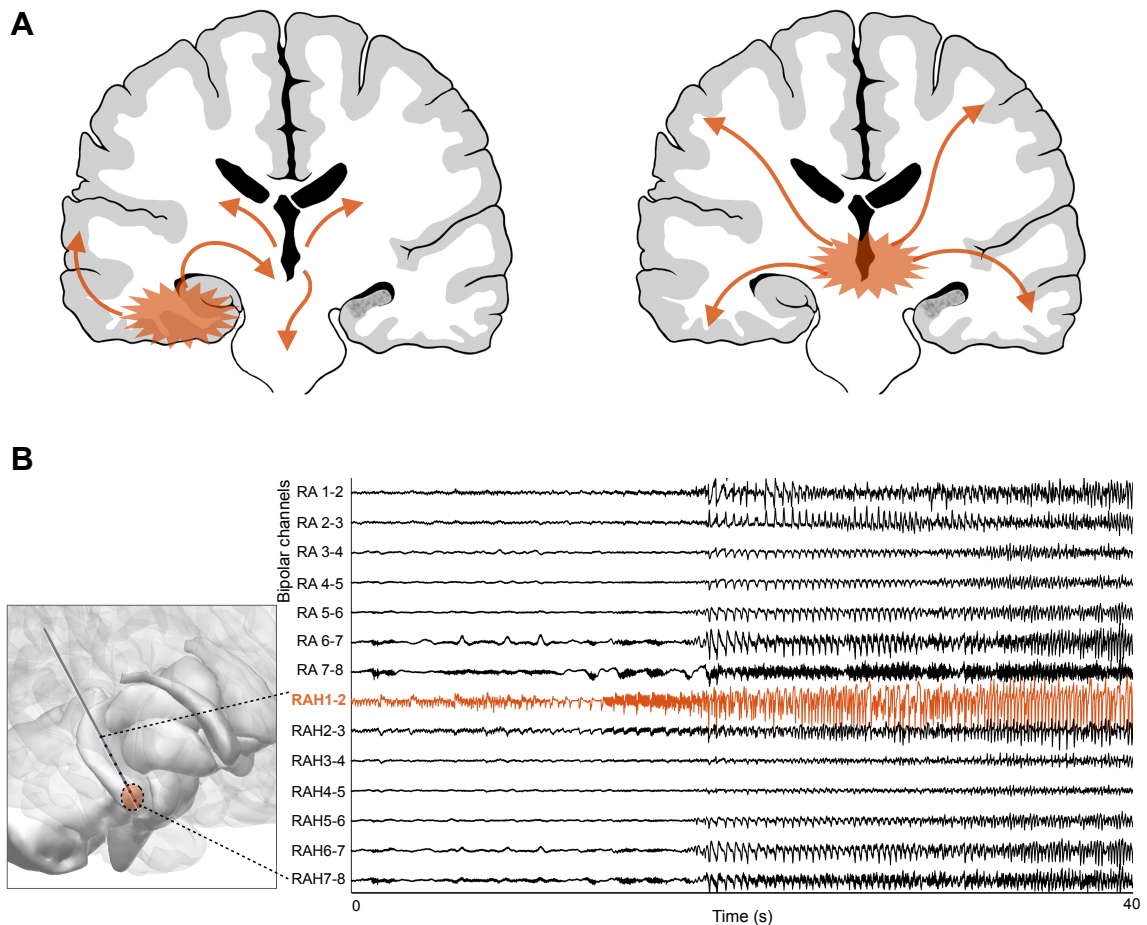


**Figure 1-1. (A) Scheme showing the pathway of partial seizure originates from temporal lobe (left) and primary generalized seizure (right). (B) Forty seconds of intracranial EEG recording segment.**

Nearly 30% of epilepsy patients remain refractory to drug treatment, making surgical resection of epileptogenic zone an optimal solution to produce seizure freedom (Kwan and Brodie, 2000; Rosenow and Lüders, 2001). The success of resectional surgery depends critically on the localization of epileptogenic zone. Continuous electroencephalography (EEG) with video monitoring is utilized as a routine approach for non-invasively collecting signals through scalp electrodes. Structural and functional imaging (MRI, PET and ictal-interictal SPECT) also contributes to a comprehensive non-invasive presurgical workup. However, due to the interference from the dura, skull, and scalp, the sensitivity of EEG recording can be low (Yang, Hakimian and Schwartz, 2014). It has been discussed that scalp video-EEG is generally necessary yet not sufficient in the evaluation of the majority of surgical candidates. Scalp EEG sometimes exhibits propagated epileptiform discharges more predominantly than those generated at the seizure onset zone (SOZ). For instance, patients with large and unilateral early-onset cortical lesions sometimes show generalized or even falsely lateralized epileptiform discharges on scalp EEG. Such an unwanted phenomenon is also observed in magnetoencephalography (MEG) (Asano, Brown and Juhász, 2013). There exist many other circumstances where non-invasive monitoring might fail to lateralize or localize the epileptogenic focus entirely. Studies showed that scalp EEG can localize SOZ successfully only in approximately 50% of the patients with neocortical epilepsy, and is likely to falsely define the site of seizure onset in 5% – 10% of patients. In patients with hypothalamic hamartoma (HH) associated epilepsy, scalp EEG may show diverse features. The majority of gelastic seizures fail to demonstrate changes in the EEG signal,

suggesting the utility of EEG is limited in the evaluation of these patients. This absence of ictal discharges may be due to the large distance between recording electrodes and the seizure generative locations (Asano et al., 2013; Troester et al., 2011). Simultaneous EEG recording during PET and SPECT imaging is believed to provide a more reliable interpretation when localizing SOZ. Nevertheless, in pediatric epilepsy surgery, neuroimaging may present normal in spite of the clinical evidence of localization-related epilepsy. In such cases, data recorded by invasive monitoring provides invaluable for SOZ localization and directing the surgical resection.

Intracranial EEG (iEEG) is a monitoring method in which the electrodes are directly placed over the brain cortex that is surgically exposed inside or outside the operating room. For over six decades, it has been widely used by neurologists during the epilepsy surgery for the purpose of precisely identifying seizure foci and facilitating epilepsy surgery (Yang et al., 2014). Intracranial EEG recordings are indicated for surgical treatment of refractory epilepsy when other tests to identify the seizure focus are conflicting or inconclusive, when there is no abnormality shown in neuroimaging, when the SOZ is close to eloquent cortex (including many lesional cases), with dual or multiple pathology (e.g., hippocampal sclerosis plus a lesion), and occasionally in other scenarios (Ritaccio et al., 2013). The relatively high spatial resolution and signal to noise ratio of iEEG provides accurate seizure onset information, which greatly benefits the preoperative evaluation and management for the epileptic surgery (Engel et al., 2013; Freeman et al., 2000). Comparing to non-invasive techniques, iEEG recording also has higher bandwidth, and is less prone to artifacts (Ball et al., 2009). Therefore, iEEG is

preferred in many clinical procedures, such as presurgical evaluation, epilepsy diagnosis, SOZ localization (Rosenow & Lüders, 2001), and in electrical stimulation mapping (Uematsu et al., 1992). Moreover, current devices are capable for recording chronic ambulatory iEEG that may allow seizure prediction and warning. Such devices would improve patient safety and quality of life, as well as allow effective treatment for seizure prevention (Ritaccio et al., 2013). Till present, invasive EEG recording is still the gold standard that helps recognize the patient population who may profit from surgery (Baghdadi and Najjar, 2010). For over six decades, it has been widely used by epileptologists during the epilepsy surgery for the purpose of precisely identifying seizure foci. Meticulous implantation of intracranial electrodes and judicious interpretation of their data is a definite need in a successful epilepsy program. To accurately delineate the epileptogenic region, iEEG is recorded in the epilepsy monitoring unit (EMU) over days where multiple stereotypical clinical seizures are recorded to provide information about the SOZ. Figure 1-2 (B) shows an example of iEEG data trace recorded by two depth electrodes that were implanted in the mesial temporal lobe (MTL) structures. As it is shown in the figure, the SOZ (in red) was identified as the deepest two contacts in the right anterior hippocampus (RAH), where the low-amplitude fast oscillatory activities started at channels 105 – 106 and propagated to other locations.

Detection of epileptogenic zone requires invasive EEG monitoring over an extended period of time and detailed visual inspection of collected data by medical experts. The prolonged monitoring in the EMU adds to the risk of complications, increases the cost and places a high demand on the clinical service (Nagarajan et al., 2015). The rates of

reported complications related to invasive monitoring differ widely between studies, from no complications at all (Ross et al., 1996) up to 26.3% (Hamer et al., 2002). Problems related to implanted electrodes, including the risk of being pulled out by the patients, represent a unique challenge associated with invasive EEG monitoring, especially in pediatric cases (Arya et al., 2013). The potential complications associated with prolonged iEEG monitoring may include trivial issues, such as pain and discomfort, but may also include more serious issues, such as intracranial bleeding, meningoenephalitis, and death. According to retrospective studies, all complications associated with invasive monitoring are significantly more common in children than in adults (Roth et al., 2014). The overall frequency of complications is five times higher in the pediatric population (Arya et al., 2013; Hader et al., 2013). Moreover, complication risk is also correlated with younger age at the time of surgery and longer hospitalization (Roth et al., 2014). Longer duration of monitoring is found to be significantly associated with more frequent adverse events. The risk of adverse events per patient increases by about 4% per day after 7.8 days of monitoring (Arya et al., 2013). Study showed that the decrease of infection rate (18% to 6%) was correlated with a shorter monitoring period (13 days vs. 9 days) (Hamer et al., 2002). Other than the risk of complications, EMU monitoring procedure extends the duration of therapy and causing long waiting periods for other patients requiring immediate treatment in countries with limited resources. The financial cost of a prolonged hospital stay and monitoring fees can be substantial (Sun et al., 2015). For pediatric patients, prolonged monitoring would result in missed school for the child,

missed work for the parents and disruption for the family because the parent and child are away from home, and overall increased parental anxiety, in general.

In order to reduce the duration of prolonged monitoring and related cost, as well as the risks to patients whose seizures could result in fatal condition, there is urgent need to conduct research involving neurobiomarkers for the fast and accurate identification of seizure generating zone in epilepsy. Extraction of predictive patterns in iEEG can open the door of efficient diagnosis of SOZ, and may eliminate the need to wait for spontaneous epileptic seizures to occur over days in the hospital setting.

In this project we mainly concentrate upon the computational analysis of iEEG datasets because the recent advancement in clinical-practical high-band signal recording and data mining technologies has provided tools for the extensive investigation of local field potentials in human epilepsy patients, and introduced recordings in high temporal and spatial resolution where new possible electrophysiological signature for the epileptogenic network is emerging. Such neurobiomarkers in milliseconds time scale,

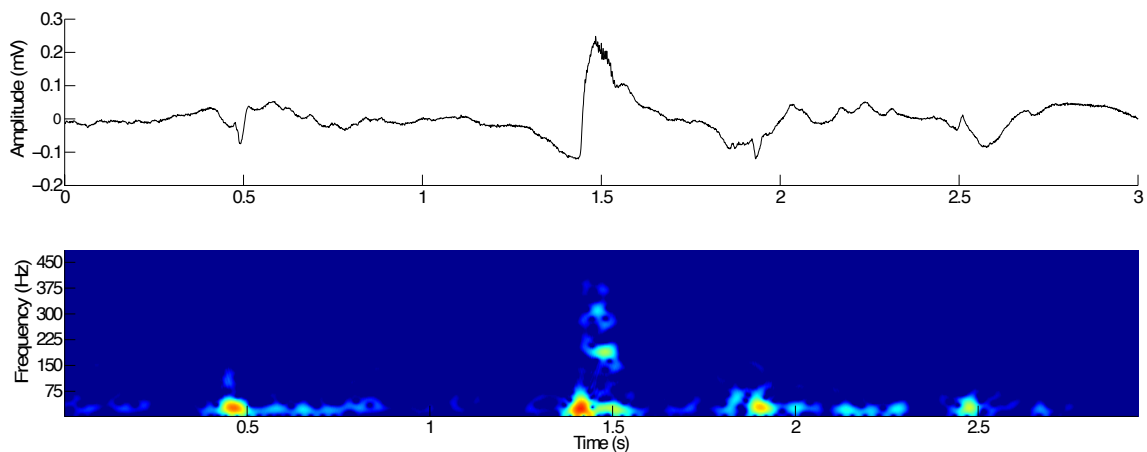


**Figure 1-2. Three seconds of raw iEEG data (top) and its time-frequency representation (bottom). A fast ripple occurs at the center with its primary high-band energy peak extending beyond 200 Hz.**

termed high frequency oscillations (HFOs), are transients with frequency spanning from 80 to 500 Hz, far beyond the traditional EEG bandwidth. In figure 1-2 we provided an example of representative HFO centered in a 3-seconds iEEG signal. HFOs are distinctive compared to the classic Berger frequency band (0.3 – 70 Hz) and people believe that HFOs recorded from epileptic structures are generated by unique pathological mechanisms associated with epileptogenesis.

Unlike the conventional non-invasive scalp EEG studies where data is commonly collected from both patient and healthy control cohorts, the investigation of invasive EEG are essentially limited to patients with partial epilepsy where intracranial macro-electrodes are surgically implanted to monitor the ictal activities. Therefore, validation of the specificity of HFOs, interictal spikes and other neuronal activities recorded in iEEG is challenging (Worrell et al., 2012). One of the metric to assess the clinical utility of HFOs as SOZ localizing indicators will be examining the correlation of HFO properties with clinician defined epileptogenic zone as well as the postsurgical outcomes after the removal of the epileptogenic region. Before any ultimate conclusion can be made, however, a more practical challenge should be undertaken, which is the development of computational tools for the accurate and efficient identification of HFO in the continuous multi-channel iEEG recordings. Thus, a better understanding in the mechanism of HFO generation – either pathologically or physiologically – can be achieved by exploring the HFO spatial and temporal characteristics using tremendous amount of data obtained in large patient cohorts without human intervention which may put bias arising from visual validation, channel pre-selection and data reduction.

## 1.2 Aims and Contributions

This dissertation is concerned with the role of HFOs in clinical epilepsy for the accurate and efficient localization of SOZ. We particularly focus our attention to the automatic HFO detection and its clinical applications to facilitate presurgical evaluation with two major objectives: i) *the development of HFO detection algorithm*, and ii) *the investigation of HFO and its prognostic value in clinical epilepsy*. For the first aim, we proposed unsupervised detection approaches and tools to efficiently identify HFOs in massive clinical iEEG datasets in an automated fashion that is capable of isolating different subtypes of HFOs from interictal spikes and other non-neuronal events/artifacts. For the second aim, we demonstrated that the automatically detected HFOs could be used to provide specific information regarding the epileptogenic regions in different types of epilepsy in different states, and observed distinctive waveform patterns in physiological and epileptic HFOs which could be applied to distinguish SOZ from non-epileptic functional areas. The temporal attributes of HFO and its application in the early prediction of SOZ were also examined.

This thesis is structured in a way described as following: first, a brief review of the literature on HFOs studies is given in Chapter 2. It includes the definition of HFO and its putatively described subtypes, namely “ripple” and “fast ripple (FR)”, distinguished by the different frequency bands. The clinical significance and previous studies focusing on the computational analysis of HFO are also discussed. Chapter 3 reports the methodological contributions of the thesis. A novel algorithm is introduced for the detection of HFO as well as the localization of SOZ, and the results are correlated with

clinician-defined SOZ, which is also known as the gold standard. We further validated the method in different types of epilepsy, including some of the challenging cases where the ictal pattern was difficult to determine, and where both epileptogenic zone and eloquent brain regions were involved in the invasive monitoring, some of the representative results are given in Chapter 4 in the form of case studies. Chapter 5 and 6 report the original scientific contributions of the thesis, including a new pattern in the pathological HFO waveforms, and the temporal variation of HFOs in long-term recordings. Finally, in Chapter 7 we summarize the significance and conclusions of the dissertation, with ideas for future extensions of the work.

## CHAPTER 2 REVIEW OF PRIOR WORK

### 2.1 Definition of High Frequency Oscillations

High frequency oscillations (HFOs) are field potentials that reflect short-term synchronization of neuronal activity (Zelmann et al., 2012). It was firstly recorded in rat hippocampus and entorhinal cortex, and then was discovered in human subjects with medial temporal lobe epilepsy recorded using microwires (Bragin et al., 1999). Since then, the mechanism of HFO as well as its relationship to epileptic spikes and other brain activities has been broadly studied. The definition of HFOs varied in literature. Investigators generally agree that HFOs are spontaneous neuronal activities between 80 to 500 Hz that “clearly stand out from the baseline and persist for at least four oscillations cycles” (Zijlmans et al., 2017). The mechanism underlying the generation of HFO is to a large extent unclear. Recent studies support the view that HFOs are likely generated by multiple mechanisms at the cellular and network level, including synchronized inhibitory postsynaptic potentials with sparse pyramidal cell firing (Buzsáki et al., 1992) or principle cell action potentials (Bragin et al., 2011).

There has been an assumption that ripples (80 – 200 Hz), which have been well described in hippocampus and associated structures in normal animal brains, reflect physiological brain activities, whereas fast ripples (FRs, 200 – 500 Hz) reflect pathological hypersynchronous events that are crucially associated with seizure genesis (Staba et al., 2002). Scientists hold the view that ripples and  $\gamma$  activities (30 – 100 Hz) could be sharing similar mechanisms since they involve the same networks (Belluscio et al., 2012; Sullivan et al., 2011). Frequently found occurred with sharp waves, ripples are

considered as the production of periodic perisomatic inhibition generated by hippocampus. FR transients, by contrast, are more likely to be embedded in or following the inter-ictal spikes. Reports suggested that FRs can be production of the out-of-phase firing pyramidal cells, which otherwise produce epileptic spikes (Jefferys et al., 2012; Gulyás and Freund, 2014).

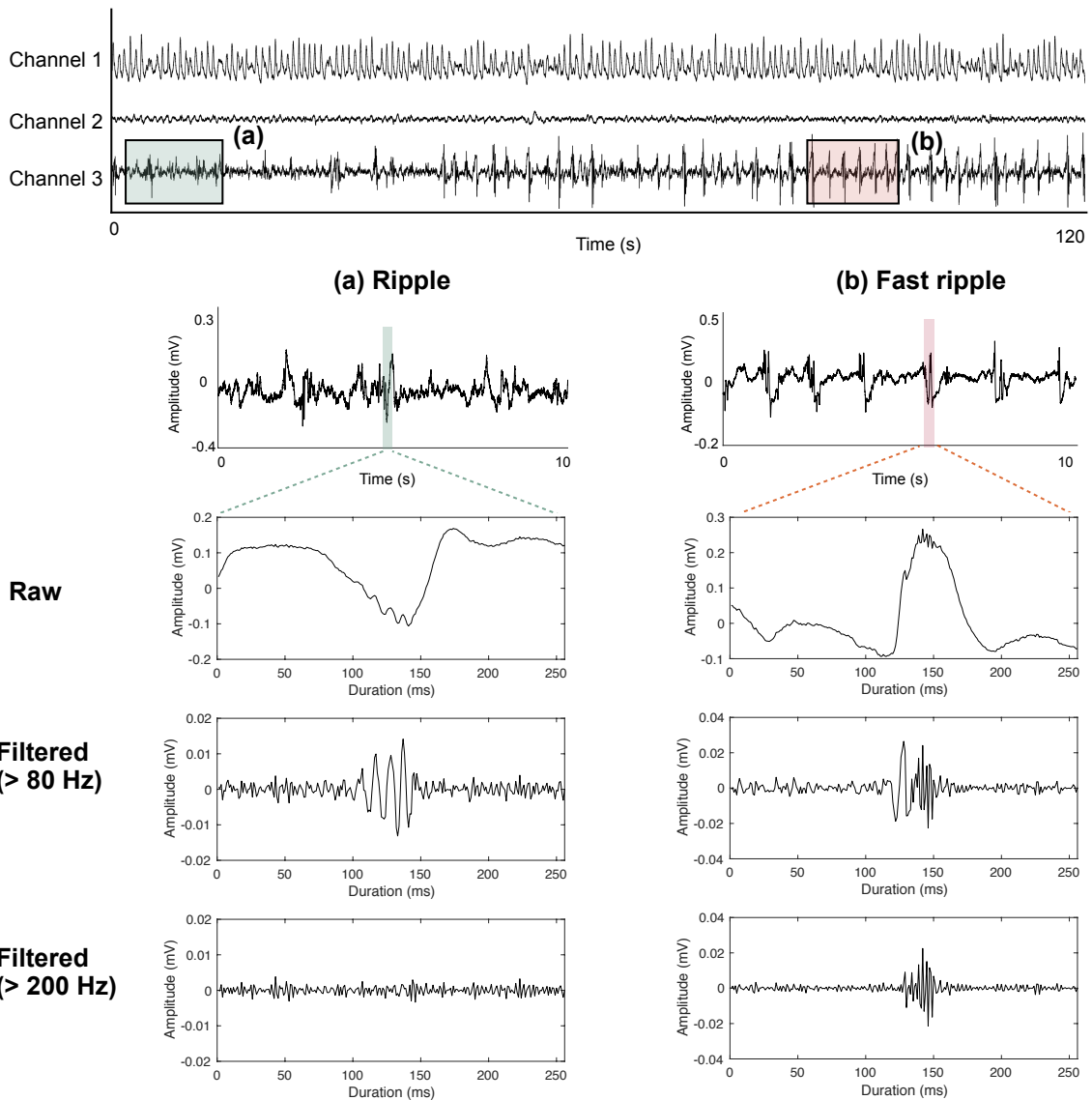


**Figure 2-1. Examples of ripple (left) from 10-second window (a) and fast ripple (right) from window (b). For both events, the raw and filtered signals above 80 Hz and 200 Hz are shown.**

However, studies have demonstrated important aspects about HFOs, that is, both epileptic and physiologic process may generate HFOs with peak frequency in the identical band. The considerable overlap in spectral frequency between normal and epileptogenic oscillations makes the definition of physiological and pathological HFOs still controversial (Engel et al., 2009). Not only that ripples and FRs recorded from clinical macro-electrodes or micro-wires both increased in seizure generating brain regions (Jacobs et al., 2008b), FR activities in normal brain functioning that reflect neuronal network coordination related to attention, learning and memory are also reported in several recent studies (Kucewicz et al., 2014). Apparently, it is inappropriate to group normal and epileptic HFOs on the basis of their frequency bands alone.

## **2.2 HFOs in Clinical Epilepsy**

HFOs are believed to be clinically significant, and thus could be used for seizure localization. In 2006, HFOs were recorded with a clinical setting for the first time, revealing that high-frequency EEG activity can be recorded with macro-electrodes in humans. The recorded HFOs underwent consistent modifications after spikes, and showed an increase trend in SOZ (Jirsch et al., 2006). Subsequent studies used macro- and micro-electrodes to record HFOs, indicating that HFO events captured by both of these two types of electrodes were increased in seizure generating brain regions (Schevon et al., 2009b; Worrell et al., 2008b). Despite that there is yet no evidence showing the high frequency activities recorded by macro- and micro-electrodes are exactly same kind of events, macro-electrode recordings has been considered to have the advantage of filtering out physiological HFOs and preferentially leave the pathological ones, making it

possible to evaluate HFOs as markers of epileptogenic areas for clinical practice (Crépon et al., 2010; Jacobs et al., 2008b).

HFOs are highly valued as promising clinical biomarkers for epilepsy. The identification of HFO generative locations produces direct connections to successful surgical evaluation. In general, presurgical localization in epilepsy is a combination of the identification of the irritative zone, the SOZ, the epileptogenic lesion, and the functional deficit zone (Zijlmans et al., 2012). The fact that HFOs usually occur superimposed on interictal spikes indicates that HFOs are associated with irritative zone. Study also shows that the rates of spikes and HFOs are higher inside than outside the SOZ, and that HFOs are more specific and accurate than spikes to delineate the SOZ in epileptic patients without a visible brain lesion, which implied a clear link between HFOs and the SOZ (Andrade-Valença et al., 2012). Moreover, it has been proved that the occurrence of HFOs can reflect focal cortical dysplasia lesions (Kerber et al., 2013). A series of studies illustrated that the removal of HFO generative regions within and outside the SOZ in children and adult patient population was correlated with seizure-free outcomes, suggesting HFOs can be excellent surrogate markers of epileptogenesis, and therefore should be recommended as the guide of surgical resection (Akiyama et al., 2005; Cho et al., 2014; Jacobs et al., 2010; Ochi et al., 2007; Wu et al., 2010).

Recent studies have been focusing on the investigation of different HFO patterns and their relationship to different epileptogenic areas and seizure propagation. Reports suggested that ripples co-existed with distinctive background EEG activities might have different interpretations. Only the removal of those areas where HFOs occurred in a flat

background was significantly associated with good surgical outcomes (Kerber et al., 2014). The relationship between HFO patterns and different epilepsy phenotypes is still under investigation. HFOs are considered more related to SOZ than to brain lesion (Jacobs et al., 2009). Data recorded with micro-electrodes provided evidence that FR was linked with volume reduction of hippocampus in epileptic subjects (Ogren et al., 2009). In one study, researchers highlighted that FR activities should also be considered for its potential in the presurgical workup of non-lesional epilepsy (Jiruska et al., 2010). Some groups argued that HFOs in ictal, preictal, and interictal stages presented different appearance, suggesting that the identification of HFO might be helpful in the clinical practice of epilepsy surgery (Jacobs et al., 2012; Jirsch et al., 2006; Zijlmans et al., 2011). Further, the pattern by which high frequency activities are propagated is believed to be helpful in identifying epileptogenic network nodes relevant to surgical planning (Korzeniewska et al., 2014). Additional study is needed to reveal whether there is a clear relationship between HFO patterns and different type or distinct phase of seizures.

### **2.3 Identification of HFO in Human Intracranial EEG**

Although it is possible that HFOs being spotted directly from raw EEG data traces, they are more likely to become visible and detectable after band-pass filtering. Using the band-pass filtered data one is able to discover the high frequency events as oscillatory waveforms that “pop-out” from the background. Based on this theory, a basic HFO detector is built up by setting a threshold that would distinguish candidate events with a higher energy than the background. However, there are many types of brain signals, such as epileptic spikes, impulse-like artifacts, or non-sinusoidal oscillatory activities with

harmonics, which may contain residual energy in the high-band and show similar waveform patterns with HFOs, after straightforward filtering and thus resulting in “false” ripples that might easily be confounded with “genuine” ripples.

Discussion regarding to this issue have been addressed. Figure 2-2 (A) shows a series of iEEG transients with similar appearance after high-pass filtering process, which is

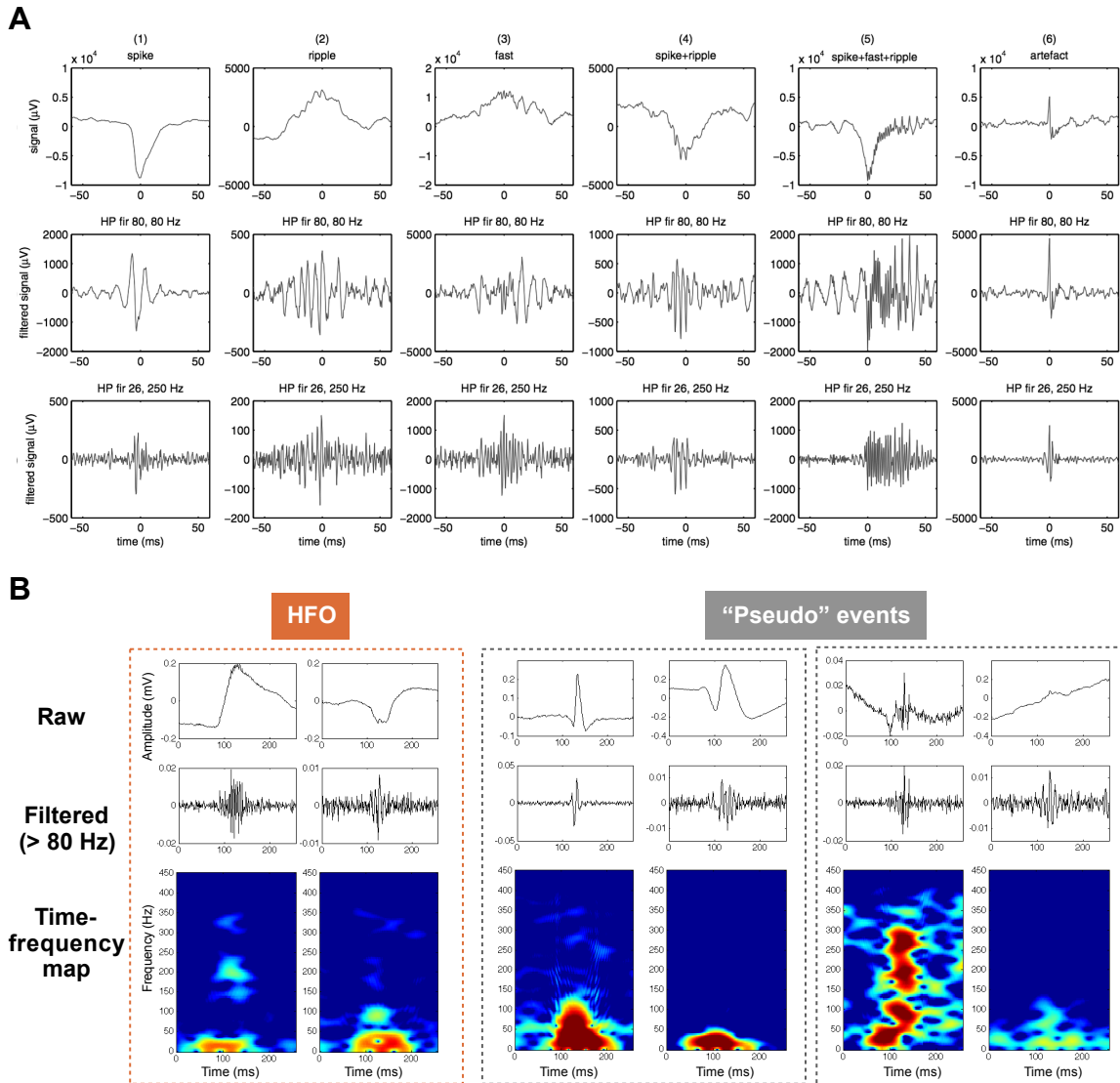


**Figure 2-2. (A) Previous study demonstrating the pitfalls associated with straightforward filtering. (B) The distinctions between HFOs and “pseudo” events are clearer by inspecting the time-frequency characteristics.**

reported in a recent study by Bénar and colleagues (Bénar et al., 2010). A set of detection criteria has been brought up considering the natural properties of HFOs, that is, its amplitude range (10 – 1000  $\mu$ V) and duration (30 – 100 ms) (Worrell et al., 2012). An alternative method to identify HFO is by viewing its time-frequency contents after short Fourier transform or wavelet transform. The high frequency component can be seen well isolated in the time-frequency panel, different from the pattern in pure spikes or sharp noise. Examples of HFO, spikes and other false detections are presented in figure 2-2 (B). The time-frequency representation of these events shows distinct characteristics and facilitates the visual verification of HFOs. Some studies have been using this technique in HFO studies for visual inspection, or seizure detection, with or without a preliminary auto-detector (Burnos et al., 2014; Park, Lee and Chung, 2014; Schevon et al., 2009b; Tzallas, Tsipouras and Fotiadis, 2009).

Due to its significant value in clinical use, scientists are dedicated to the investigation of this standalone transient. Staba et.al recorded intracranial EEG data during rapid and non-rapid eye movement (REM, NREM) sleep as well as waking state of patients with epilepsy. They used a root mean square (RMS) detector to distinguish HFOs, suggesting that both ripple and FR could be detected during waking and sleep segments, and that the highest rate of occurrence was found during NREM sleep (Staba et al., 2002, 2004). In order to validate the HFO as an applicable clinical biomarker, researchers need to clarify whether inter-ictal spikes with pathological HFOs are more reliable to indicate epileptogenesis than spike itself, and whether HFOs that are not associated with spikes have the identical connection to epileptogenicity as those co-exist with interictal spikes.

Existed studies indicated that HFO underwent consistent modifications after EEG spikes (Urrestarazu et al., 2006). By visual observation using 10-minute data during slow wave sleep, researchers demonstrated that spikes were more likely to co-occur with ripples rather than FR. Furthermore, the rate of FRs and of spikes with FRs showed the highest sensitivity in indicating the SOZ (Jacobs et al., 2008b). In other studies where HFOs, spikes and other waves were marked by human visualization, results implied that HFOs occurred to a high degree independently of spikes, and that when they co-occurred with spikes, it seemed to be more often the case in SOZ areas (Gardner et al. 2007).

The detection and investigation of HFO provided a better understanding of the inner relationship between this particular type of activity and epilepsy. However, due to the massive size of modern iEEG datasets and the short duration, low amplitude of the transient, visually marking the events in long-term recordings is not feasible, which stressed the necessity to introduce a robust, reliable auto-detector that is applicable for quantitative data analysis in large-scale modern iEEG database.

A summary of existing HFO studies and the utilized HFO identification approaches is given in table 1-1 (A). While majority of the research performed visual identification, some of the studies adapted a sensitive amplitude based detector followed by visual validation. One of the existing benchmark detection method is to compute the root mean square (RMS) of band-pass filtered data (100 – 500 Hz) using a 3 ms window as the measurement of background energy. Successive RMS with amplitude greater than 5 times of standard deviation (SD) above the overall mean RMS value and a minimum duration of 6 ms were selected as putative HFO events, and were subjected to the additional

criteria, which was defined as containing at least 6 peaks greater than 3 SD above the mean value of the rectified band-pass signal (Staba et al., 2002). Following optimized detectors were using diverse parameters, including filter settings and adaptive threshold; HFO duration and minimum event interval definition also differs among several studies (Gardner et al., 2007; Worrell et al., 2008; Blanco et al., 2010, 2011). Other than the RMS based detector, several studies utilized the “short time line-length” for baseline detection, which is a technique based on fractal dimension method that was firstly proposed for seizure detection in 2001 (Esteller et al., 2001). The line-length of a signal can be described as the sum of the absolute differences between successive samples of the signal, and is treated as a measure of the combined amplitude-frequency features of the signal (Esteller, Echauz and Tchong, 2004). Line-length has been one of the most preferable features in seizure and epileptic event detection, due to its sensitivity to amplitude and frequency fluctuation and its low computational burden (Esteller et al., 2004; Guo et al., 2010; Koolen et al., 2014; Paz et al., 2013). Using 85 ms window without additional ripple count criteria, line-length based detector window showed a more robust performance when compared to the conventional RMS detector, yet tended to over-detect especially to the artifacts, spike-like events and events with low amplitude and short high frequency component (Gardner et al., 2007). Another group utilized line-length detector with 200 ms long, 50 ms overlapped sliding window to identify pathological HFOs in epileptic subjects, associated with expert visual validation. The result showed that the majority of HFOs occurred with epileptiform sharp wave transients (Matsumoto et al., 2013).

The critical methodological difference among variety types of detectors lies on the functions used to compute the energy of the filtered signal. Besides, HFO detectors may be semi- or fully-automatic, depending on their post-processing techniques to prune false detected events. In both cases, the initial detector should have a high-sensitivity, low-specificity property in order to successfully distinguish all the high frequency candidate events from the background signal. This preliminary detector can be built using RMS or line-length method, as described above, or other approaches such as computing signal envelope using Hilbert transform (Crépon et al., 2010) and the autocorrelation of the signal to build a baseline model (Zelmann et al., 2012). Several studies used a combination of the benchmark detection methods to optimize the performance of the detector (Biro et al., 2013; Dümpelmann et al., 2012; Schevon et al., 2009b).

Many of the existing HFO detectors are so-called “semi-automatic” because of its 2-stage processing strategy, where an automated detector is used in the first place, and then visual inspection is performed in the second place (Crépon et al., 2010; Schevon et al., 2009b; Worrell et al., 2008b). Several research groups have been working on the development of fully automated algorithms for HFO detection. Either supervised classification procedure or advanced signal-processing steps are executed after initial detection (Burnos et al., 2014; Chaibi et al., 2013; Dümpelmann et al., 2012; López-Cuevas et al., 2013). However, due to the highly-intensive labor cost associate with the manual labeling of the events, these proposed supervised detectors commonly investigated short data segments or performed data reduction/channel pre-selection to decrease the work load. As it is given in table 1-1 (B), most of the automatic techniques

executed HFO analysis using 1 to 10 minutes of data. A recent study introduced an unsupervised approach implemented by means of clustering (Blanco et al., 2011, 2010a), where the unlabeled, detected events are automatically grouped into several clusters based on their distinctive features and then inspected by the authors. This approach further deducts human inspection; hence it should be applicable for massive data processing. Additionally, it is likely to provide objective evidence showing the essential distinction of different HFO patterns that have been taken largely for granted. Nevertheless, in the existing clustering based study the authors did not perform validation of the detected HFOs. Till present, few reports correlated the HFO findings with the clinical information, and little is known whether the automatic detection of HFO can be employed to serve the accurate localization of SOZ.

**Table 1-1 (A) Review of HFO characterization studies**

<b>Study</b>	<b>Method</b>	<b>Study</b>	<b>Method</b>
Staba et al., 2004	<i>RMS + visual inspection</i>	Blanco et al., 2010, 2011	<i>Automatic (k-means clustering)</i>
Jirsch et al., 2006	Visual inspection	Zelmann et al., 2010, 2012	<i>Automatic (MNI: wavelet entropy + RMS)</i>
Gardner et al., 2007	<i>Line length + visual inspection</i>	Zijlmans et al., 2011, 2012	Visual inspection
Worrell et al., 2008, 2010	Line length + visual inspection	Gotman et al., 2011, 2013	Visual inspection
Urrestarazu et al., 2007	Visual inspection	Valença et al., 2012	Visual inspection
Jacobs et al., 2008, 2009, 2010, 2015	Visual inspection	Dümpelmann et al., 2012, 2015	<i>Automatic (neural network, ripple only)</i>
Bagshow et al., 2009	Visual inspection	Pearce et al., 2013	Automatic detection (k-means clustering)
Schevon et al., 2009	RMS + visual inspection	Cho et al., 2014	RMS + visual inspection
Crepon et al., 2010	Envelope + visual inspection	Burnos et al., 2014	<i>Automatic (time-frequency analysis)</i>
Wu et al., 2010	Visual inspection	Klink et al., 2014, 2015	Visual inspection

**Table 1-1 (B) Review of HFO auto-detection techniques**

<b>Study</b>	<b>Data</b>	<b>Method</b>	<b>Validation</b>	<b>Note</b>
Staba et al., 2002	<i>Ten-min</i> segments from 5 patients, NREM sleep	RMS	/	Benchmark detector
Gardner et al., 2007	<i>Three-min</i> single channel data from 2 patients	Line-length	1330 HFOs were validated by human reviewers	
Blanco et al., 2010	Continuous recording from 9 patients, approximately <i>3 hours multichannel recording per patient</i>	RMS + Unsupervised clustering	/	
Zelmann et al., 2010	<i>One-min</i> sections from 19 patients, totally 373 channels. Bad channels excluded	MNI detector: wavelet entropy + RMS	7994 HFOs were visually marked by 2 reviewers	<i>“It takes 10h to mark HFOs in a 10-channel 10-min recording”</i>
Dumpelmann et al., 2012	<i>Three-min</i> recording from 11 patients, totally 128 channels.	Neural network	41722 HFOs were visually marked by an experienced reviewer	Ripples only
Burnos et al., 2014	<i>Five-min</i> recording from 7 patients, totally 36 channels	Time-frequency analysis	Correlated the HFO channels with SOZ	Selected a subset of channels

# **CHAPTER 3 UNSUPERVISED HFO DETECTION USING MULTICHANNEL IEEG RECORDINGS IN PATIENTS WITH EPILEPSY**

## **3.1 Introduction**

High frequency oscillations (HFOs) in the frequency range of 80 to 500 Hz are proposed as putative clinical neurobiomarkers for epilepsy, with their potential to improve the postsurgical outcomes of SOZ removal operations in patients with epilepsy resistant to medication. The duration an HFO may possess range from a few milliseconds to tens of milliseconds depending on the minimal frequency component that outlines the event (Zijlmans et al., 2017). Due to the short duration and low amplitude of the transient, as well as the massive data size, visually annotating the event in long-term recordings could be exhausted and cumbersome, making it an obstacle to introduce HFO into clinical routine. This stressed the necessity to introduce a robust, reliable technique that is applicable for quantitative data analysis in large-scale iEEG database.

Similarly to epileptiform spikes, some artifactual sharp waveforms and physiological neuronal events associated with normal brain functions may contain high-frequency spectral contents that overlap with epileptic HFOs, and therefore resulting in false detections that might easily be confounded with HFOs introduced by epileptogenic networks. Discussion regarding to this issue have been addressed, and a set of detection criteria has been brought up considering the signal properties of HFOs in the high-pass filtered iEEG data. Several HFO detectors have been proposed in literature based on

these regulations in the time and frequency domain. One of the critical methodological differences among variety types of detectors lies on the functions used to compute the energy of the filtered signal. Most of the studies define background energy by computing the root mean square (RMS) or signal line length. The initial detector generally includes a high-sensitivity, low-specificity property in order to successfully distinguish all the high frequency candidates from the background EEG signal. In semi-automatic detectors, usually a visual inspection step is performed after the prior detection, whereas in fully-automatic detectors, supervised classifiers or advanced signal processing steps are required.

Despite that many efforts have been made towards the investigation of HFOs, to our knowledge, until now there exist few reports utilizing automatic detection to localize the seizure onset zone (SOZ) on account of the potential prognostic value of HFOs. The aim of this study is to identify epileptic seizure onset regions in brain using HFOs detected by an automatized technique. We developed analysis tools integrating clustering method involving  $k$ -means and Gaussian Mixture Models (GMM) to explore the time and time-frequency content of HFOs. High frequency transients were first detected by an energy-based threshold, and then were further discriminated using an unsupervised approach where the unlabeled, detected candidates were automatically grouped into several clusters according to their distinctive features. We did not perform any channel pre-selection or artifact elimination in the original datasets. The algorithm was tested using 10 minutes of iEEG data segment in the sleep, awake, and pre-ictal state of 8 patients collected from

two deferent centers. The relationship between SOZ and HFO generative regions was also discussed.

### **3.2 Data Acquisition**

A total of 8 patients with refractory epilepsy were involved in the study (3 male, 5 female, ages 28 – 55). The iEEG data of 5 patients (P1 – P5) with focal and generalized tonic-clonic seizures were recorded for 6 – 14 days at the Fairview Hospital at the University of Minnesota. The iEEG data was digitized at 2 kHz sampling frequency by using a multichannel bioamplifier with XLTEK EMU128FS system (Natus Medical Inc, CA), which had an anti-aliasing filter set to 1 kHz. The iEEG data of 3 patients (P6 – P8) were recorded at Capa Hospital of Istanbul University (Istanbul, Turkey) with Nicolet C64 amplifier (Natus Medical Inc, CA) at 1 kHz sampling frequency for 5 – 6 days, with 150 Hz anti-aliasing filter implied. All patients were suffering from medically refractory epilepsy and underwent monitoring with clinical grid and/or depth electrodes. Detailed description of patient characteristics, electrode implantation information, MRI and PET characterization are shown in table 3-1. Data collection and scientific workup was approved by the University of Minnesota institutional review board and the ethical committee of Istanbul University, respectively.

We defined 10-minute segments in sleep and waking state as sleep baseline (SB) and waking baseline (WB), which was at least 60 min away from the onset of the first seizure of each day. The pre-ictal (PI) data was defined as 10-minute segments before the seizure onset. For each subject, all channels were used for data analysis. The SOZ was defined as the contacts where a seizure was firstly occurred during the EEG monitoring, which was

identified by neurophysiologists, and was taken as the gold standard for result validation. Sample bipolar raw and 80 – 500 Hz band-pass filtered iEEG data in three states is shown in figure 3-1. Channel pair where a seizure first occurred was marked in red.

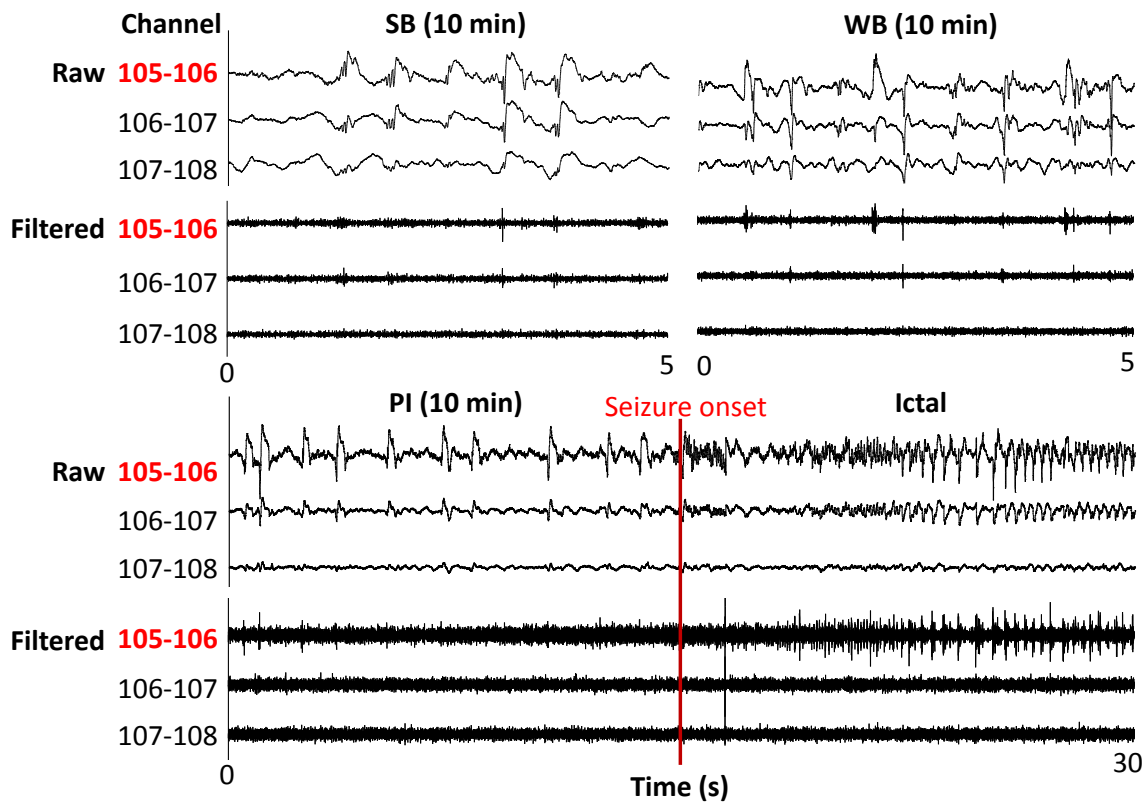


**Figure 3-1. Data collection protocol with sample bipolar raw and 80 - 500 Hz band-pass filtered iEEG data. Only 5 seconds of SB/WB, and 15 seconds before and after the seizure onset are shown.**

**Table 3-1. Patient demographics**

ID	Sex	Age	Seizure types <sup>a</sup>	SOZ <sup>b</sup>	Chan No.	Electrode types	MRI	SZ No.	SB No.	WB No.	Surgery Outcome <sup>c</sup>
P1	M	30	FS	RAH (18)	28	Strip; Depth	Right mesial temporal sclerosis	6	6	6	Engel class I
P2	F	28	FS	LA, LAH, LPH (4,11,18)	52	Strip; Depth	Left mesial temporal sclerosis	4	4	7	Engel class I
P3	F	35	FS and GTC	RA, RM, RP (28,36,43)	56	Depth	Normal	5	4	6	Engel class III
P4	M	44	FS and GTC	RA, RAH, RPH (31,32,38, 45)	60	Strip; Depth	Normal	4	13	14	Engel class I
P5	F	32	FS	LA, LAH, LPH, RA, RAH, RPH (8,15,22,23,29,36,43)	56	Strip; Depth	Foci of cortical thinning in the left frontal operculum and left temporal lobe	11	5	5	Engel class I
P6	M	38	FS	LOL(20-23,25-27)	52	Strip; Depth	Normal	5	6	6	Engel class I
P7	F	55	FS	RTL (14-16,23)	32	Depth	Normal (wide spread small sized hyper-intensities in WM)	4	6	6	Engel class I
P8	F	30	FS	RH (1,2)	24	Depth	Right hippocampal sclerosis	3	2	2	Engel class I

<sup>a</sup> FS: focal seizures. GTC: secondary generalized tonic-clonic seizures.

<sup>b</sup> LAH: left anterior hippocampus. LPH: left posterior hippocampus. RAH: right hippocampus anterior. RPH: right hippocampus posterior. LA: left amygdala. RA: right amygdala. RM: right mid-temporal. LOL: left occipital lobe. RTL: right temporal lobe. RH: right hippocampus. For each patient, SOZ channel indices are shown in parenthesis.

<sup>c</sup> Engel Class: the classification of postoperative outcomes for epilepsy surgery. Class I: free from disabling seizures; class III: worthwhile improvement (Engel et al., 1987).

### **3.3 Proposed Algorithm**

The approach was performed in three stages as depicted in figure 3-2 (A): HFO detection, time-frequency analysis and feature extraction/clustering. All data analysis procedures were implemented in MATLAB (Mathworks, MA) environment. An HFO investigation tool integrating HFO detection and unsupervised clustering was developed and used to analyze all segments as shown in figure 3-2 (B).

#### **3.3.1. Initial Detection**

A high sensitivity automatic detector was built based on the existing technique proposed by Staba et al. (Staba et al., 2002) with modification to minimize noise/artifact and other false detections. Raw data of multichannel iEEG segments were first processed using a 64-order FIR digital band pass filter in 80 – 500 Hz range. The data was filtered in forward and reverse directions to avoid phase distortion using *filtfilt* function in MATLAB. We computed the standard deviation (SD) of the band-pass filtered signal in 100 ms windows. Then an amplitude threshold was set to 5 times the median of the SDs. For all samples with amplitudes larger than the threshold, an epoch of 128 ms before and

after the sample were extracted on the raw data. In order to give a flavor of typical events captured by the initial threshold, we provided raw and band-pass filtered iEEG waveforms, and their time-frequency maps in figure 3-3. These events then went through the HFO sieving procedure based on the assumption that HFOs are transients with protruding oscillatory components that “pop out” from the background signal (local baselines) after high-pass filtering.

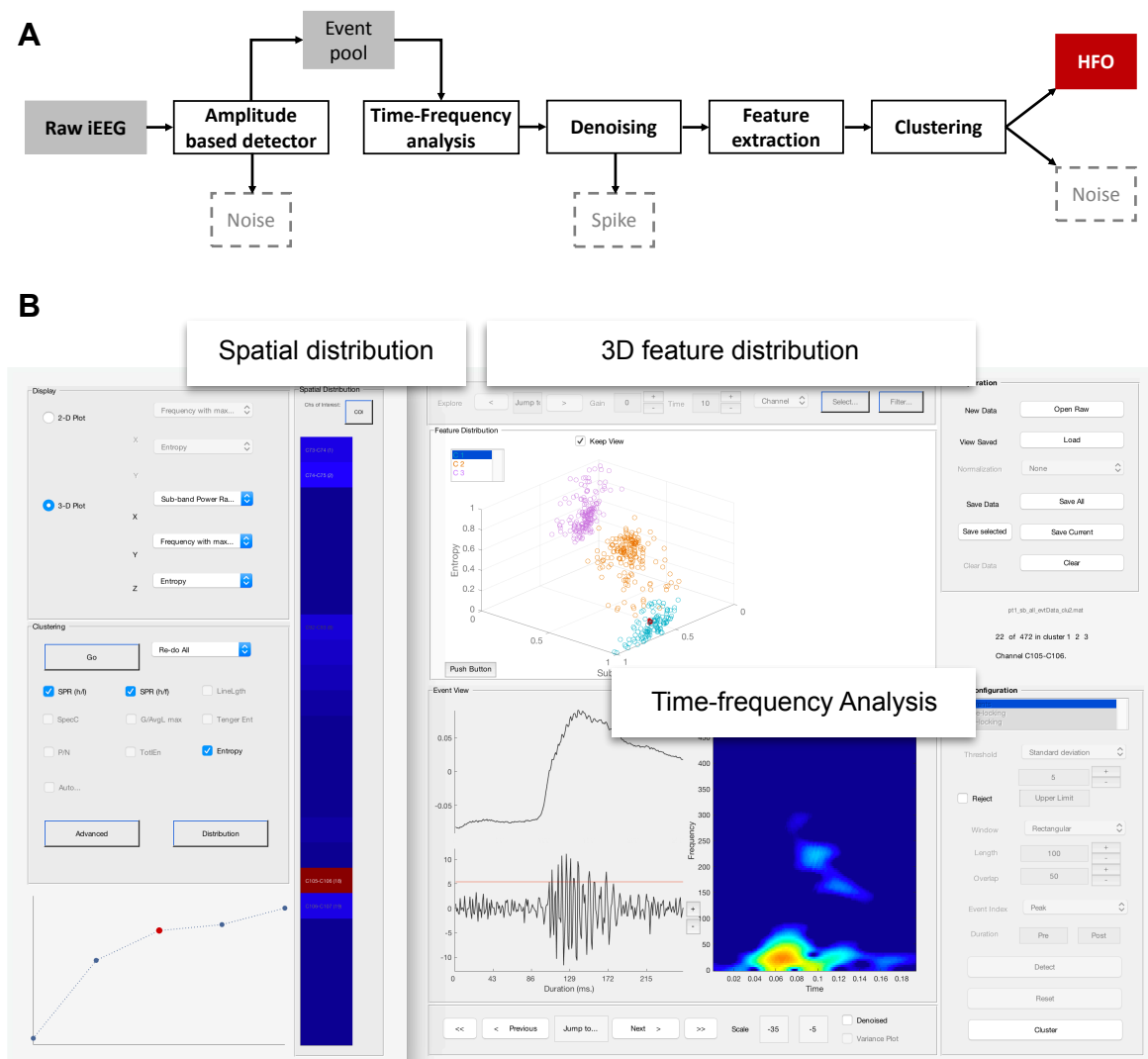


**Figure 3-2. (A) Schematic diagram of the algorithm. (B) Interface of the customized HFO investigation tool.**

More specifically, raw data with a zero-crossing number larger than 10 were considered artifacts, and therefore were excluded from the event pool. After band-pass filtering the raw iEEG within 80 – 500 Hz range, the signal envelope was computed using the Hilbert transform for each extracted segment. A threshold defining the local background activity was set to three times of the median of the background envelope, which was obtained from the first and last 80 ms segment. In addition, the protruding part of the bell-shaped envelope with an amplitude exceeding the threshold should be well localized in the center, lasting for 30 – 100 ms. The threshold-crossing number of the filtered data should be no less than 8 times to ensure at least 4 successive peaks standing out from the background. Figure 3-3 describes the HFO sieving criteria during initial detection. As it is shown in the figure, the spike was discarded as its threshold-crossing number was less than 8. The first noise example was excluded since the raw waveform crossed zero-baseline for more than 10 times. The second noise example was excluded for its threshold crossing number being less than 8.

### **3.3.2. Time-Frequency Analysis and “Denoising”**

In the past, feature extraction techniques were generally employed on the band pass filtered iEEG data. However, the noise and spikes generally have residual energy in the HFO band and it becomes difficult to isolate these events from real HFO when the analysis is restricted to a certain portion of the available bandwidth. Here, we explored the time-frequency content of the raw iEEG in the 0 – 500 Hz band around each HFO candidate that survived the initial detection. We observed that, not only high frequency, but also low bands below 80 Hz played a crucial role in distinguishing HFOs from other

events such as epileptic spikes. We used a short time Fourier transform (STFT) to observe the time-frequency content of iEEG around each HFO candidate. Moreover, a denoising procedure was executed to improve the detection accuracy. The STFT was computed in a 256 ms segment starting 128 ms before the center of HFO and extending 128 ms after it. The Fourier transform was computed in a 64 ms *Hanning* window which was shifted sample by sample to create a time-frequency map.

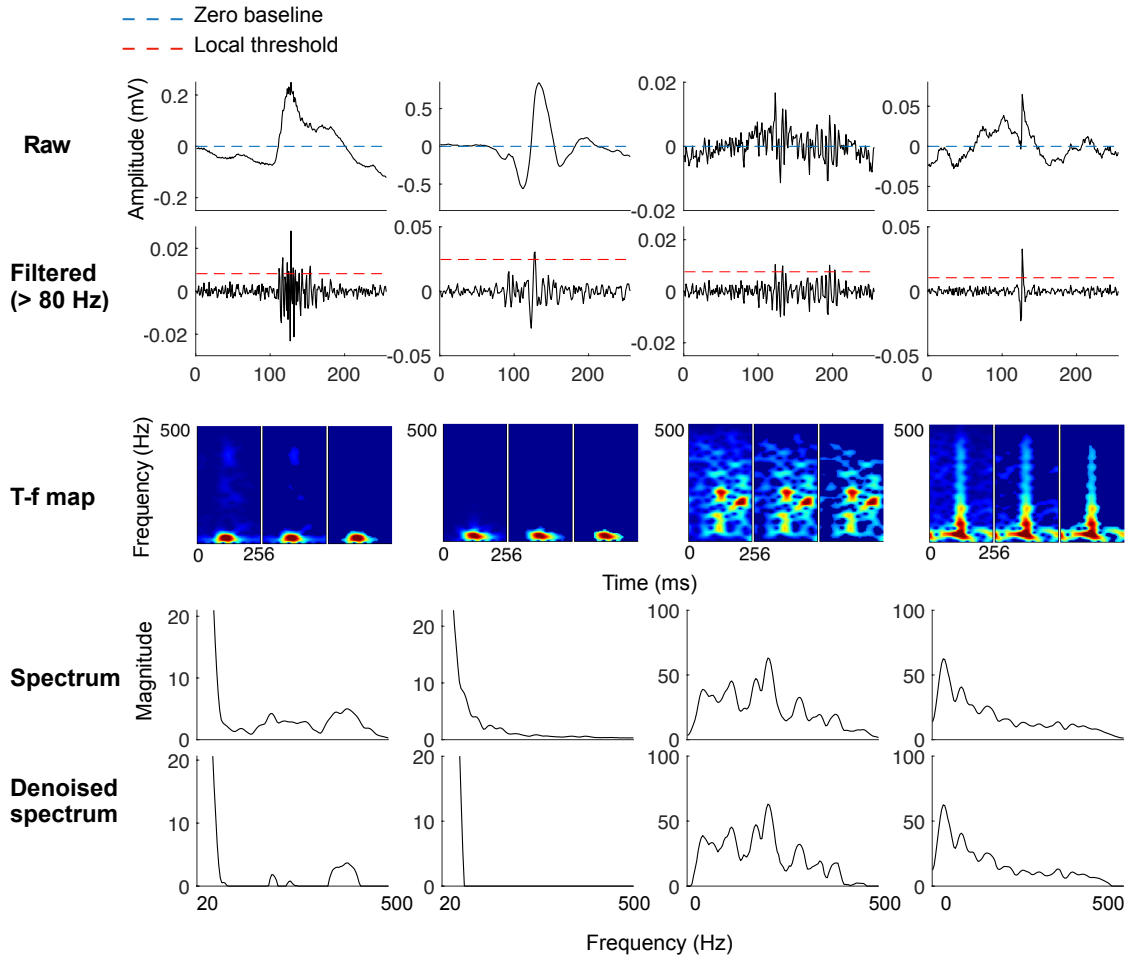


**Figure 3-3. HFO sieving and denoising step. Appropriate denoising would reveal the high frequency component of an HFO. The spectrum was derived from the original and denoised time-frequency map.**

Generally, these time-frequency maps were quite noisy due to background noise, making it difficult for visual exploration. To remedy this, we performed a denoising procedure in which we first computed the cumulative energy of the time-frequency map using the expansion coefficients for each event, then retained only the components that made up the majority of the total energy and omitted the rest. In figure 3-3 the time-frequency maps of a representative HFO, a non-HFO spike, and two types of noise samples were provided before denoising and after denoising (with 97% and 90% energy preserved respectively). We observed that these maps were extremely useful in visual inspection, and noted that no residual energy remained above 80 Hz in spikes following the denoising step (i.e., no spectral peak left after denoising), whereas The HFOs were represented with two isolated components, one located in low frequency band and the other as a blob in 80 – 500 Hz band whereas the spikes were represented with a single component in the low band. With this motivation, we eliminated those spikes with no residual energy above 80 Hz from the event pool, and used the surviving candidates with clear high-band spectral peaks standing out from the background in the feature extraction step.

### **3.3.3. Feature Extraction**

Three HFO distinctive features were extracted from the frequency and time-frequency domains and an unsupervised clustering step was implemented on these features to cluster similar events, which include HFOs, inter-ictal spikes, sharp waves and many other pseudo events due to noise.

- **Frequency corresponding to maximum peak to notch energy ratio.**

In the denoised time-frequency map of an HFO, the high-frequency component is clearly revealed with a “gap” between the low frequency component (see figure 3-3 for examples). The peak to notch feature is designed to quantify this discriminant information. Figure 3-4 gives detailed explanation of the feature. As an initial step, two power spectra of the HFO was computed from a segment that centered on 100 ms of the original and denoised time-frequency map. In the following step, we further processed the remaining anomalies by searching for the peaks in the high-band using their original and denoised power spectrum. In each candidate, we first localized the frequency with the minimum energy between 40 and 100 Hz ( $f_m$ , marked with green arrow in the figure), and then in the denoised spectrum, we stored all the energy peaks above  $f_m$  (magenta dots, A and B) together with their corresponding frequency indices. Then we searched for the local minimum within the 50 Hz band below the frequency corresponding to in the

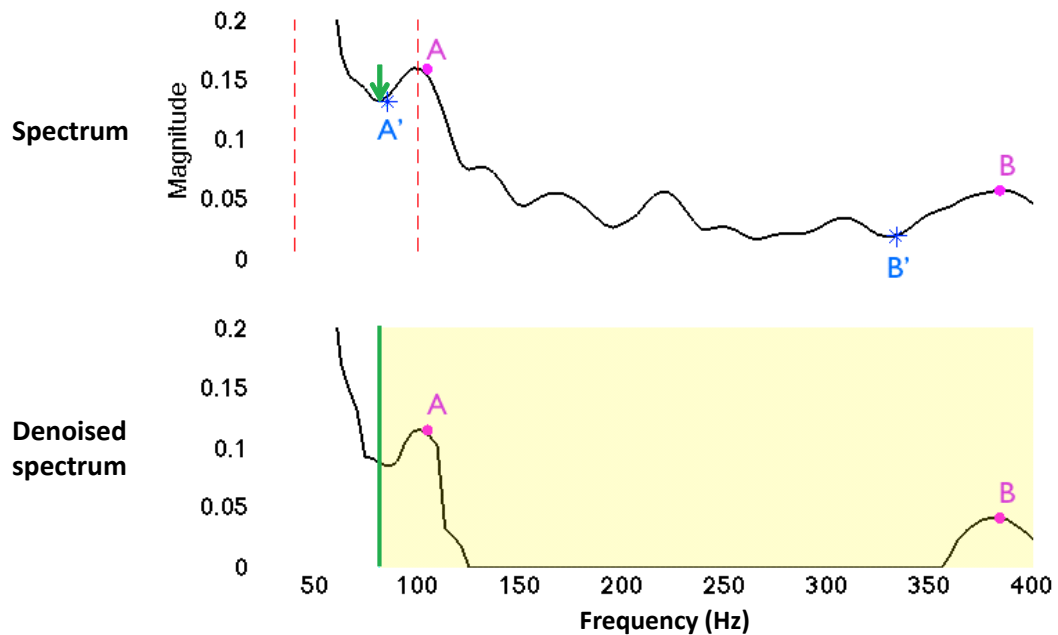


**Figure 3-4. Frequency corresponding to maximum peak to notch ratio.**

original power spectrum (blue stars, A' and B'). The frequency with the maximum energy ratio was used as a feature to identify genuine HFOs from other events. In the sample event given in figure 3-4, although the maximum energy occurred at point A, the maximum peak to notch ratio is corresponding to B which corresponds to fhFO.

- **Sub-band power ratio.**

For each candidate, we computed the ratio of the signal power in the presumed HFO band (80 – 500 Hz) to the power in low band (16 – 80 Hz) using the following equation:

$$\frac{P_{[80-500]}}{P_{[16-80]}}, \quad (3-1)$$

where  $P$  is the power spectrum density (PSD) defined as

$$P_{[a,b]} = \sum_{\{k \in Z | \zeta(a) \leq k \leq \zeta(b)\}} \left| \hat{P}_k \right|^2, (a < b) \in (0, \frac{f_s}{2}), \quad (3-2)$$

with  $f_s$  representing the sampling frequency, and  $\hat{P}_k$  representing a multitaper power spectral density estimate, in our case, the periodogram derived by using Welch's method:

$$\hat{P}_k = \frac{1}{U} \sum_{u=1}^U \hat{P}_M, \quad (3-3)$$

where  $\hat{P}_M$  denotes the modified periodogram of the  $u^{\text{th}}$  measurement in the signal.

- **Spectral entropy.**

For each candidate, the denoised spectrum was normalized by its sum to construct a probability function. The signal entropy was thereafter obtained by:

$$H = - \sum_f s(f) \log[s(f)], \quad (3-4)$$

where  $s(f)$  represents the normalized signal spectrum.

Here the entropy measures the sharpness of the spectrum and serves as a useful feature in distinguishing HFO from irrelevant events.

### 3.3.4. Unsupervised Clustering

After feature extraction, unsupervised GMM clustering was used with these three features to map survived candidate events into different categories, and the resulting groups were presented to experienced reviewers with their temporal and spatial patterns. In GMM, the feature distribution is presented by a weighted combination of  $K$  Gaussian components, with its probability density distribution (*pdf*) characterized by:

$$p(x) = \sum_{k=1}^K \pi_k \eta(x | \mu_k, \Sigma_k), \quad (3-5)$$

where  $\pi_k$  is the weight of each component satisfying

$$\sum_{k=1}^K \pi_k = 1, \quad (3-6)$$

and  $x$  is the measurement of features,  $\pi_k$  ( $k = 1, 2, \dots, K$ ) represents the weight of each component,  $\mu_k$  and  $\Sigma_k$  stands for the means and covariance,  $\eta(x | \mu_k, \Sigma_k)$  is the component Gaussian density represented as:

$$\eta(x | \mu_k, \Sigma_k) = \frac{1}{(2\pi)^{D/2} |\Sigma_k|^{1/2}} \exp\left(-\frac{1}{2}(x - \mu_k)^T \Sigma_k^{-1} (x - \mu_k)\right). \quad (3-7)$$

Here,  $D$  is the dimensionality of the data. The component density parameters  $\pi_k$ ,  $\mu_k$  and  $\Sigma_k$  are estimated by a probabilistic approach that maximizes the likelihood of the sample:

$$\prod_{i=1}^N p(x_i). \quad (3-8)$$

The standard GMM clustering generally starts with a random selection of  $K$  samples as the initial centroids. Here the initialization of the iteration process was conducted based on an optimized version of the Partitioning Around Medoids (PAM) algorithm, also known as  $k$ -medoids (Kaufman and Rousseeuw, 1987), which is a variant of  $k$ -means. This classic partitioning technique was chosen to define the initial centers of GMM because of its low computational complexity and robustness.

In  $k$ -means, given a set of observations  $(x_1, x_2, \dots, x_N)$ , where each observation is a  $D$ -dimensional real vector,  $k$ -means clustering partitions the  $N$  observations into  $k$  sets ( $k \leq N$ )  $C = \{C_1, C_2, \dots, C_k\}$  so as to minimize the within-cluster sum of squares:

$$\operatorname{argmin} \sum_{i=1}^k \sum_{x_j \in C_i} \|x_j - \mu_i\|^2, \quad (3-9)$$

where  $\mu_i$  is the mean of observations in  $C_i$ . The initial centers are 2 random samples, and the algorithm iteratively compute the new centroids through the assignment step:

$$C_i = \left\{ x_q : \|x_q - m_i\|^2 \leq \|x_q - m_j\|^2 \forall j, 1 \leq j \leq k \right\}, \quad (3-10)$$

where each observation is assigned to the cluster whose mean yields the least squared Euclidean distance (update step):

$$m_i = \frac{1}{|C_i|} \sum_{x_j \in C_i} x_j, \quad (3-11)$$

which is intuitively regarded the nearest mean.

The proposed algorithm uses the  $L1$  norm (Manhattan distance) as distance metric in the update step, where the medoid of each cluster (i.e. the most centrally located datapoint in each cluster) is computed, yielding the  $k$ -medoids approach. Considering that the initial random selection of medoids will increase the number of iteration, a specific way of choosing centers was applied (Arthur and Vassilvitskii, 2007). Briefly, after initial center was randomly chosen among all datapoints, the algorithm computes the distance between and the nearest medoid, then the new medoid is determined with weighted probability distribution (Jiang and Zhang, 2014).

After initial centers were found, the parameters of the model were determined by expectation maximization (EM) approach (Dempster, Laird and Rubin, 1977). During the E-step, the algorithm computes the posterior probability for each sample as a member of the  $K^{\text{th}}$  component:

$$p_i(k) = \frac{\pi_k \eta(x_i | \mu_k, \Sigma_k)}{\sum_{j=1}^K \pi_j \eta(x_i | \mu_j, \Sigma_j)}, \quad (3-12)$$

then re-estimate the parameters through M-step:

$$\mu_k = \frac{1}{N} \sum_{i=1}^N p_i(k) x_i, \quad (3-13)$$

$$\Sigma_k = \frac{1}{N} \sum_{i=1}^N p_i(k) (x_i - \mu_k)(x_i - \mu_k)^T, \text{ and} \quad (3-14)$$

$$\pi_k = \frac{N_k}{N}, \quad (3-15)$$

where

$$N_k = \sum_{i=1}^N p_i(k) . \quad (3-16)$$

The entire procedure was repeated until model parameters converged. Each observation was assigned to the Gaussian component that provided the highest posterior probability. Consequently, the number of cluster is defined by the number of Gaussian components.

In order to find the optimal number of mixtures,  $K$ , for each dataset, we plotted  $p_i$  with respect to different  $K$  values. This curve represented the change in log-likelihood when increasing the number of mixtures. We observed that following an initial increase after a few mixtures, the log-likelihood reached a plateau. By inspecting this plot we selected the elbow of the curve to determine the optimal mixture number.

### 3.3.5. Validation

The cluster validity was measured by computing the well-accepted validation index Silhouette coefficient (Rousseeuw 1987) defined as:

$$S = \frac{1}{N} \sum_{i=1}^N \left( \frac{d_i - l_i}{\max \{l_i, d_i\}} \right), \quad (3-17)$$

where  $l_i$  is the average distance of element  $x_i$  with all other members in the same cluster, and  $d_i$  is the minimum average distance of  $i$  with elements that belong to any other cluster. This method measures for every point its cohesion to its separation. The result ranges from -1 to 1, a higher value indicates an object is well assigned to its own cluster. A Silhouette value greater than 0.7 is preferable (Chen, Ibekwe-SanJuan and Hou, 2010).

The detected HFOs were used to identify the seizure onset areas. With varying denoising levels ranging from 90% to 100% (i.e., no denoising executed), we investigated the spatial distribution of automatically clustered HFOs. The SOZ detection accuracy was measured by assessing the overlapping rate of HFO generative channels and the gold standard – clinician-determined SOZ. A channel was considered true positive if it was overlapped with the seizure onset location identified by neurologists and was considered false positive if it lied outside of the SOZ. The sensitivity (SE) and specificity (SP) was evaluated by:

$$SE = \frac{TP}{TP + FN} \text{ and} \quad (3-18)$$

$$SP = \frac{TN}{FP + TN}, \quad (3-19)$$

where TP stands for true positive, TN stands for true negative, FP stands for false positive, and FN stands for false negative (Burnos et al., 2014).

We compared these HFO channels with seizure onset channels in different states of each patient. The efficacy of the algorithm was tested by using a leave-one-subject-out cross validation procedure. Each time, one patient was separated from the entire patient population. Data from the remaining patients were used for learning the optimum denoising level, and this learned parameter was tested on the iEEG data of the left-out patient. This procedure was repeated for all patients, rotating the left-out subject. The performance was compared with another existing SOZ detection algorithm (Geertsema et al., 2015). Statistical analysis was implemented using paired Wilcoxon test with a confidence interval of 95%.

### 3.4 Results

#### 3.4.1. Feature Distribution of Detected Events

Across all 8 patients, a total of 10,188 events were accepted by the initial threshold detection and spike elimination steps, and then grouped by the clustering method. In general, 2 to 5 clusters were identified by the algorithm in each state of each patient, where one or two of them appeared to be HFOs, others were artifacts. The two HFO sub-clusters presented diverse energy distribution in the high band. One cluster was comprised by HFOs with their energy extending above 200 Hz, we referred them as fast HFO (fHFO); the other cluster presented oscillatory activity around 80 to 100 Hz and was interpreted as slow HFO (sHFO). In three patients with 1 kHz sampling rate (P6 – P8), no fHFO was detected due to the built in anti-aliasing hardware filter of the amplifier which was set to 150 Hz. For each individual patient, the number of HFO cluster was always fixed (either one or two) in all states. In patients where two HFO clusters were generated, we used fHFO cluster for the SOZ detection.

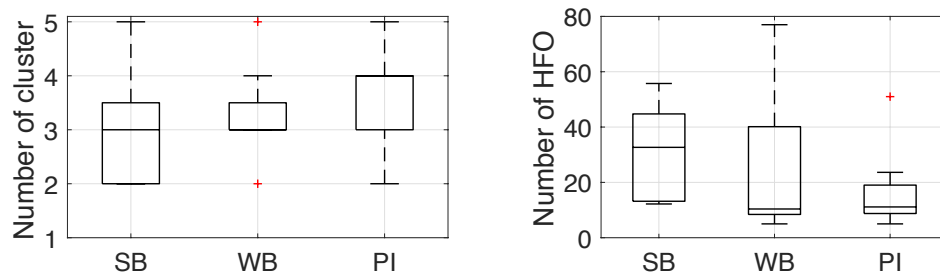


**Figure 3-5. Number of cluster (left) and HFOs detected per 10-minute segment (right) in different states ( $P_{SB-WB} = 0.30$ ;  $P_{SB-PI} = 0.10$ ;  $P_{WB-PI} = 0.17$ ) and HFO numbers ( $P_{SB-WB} = 0.09$ ;  $P_{SB-PI} = 0.14$ ;  $P_{WB-PI} = 0.71$ ).**

**Table 3-2. Cluster number and average event number per data segment**

ID	Cluster No. (HFO No <sup>a</sup> ./ candidate No.)			S-value (average)
	SB	WB	PI	
P1	2 (13/31)	2 (8/24)	2 (6/12)	0.82
P2	3 (56/102)	4 (60/259)	4 (9/79)	0.72
P3	3 (48/121)	3 (92/232)	4 (43/147)	0.67
P4	4 (14/73)	3 (20/54)	3 (11/55)	0.92
P5	2 (12/21)	3 (10/22)	3 (24/50)	0.60
P6	5 (29/73)	5 (9/31)	4 (18/46)	0.82
P7	2 (36/39)	3 (11/18)	5 (7/36)	0.72
P8	3 (42/86)	3 (5/17)	4 (93/156)	0.74

The current clustering solution yielded an average Silhouette value of 0.74 (ranging from 0.60 to 0.92), suggesting a desirable clustering result. A lower Silhouette value was found in P5 due to the large number of noisy events detected in this patient. The number of clusters, and the amount of HFO events in each cluster is given in table 3-2. Overall, the algorithm found smaller number of clusters in SB. This could be due to the low level of noise/artifacts in the data originating from the movements of patients as the patients are not active during sleep. As it is shown in figure 3-5, the HFO amount captured per data segment tended to be greater in SB compared to WB and PI, although the difference was not statistically significant ( $P_{SB-WB} = 0.09$ ,  $P_{SB-PI} = 0.14$ ). Figure 3-6 shows the feature distribution in two patients where 2 and 3 clusters were generated, respectively. For each cluster (sHFO/fHFO/artifact), typical waveforms and averaged time-frequency map of 20 random selected members are presented.

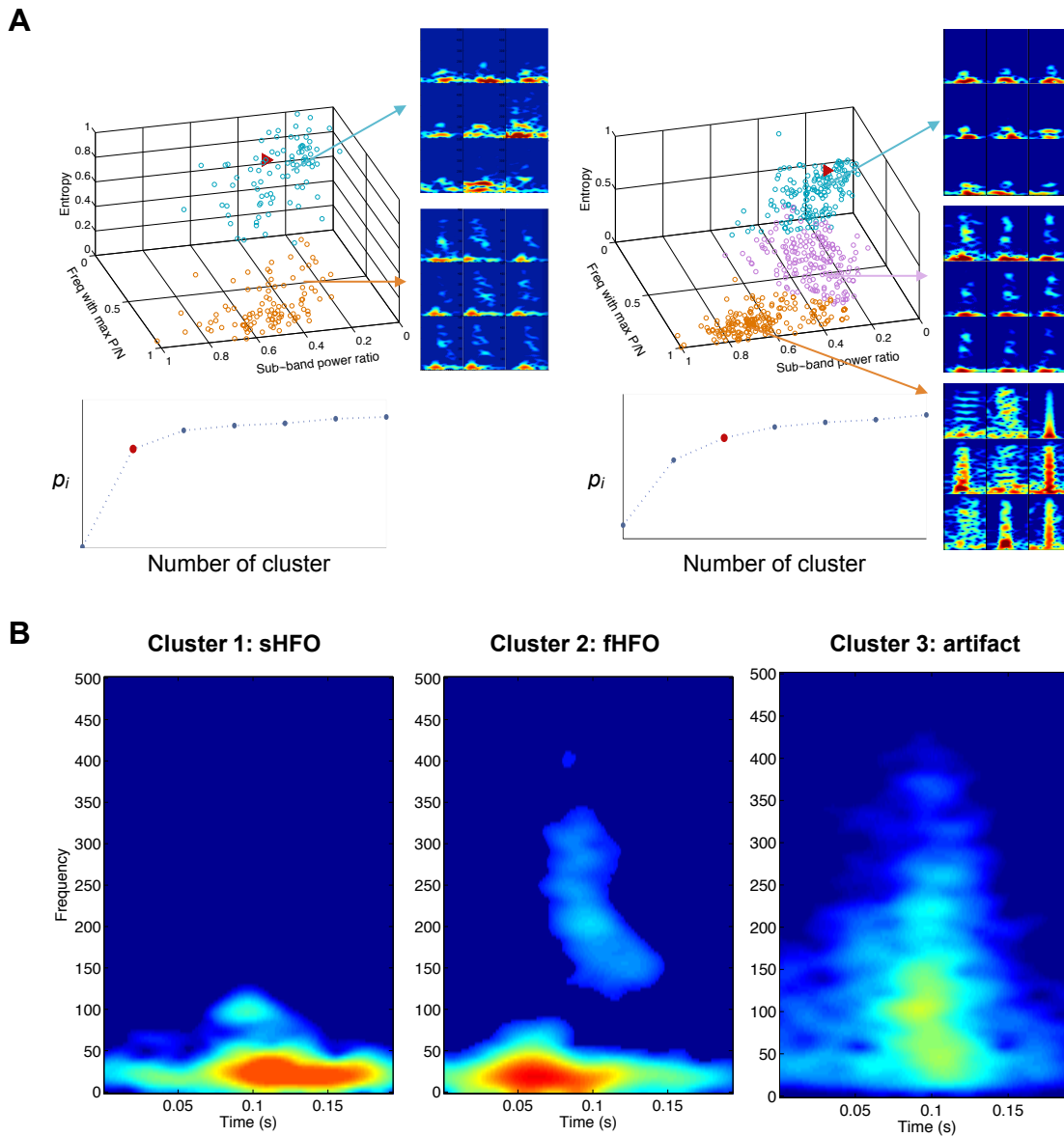


**Figure 3-6. (A) Feature distribution and the curvature of log-likelihood with respect to  $K$  values of GMM in 2 patients. (B) Time-frequency maps averaged from randomly selected 20 events in each cluster.**

### 3.4.2. Localization of the Seizure Onset Zone

In each state of each patient, clustered candidates were displayed and explored by using the HFO investigation tool. For those patients with one cluster composed of HFO,

that particular cluster was selected for the spatial distribution analysis; for those patients with two different HFO clusters, the one composed of faster oscillations was selected to explore its spatial distribution. Figure 3-7 (A) illustrates the spatial distribution of HFO among all bipolar channel pairs in each state of each patient. Each row in a single panel represents a different state (SB-WB-PI); the color strips display the HFO numbers located in each channel pair. The SOZ identified by neurologists are marked by red and yellow arrows (red arrows indicate the channels with highest seizure frequency). In all patients, HFOs were sparsely distributed and well localized in a few channels. In all patients except P3, the channels with maximum number of HFOs identified the SOZ. In P3, the HFO generative areas were found in the contralateral site of the presumed SOZ. The postsurgical outcome of P3 was poor. Although there was an improvement in seizure frequency of the patient, it was less than 80% of reduction. The patient continued to have monthly seizures after the surgery. We therefore excluded this patient from successive analysis.

Seven patients with Engel class I outcome were used to evaluate the SOZ detection performance. Overall, 11% of the total channels were delineated as SOZ (28/251). In each patient, 1 – 7 contacts were visually marked by neurologists and were used as the gold standard. During cross-validation, a denoising level of 97% was learned for testing in all except one patient in all states. In SB of P6, a denoising level of 90% was used. The algorithm resulted in sensitivities of 81%, 63%, and 74%, with specificities of 96%, 96%, and 94% in SB, WB and PI, respectively. We observed that none of the 14 corrupted channels was identified as the SOZ. In all states of P1, the seizure onset channels were

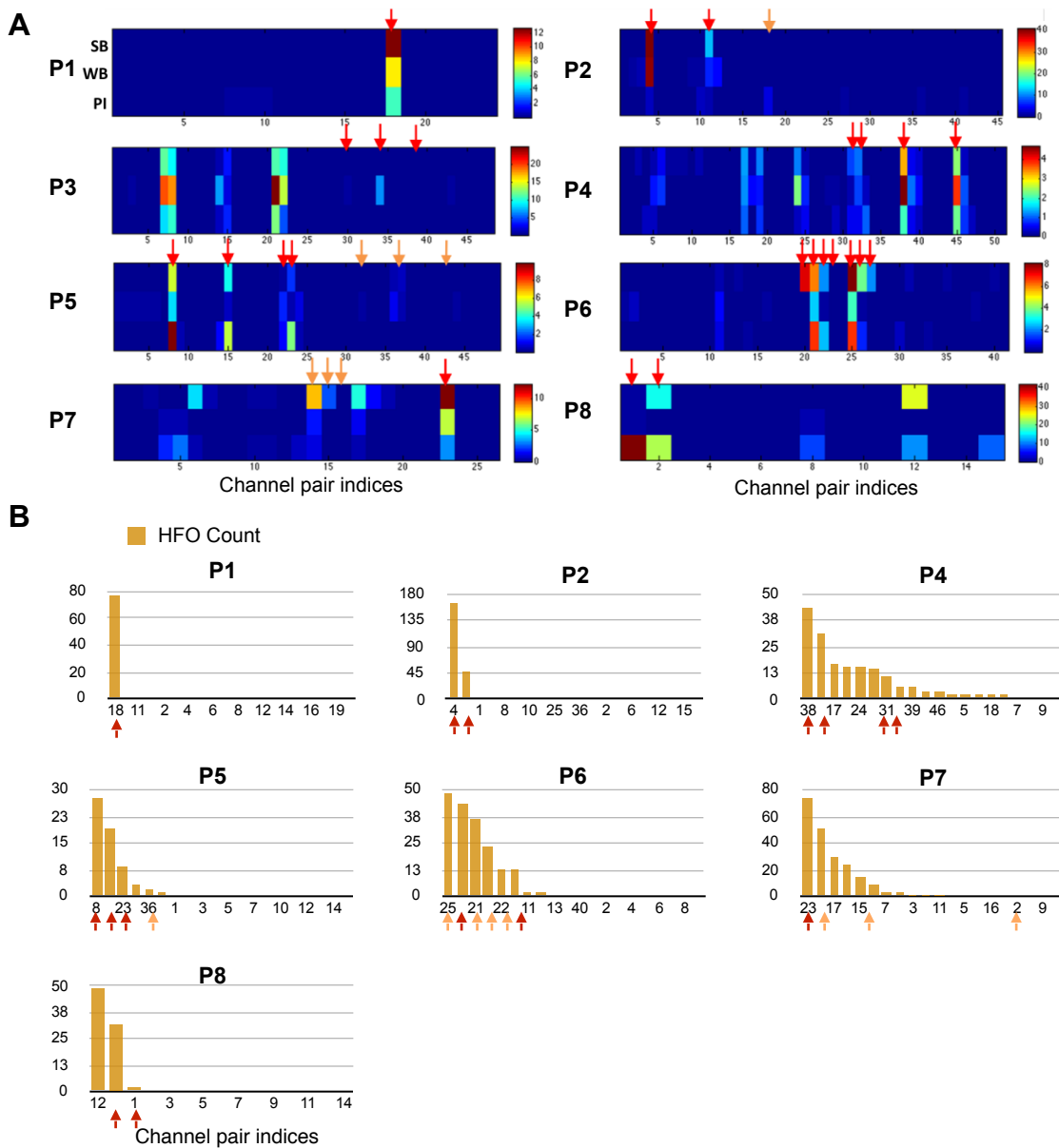


**Figure 3-7. (A) HFO spatial distribution in SB, WB and PI. (B) For each Engel class I patient, all channels are sorted according to their HFO numbers (up to 20 channels are shown).**

perfectly detected by the algorithm, leading sensitivity and specificity to 100%. In P5, where a larger number of channels were identified as SOZ, the majority of fHFOs were localized ipsilaterally in the left hemisphere, causing the lowest SE of 48% on the

average. Considering different states, the sensitivity result was significantly higher using data in SB comparing to WB ( $P < 0.001$ ), whereas no evidence showing a significant difference existing between SB and PI ( $P = 0.32$ ). The detection results are shown in table 3-3.

We ranked all channels according to their HFO densities, the result is presented in figure 3-7 (B). In 5 out of 7 patients, the channels that generated most of the HFOs correctly identified the locations where seizures occurred more frequently (marked by red arrows).

**Table 3-3. SOZ detection results**

ID	Channel No.	SOZ Channel No.	SB		WB		PI	
			SE	SP	SE	SP	SE	SP
P1	24	1	100%	100%	100%	100%	100%	100%
P2	45	3	66.7%	100%	66.7%	92.9%	100%	95.2%
P4	51	4	100%	93.6%	100%	95.8%	50%	95.7%
P5	49	7	42.9%	100%	42.9%	100%	57.1%	97.6%
P6	41	7	80%	97.2%	28.6%	97.1%	57.1%	100%
P7	26	4	75%	86.4%	50%	95.5%	50%	90.9%
P8	15	2	100%	92.3%	50%	92.3%	100%	76.9%
Average			<b>80.7%</b>	<b>95.7%</b>	62.6%	96.2%	73.5%	94.1%

### 3.4.3. Spatial Distribution of sHFO, fHFO, and Spikes

Compared to sHFOs, the vast majority (90%) of fHFOs were generated from only 7% of the total channels. In contrast, sHFOs were detected in 24% of the total channels,

including many of the neighboring regions of the SOZ, even the contralateral sites to the SOZ. Although the sHFO can be observed bilaterally, we noted that their occurrence was much higher in the ipsilateral side to the SOZ ( $P = 0.001$ ). The boxplot for sHFO distribution is shown in figure 3-8 (C).

We inspected the spatial characteristics of fHFO, sHFO and spikes using SB data segments in 5 patients where both sHFOs and fHFOs were successfully captured, the clustering results and samples of captured events are provided in figure 3-8 (A). Unlike HFOs, the spatial distribution of spikes appeared to be more wide-spread and inconsistent. In figure 3-8 (D) we show the boxplots demonstrating the distribution of three types of activities with respect to their relationships to SOZ, computed from all patients with Engel Class I outcome. Overall, 95% of the fHFOs captured by the algorithm were located inside of SOZ. On the contrast, 65% of the sHFO and only 38% of the spikes occurred inside of the SOZ. Most of the spikes were found extending well beyond the SOZ regions, spreading neighboring locations as well as contralateral sites of the seizure onset channels.

Using different types of events identified by the detector, we assessed the efficacy of fHFOs, sHFO and spikes as indicators to SOZ localization in all patients with favorable surgical outcomes. The average sensitivity and specificity across 4 patients were 70% and 100% for fHFOs, 81% and 82% for sHFOs, 92% and 76% for spikes, respectively.

#### **3.4.4. Comparing with existing techniques**

We compared our detector with an automatic SOZ detector established by Geertsema et al. (Geertsema et al., 2015), which is based on the evaluation of autoregressive model

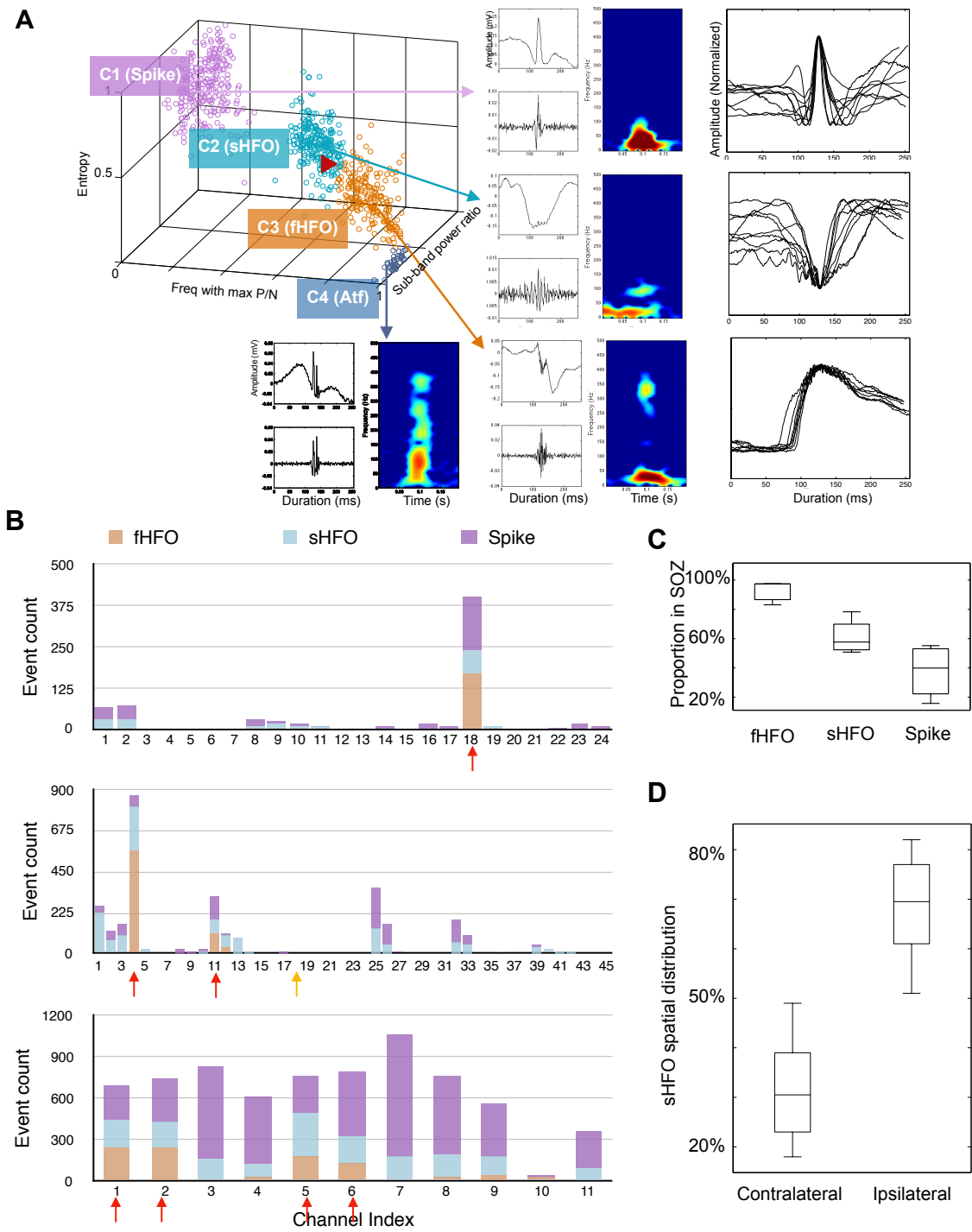


**Figure 3-8. (A) Feature distribution for spikes and HFOs in P3. (B) Spatial distribution for sHFO, fHFO and spikes in 3 patients. (C) Proportion of events inside the SOZ. (D) Spatial distribution for sHFO.**

residual variation (ARR). This recently proposed method estimates the time-variation of residuals from autoregressive models of iEEG windows computed from each channel, by obtaining the normalized standard deviation (CV, coefficient of variance) of the residuals. In order to reproduce the algorithm, we applied the same parameters as in the report, and computed the CV value for each channel in each 10-minute data segment. In each state, the receiver operating characteristic (ROC) curve was obtained by assessing the SE and SP for various thresholds from the training population. An optimal threshold was chosen when the ROC curve reached its elbow, and then was used to test the left-out patient.

The ARR detector obtained SE of 60%, 60%, 40% with SP of 70%, 69% and 80% in SB, WB, and PI, respectively. Comparing to ARR detector, the overall performance of our detector was significantly higher in terms of both sensitivity ( $P = 0.02$ ) and specificity ( $P < 0.001$ ).

### **3.5 Discussion**

#### **3.5.1. Main Contributions**

In this study, we showed that localizing SOZ using HFOs identified in 10-minute of SB data provided significantly higher overall sensitivity compared to WB in both centers. Using 10-minute baselines and pre-ictal data, the algorithm successfully detected HFOs, and localized the seizure onset areas in 7 out of 8 patients, where the HFO spatial distribution was closely overlapped with the electrodes that were placed over the regions where the seizures were thought to originate, suggesting the good prognostic value of HFOs captured by automatic technique.

HFO detection techniques have been widely discussed over recent 10 years. Conventional methods use high-pass or band-pass filtering to expose those high frequency transients of interest, followed by amplitude thresholding in time domain. However, some components in brain signal may present a broadband characteristic, and could be confounded with actual oscillatory activities after filtering. Nevertheless, traditional HFO detection has been suffering from false positives introduced by epileptic spikes or non-sinusoidal oscillatory events that contain harmonics. The pitfalls related to straight forward filtering of iEEG were recently addressed in two reports (Bénar et al., 2010; Mina Amiri et al., 2016) which once again emphasized the need for new algorithms for the accurate detection of HFOs. Our proposed algorithm refined the detection by introducing additional HFO criteria considering its morphometric features. Without channel pre-selection, the algorithm was able to keep out the non-neuronal events resulting from the contaminated channels, as none of these visually identified corrupted channels was classified as SOZ. Moreover, we assume that one of the critical aspects of HFO identification in human examination is the existence of well-isolated high frequency component that could be distinguished from other oscillatory events after time-frequency analysis. We introduced a denoising step to pinpoint the frequency in correspondence with this prominent power increase in the high-frequency range after proper compression of the background noise. In this way we were able to eliminate spikes without HFO components from subsequent steps. By clustering, we further purified the detected HFO candidates and provided evidence of the existence of diverse HFO patterns, which is

usually pre-assumed in the forms of ripples (80 – 200 Hz) and fast ripples (200 – 500 Hz) in many of the previous studies.

We analyzed human iEEG data recorded in real clinical cases, which is essentially different from most of the previous reports where experimental data with better signal fidelity is commonly used. We were able to reliably identify SOZ using clustered HFOs, supporting the assumption that HFOs are good indicators for the epileptogenic zone. When the spatial distribution of the entire HFO group was used, we observed a SOZ identification accuracy with 81% sensitivity in SB, and 96% specificity in both SB and WB. Moreover, we tuned the algorithm by using different proportion of detected HFOs to determine HFO generative channels. When the spatial distribution of HFOs was shrunk to those channels capturing 55% of the total number of HFOs, the algorithm obtained an overall specificity of 99% in SB, 98% in WB, and 100% in PI state. In 5 out of the 7 Engel class I patients, the detector achieved specificity of 100%. In this case, fewer locations were involved and classified as seizure generating areas, resulting in lower sensitivity of 42%, 44%, and 49%. This trade-off between the measures need to be further studied to meet the actual clinical demands.

### **3.5.2. Identifying SOZ in Different States**

We showed that localizing SOZ using HFOs identified in 10-minute of SB data provided significantly higher overall sensitivity compared to WB in both centers. The relationship between sleep-wake cycle and epileptiform discharges has been reported in literature. Investigation of HFOs using both short-term and long-term iEEG data shows an increment of HFO rate with non-rapid eye movement (NREM) sleep stage, especially

in subjects with epilepsy generating from temporal lobe (Crépon et al., 2010; Dümpelmann, Jacobs and Schulze-Bonhage, 2015; Jacobs et al., 2008a; Schevon et al., 2009b). Sleep activates both focal and generalized spikes and other epileptic discharges in about 1/3 of all patients due to the increased temporal and spatial synchronization caused by the hyperpolarization of cortical and thalamocortical neurons (Kotagal and Yardi, 2008). A latest report suggests that sleep slow waves, particularly the upward trend, are the specific components of NREM sleep that is responsible for the mediation of activating the epileptic activity, which may further explain the rise in occurrence of the epileptic oscillatory events (Frauscher et al., 2015). Our result suggests that obtaining sleep recordings of a sufficient interval in clinical routine should be beneficial to quantitative HFO analysis and SOZ localization.

### **3.5.3. The Prognostic Value of HFOs**

Using 10-minute baselines and pre-ictal data, the algorithm successfully detected HFOs, and localized the seizure onset areas in 7 out of 8 patients, where the HFO spatial distribution was closely overlapped with the electrodes that were placed over the regions where the seizures were thought to originate, suggesting the good prognostic value of HFOs captured by automatic technique.

In this study, we did not presuppose the existence of different HFO sub-categories. Nevertheless, in 4 out of 5 patients with 2 kHz sampling rate recordings, two distinct HFO groups with oscillation in different frequency bands were discovered by the algorithm, which was consistent with prior studies that differentiate between “ripple” and “fast ripple”. In our study, these two HFO classes were interpreted as sHFO (around 80 –

100 Hz) and fHFO (above 200 Hz) since their frequency range didn't strictly fit the definition of the terms ripple (80 – 200 Hz) and FR (200 – 500 Hz). We noticed that these two HFO groups presented some dissimilarity in waveform pattern and spatial distribution. Compared to fHFOs, sHFO distribution appeared to be more wide spread. Nevertheless, most of the sHFOs were originated from the seizure onset sites. This result shows disagreement with a previous study reporting greater number of ripple oscillations being found in sites contralateral to seizure onset (Staba et al., 2002).

There has been an assumption that ripples, which have been well described in hippocampus and associated structures in normal animal brains, reflect physiological brain activities, whereas FRs reflect pathological hypersynchronous events that are crucially associated with seizure genesis (2002). However, the considerable overlap in spectral frequency between normal and epileptogenic oscillations makes the definition of physiological and pathological HFOs still controversial (Engel et al., 2009). Apparently, it is inappropriate to group normal and epileptic HFOs on the basis of their frequency bands alone. FR activities can be physiological, as they have been reported in normal brain functioning as a reflection of neuronal network coordination related to attention, learning and memory (Kucewicz et al., 2014). Besides, not all pathological HFOs are FRs (Menendez de la Prida, Staba and Dian, 2015). Though the diagnostic value of HFOs below 200 Hz remained in doubt, we argue that it is not necessary to conclude that ripples are not associated with epilepsy, since our results have proved that sHFO generating locations still gave considerable clues to epileptogenic regions. The investigation of

different HFO patterns should attribute to a better understanding of epilepsy, and should be taken into consideration during presurgical evaluation.

HFOs and spikes are both considered reflections of dysfunctional neural networks. Clinical and experimental evidences supported that HFOs are better markers than interictal spikes to identify seizure onset zones (Zijlmans et al., 2012; Jacobset et al., 2008). To explore the relationship among spikes and two sub-categories of HFOs discovered by the algorithm, we also assessed the value of these neuronal events in SOZ approximation. Our results suggested that the majority of HFOs appeared in a subset of spike generating channels. In two patients with generalized tonic-clonic seizures (P3 and P4), the channels with most of the FRs differed from the most spiking locations, which may provide critical information for disease propagation.

Although in other seizure free patients the HFO generating areas were always consistent with SOZ, interestingly, in P8 we detected HFOs from bilateral hippocampus. This particular patient showed poor scalp EEG findings in terms of “switch of lateralization” (Sirin et al., 2013), where the seizure generated from right hippocampus, and propagated to the contralateral site immediately after onset. A series of studies illustrate that the removal of HFO generative regions outside the SOZ is also correlated with good surgical outcomes, and therefore can be used as a guide to surgical resection (Akiyama et al., 2005; Jacobs et al., 2010; Ochi et al., 2007; Wu et al., 2010). This is the first report regarding the prognosis value of HFO in an epilepsy patient with hippocampal sclerosis and “switch of lateralization” phenomenon. Whether the HFO generative region

in such patients provides additional information regarding epilepsy needs to be further investigated with a larger population.

In the only patient (P3) where the HFOs showed inconsistency with the presumed SOZ, the patient had bilateral temporal slowing and bilateral frequent independent epileptiform activities during the invasive intracranial recording. P3 had a total of 6 habitual target seizures that were reported by the patient and family during the intracranial EEG monitoring. All these 6 seizures were found to be right temporal onset. However, there were also 3 subclinical seizures recorded during the intracranial monitoring. All these 3 subclinical seizures were left temporal onset, originating from the HFO generating locations (channels 7, 8, 14, 21, and 22). Right temporal lobectomy was proposed as a palliative procedure to reduce the seizure burden and to improve the quality of life, which the patient elected to proceed with. However, P3 continued to have clinical seizures after surgical resection. P3 did not go through a second surgery to remove HFO regions, which made it difficult to validate the relationship between HFO and seizure-free outcome. HFO generative areas outside the SOZ may provide additional information, which is of substantial importance in presurgical evaluation, and should prompt further clinical investigation.

#### **3.5.4. Towards the Clinical Application**

The results of the current study indicate that the integration of time-frequency analysis of iEEG and unsupervised clustering is capable of identifying HFOs in an efficient manner, and can be employed for automatic SOZ localization. Although it is comparable to previous HFO detection reports, our proposed HFO detection technique

was tested on a small number of patients. Among the involved 8 patients, 7 had temporal lobe epilepsy (3 with hippocampal sclerosis, 4 without structural abnormalities), 1 had occipital lobe epilepsy without lesion. Due to the limited sample size and disease phenotypes, it remains unclear whether the algorithm is applicable to different types of epilepsy other than mesial temporal lobe onset, or does it have superior performance when applied to a specific patient population. It remains an open question whether or not this technique can be used as a practical tool to assist in SOZ delineation especially in neocortical onset epilepsy, where larger cerebral cortex including functional regions and eloquent areas might be involved during the intracranial EEG monitoring. In order to answer this question, in the next chapter we reported 3 cases where the unsupervised detection was applied to adult and pediatric patients with lesional and non-lesional neocortical epilepsy. It is expected that the proposed HFO detection algorithm can be applied to provide critical information regarding the SOZ in challenging cases.

A limitation of the current study is that the analysis was based on 10 minutes of iEEG data in different states. Although past research suggested the use of 10-minute of data should be sufficient for HFO analysis, we argue that data of longer intervals should be involved in future work to test the robustness of the detector and its generalization capability. This question is specifically clarified in Chapter 6 where the HFO detection was executed using iEEG data segments of extended-length in order to show the temporal variation of event rates and its possible effect on the SOZ localization.

## **CHAPTER 4 HFO AUTO-DETECTION FOR THE LOCALIZATION OF SEIZURE ONSET ZONE: CASE STUDIES**

### **4.1 Introduction**

High frequency oscillations (HFOs) are believed to be clinically significant, and thus could be used for SOZ localization (Worrell and Gotman, 2011). A series of studies have shown that the complete removal of HFO generative cerebral tissue within and outside the SOZ provides favorable surgical outcomes in patients with drug-resistant epilepsy, suggesting HFOs can be excellent surrogate markers of SOZ, and emphasized their potential to guide the pre-operative evaluation for epilepsy surgery. Human identification of HFO has been hindered by the massive data size and the short duration (in milliseconds scale) and low amplitude of the HFO transients due to the  $1/f$  nature of iEEG signals. To date, most studies on HFOs in epilepsy to large extent rely on highly human-intensive process to extract the signals of interest from multichannel iEEG. Due to difficulties associated with visual inspection and manual annotation of data over multiple channels and recordings lasting for several days or weeks, investigators typically perform dramatic data reduction steps before committing the data to statistical analysis. Such data reduction techniques and complexity associated with visual inspection, limiting the functional usage of HFO information in clinical routine.

Compared to epilepsy literature, the fields of HFOs and the related detection techniques are in their infancy states. Majority of the current existing automatic or semi-automatic HFO identification techniques focus on the supervised classification of event candidates, based on human screening and labeling the events of interest, after prior

selection of artifact-free iEEG traces (Blanco et al., 2010a). Manually identified HFO events by multiple experienced reviewers are commonly used as the target variables and detectors were forced to classify these events in pre-defined ripple and fast ripple ranges as well as other subtypes, for instance, physiologic or pathologic HFOs. Such visual identification of HFO events by medical experts reviewing hundreds of hours of data puts considerable bias to the class labels. More importantly, few reports have capitalized on the prognostic role of HFO captured by automatic detection in the localization of SOZ. No studies have explored the entire iEEG spectrum, and the functional use of HFO auto-detection in clinical practice is poorly documented. In order to fill this gap, in this chapter the HFOs identified by the proposed three-stage automatized technique were utilized as spatial markers to the epileptic seizure onset regions in the brain. The relationship among spikes and presumed discrete sub-groups of HFOs discovered by the algorithm were explored, and the spatial distribution of HFOs were compared with the clinician delineated SOZ in these representative unique cases, to assess the value of these neuronal events in SOZ approximation using data collected in real clinical environment.

#### **4.2 Data Acquisition and Analysis**

Data collection protocol is demonstrated in figure 4-1. Continuous iEEG data was recorded intra-operatively during the electrode implantation and/or post-operatively in the epilepsy monitoring unit (EMU) for 48 hours using both gHIamp system (g.tec medical engineering GmbH, Graz Austria) and Nicolet C64 system (Natus Medical Inc, CA) through a parallel recording setup, simultaneously with video monitoring thought the period. For the HFO analysis, continuous data recorded by gHIamp bioamplifier at 2.4

kHz sampling frequency and 24 bit A/D resolution was used, with an anti-aliasing filter set to 600 Hz. The signal acquisition and real-time visualization was executed with a customized Simulink model (Matlab R2014a, Mathworks, Inc) and gHIsys real-time signal processing library (g.tec medical engineering GmbH, Graz Austria).

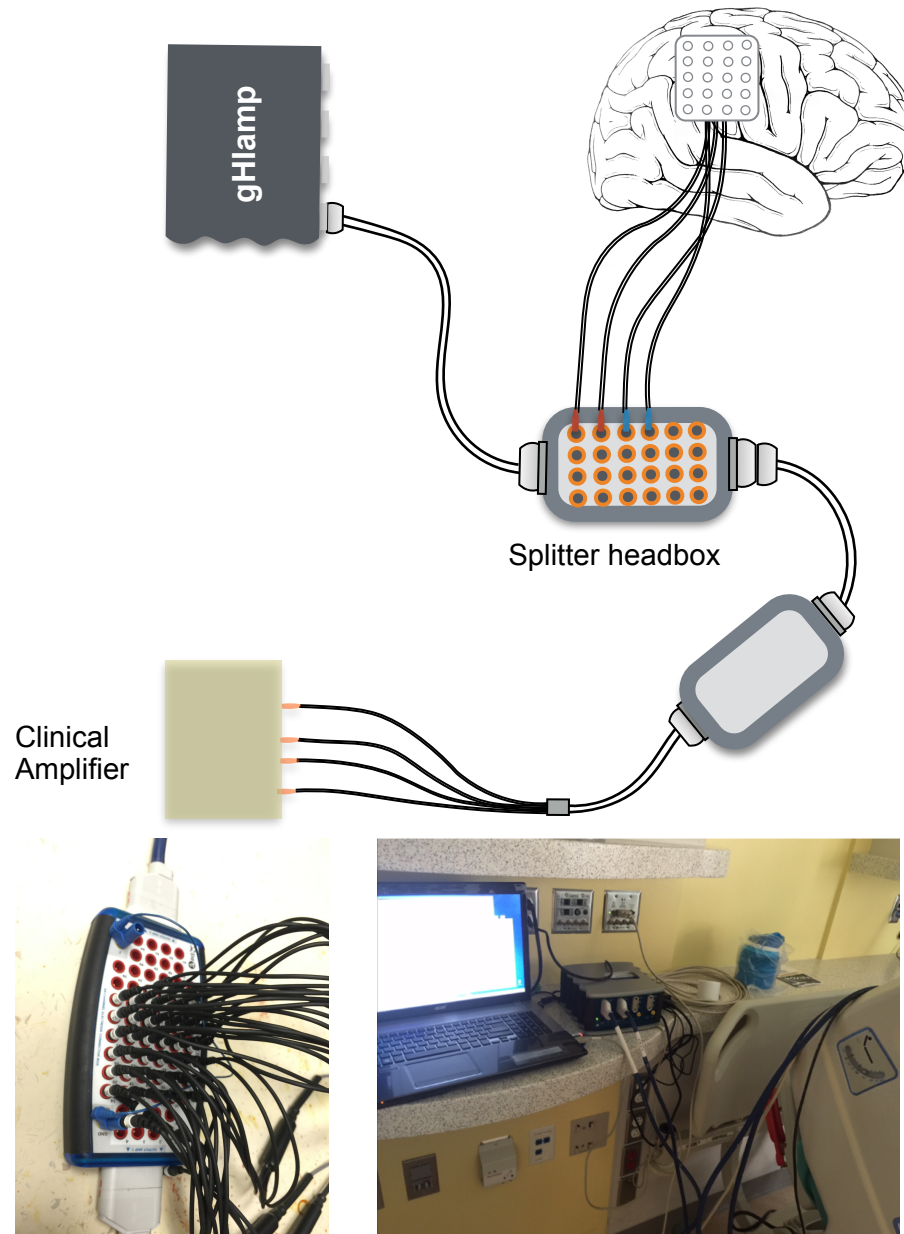


**Figure 4-1. Scheme and photos showing the data collection setup.**

The previously validated HFO detector (see Chapter 3) was used to analyze the multichannel SEEG or ECoG data (Liu et al. 2016), the workflow is given in figure 4-2. Briefly, raw data first went through band-pass filtering within the 80 to 500 Hz range and a series of HFO-sieving criteria. Next, we performed the short-time Fourier transform (STFT) and executed a denoising step on the time-frequency maps to eliminate background activity with small amplitude. Finally, we explored the entire bandwidth of surviving candidates to extract the three features: high-band to low-band power ratio, entropy, and frequency corresponding to maximum peak to notch ratio. These features were used for GMM clustering to map candidate events into different categories.

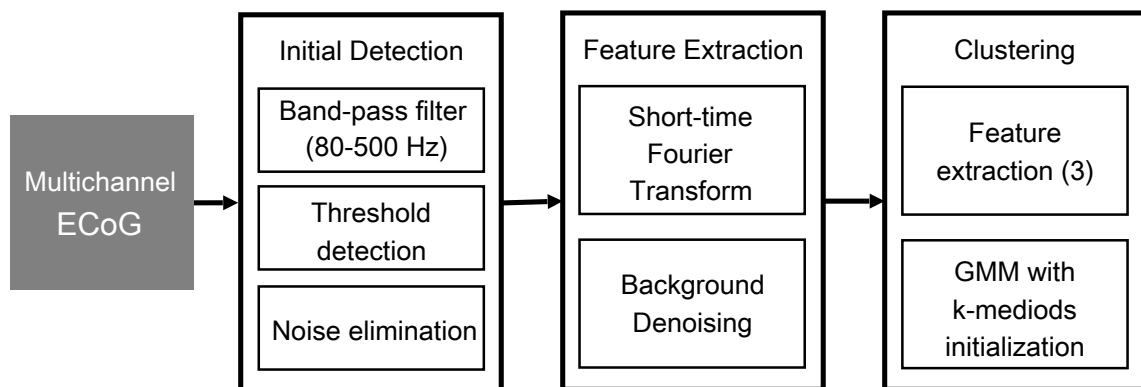


**Figure 4-2. Schematic diagram of the three-stage automatic HFO detection method.**

The grid/depth electrodes and distribution maps can be visualized by using a self-developed software application dedicated to the interactive co-registration of brain surface model or MRI volume, customized electrode model, and CT images. After loading the reconstructed MRI data of a brain template or an individual subject, one or multiple ECoG electrodes will be added by using one of the following modalities: i) each

electrode contact will be manually co-registered with the cortex model/3D rendering by referring to the surgical photographs that show the sulcal and gyral landmarks on individual anatomy, or ii) electrode models will be generated after automatic coregistration of preoperative MRI and postoperative CT that shows the electrode location in the 3D space. To accomplish this, a Matlab-based tool is developed to get the inputs from the user where two point-sets are defined by manually locating the anatomical landmarks (nasion, inion, earlobes, etc.) on both MRI and CT images. A widely applied Iterative closest point (ICP) algorithm (Besl et al., 1992) is then executed

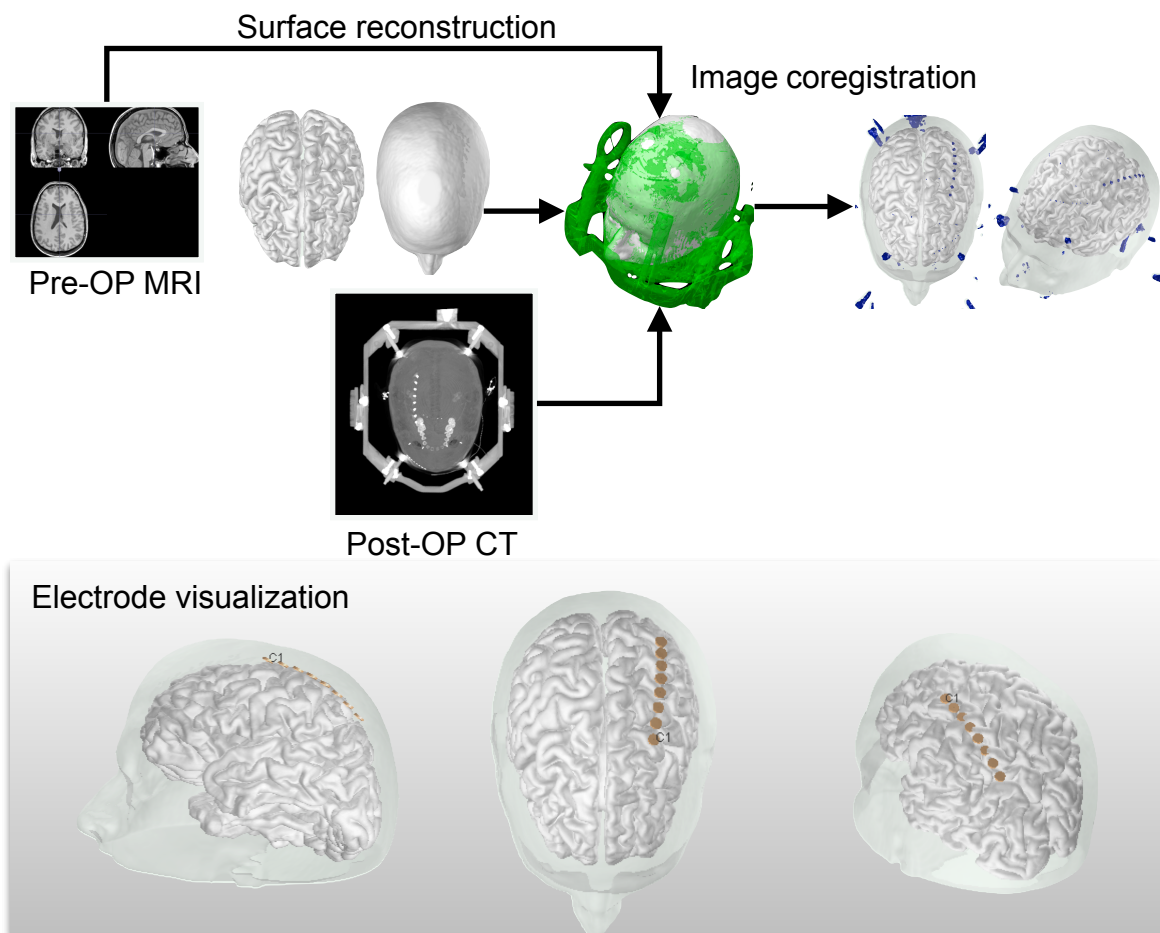


**Figure 4-3. Workflow for the coregistration of pre-op MRI and post-op CT images. A customized software is developed for the visualization of electrodes.**

to minimize the difference between two clouds of points, and to match the source image with the reference or target image. Alternatively, the electrode models can be directly generated after acquiring the contact positions defined by Talairach or Montreal Neurological Institute (MNI) coordinates. The analysis results showing the HFO spatial distribution will be mapped to the brain and visualized instantly by the software.

#### **4.3 Case 1: HFOs in Epilepsy Associated with Cavernous Malformation**

Cavernous malformations (CM) are dynamic vascular lesions in the central nervous system (Rigamonti et al., 1988). When cortical tissues are involved, CMs pose a significant risk for the development of medically refractory epilepsy that requires surgical treatment (Alonso-Vanegas, Cisneros-Franco and Otsuki, 2012; Cosgrove 1999). Invasive electrocorticography (ECoG) monitoring has been used as the gold standard for the localization of SOZ (Shah and Mittal, 2014) and has frequently been applied during the presurgical evaluation in patients with epilepsy associated with CM. By investigating the intracranial electroencephalogram (EEG) recordings, neurologists try to define the accurate location of seizure onset in relation to the CM, determine pathways of seizure propagation, and perform intraoperative mapping of cortical function before the excision, especially in pediatric cases (Bourgeois, Di Rocco and Sainte-Rose, 2006; von der Brölie, Kuczaty and von Lehe, 2014). Studies have shown that lesionectomy plus ECoG yields better seizure control outcomes; one cohort demonstrated a significant advantage with lesionectomy assisted by intracranial ECoG delineation of the SOZ (Baumann et al., 2007; Jooma et al., 1995). To this point, HFOs have not been described in pediatric patients with CM-caused epilepsy.

#### 4.3.1. Case Presentation

The 3-year-old left-handed male patient was referred to Texas Children's Hospital with focal epilepsy initially presenting as recurrent spells of loss of awareness starting at 2.5 years of age. The seizures were stereotyped and clinically consisted of eyes slowly closing and the patient swaying back and forth in association with unresponsiveness lasting 2 – 6 s. The seizures occurred in clusters of 20 – 30 events, with the clusters occurring up to 3 – 4 times per day.

Continuous ECoG data were acquired from an  $8 \times 8$  grid. Data collection and scientific workup were approved by the Baylor College of Medicine Institutional Review Board. The ECoG was recorded for 62 hours and 39 minutes. ECoG data were visually inspected for the characterization of the background activity, abnormal focal and generalized features, as well as interictal and ictal epileptiform activity. Electrical seizure activity was correlated with the clinical events of the patient recorded on video. The patient was given trials of levetiracetam, oxcarbazepine, zonisamide, and clobazam without resolution of seizures. Seizure medications have not been adjusted up to this point.

Initial scalp EEGs showed spikes that were maximal in the left frontal region (F3). They were often seen focally restricted to this region but other times were seen quickly propagating to the left mid-to-posterior temporal region (T7/P7). Brain MRI revealed a  $1.7 \text{ cm} \times 1.5 \text{ cm} \times 1.5 \text{ cm}$  lesion in the left frontal operculum as shown in figure 4-1 (A). The lesion had a heterogeneous “popcorn” appearance on T2-weighted images, with a rim of hypointensity and mild surrounding edema, consistent with a CM. Positron

emission tomography (PET) CT showed a corresponding focal area of hypometabolism, suggestive of a seizure focus, as shown in figure 4-4 (C). Figure 4-4 (D) presents the magnetic source imaging showing frequent spikes localizing to the left frontal cavernoma and posterior perisylvian region. Upon presenting the patient's case to the epilepsy surgery conference, the consensus was to implant intracranial EEG to define surgical resection borders. The sketch of the electrode and the 3-D rendering of MRI coregistered with CT image are given in figure 4-4 (E) and (F), where the CM is shown in white color.

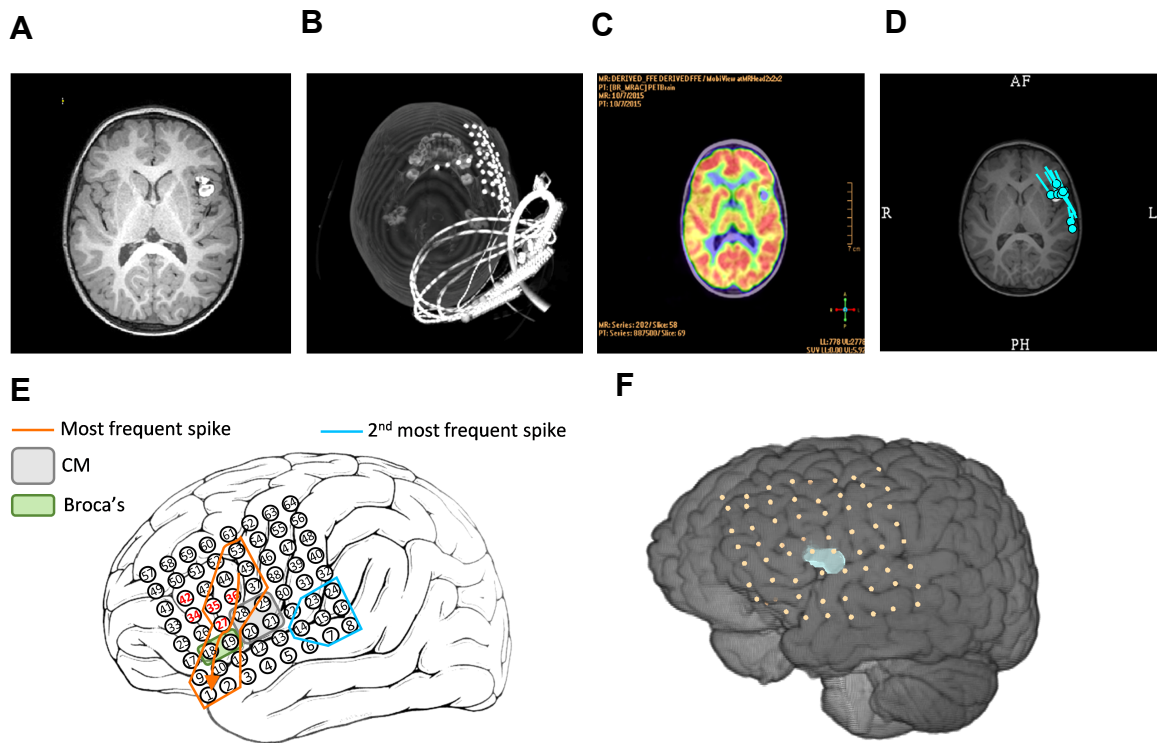


**Figure 4-4.** (A) Structural MRI (B) Postoperative CT image. (C) PET image showing hypometabolism. (D) Magnetic source imaging. (E) A schematic of grid channel orders. (F) Three-dimensional rendering of the individual brain with electrode model.

### 4.3.2. Results

Frequent epileptiform discharges were seen over much of the subdural grids. As it is shown in figure 4-4 (E), the most frequent spike population was seen at contacts 37 – 45 – 53, propagating inferiorly and anteriorly to contacts 28 – 36 – 44, 19 – 27 – 35, 2 – 10 – 18, and 1 – 9. The second-most frequent spike population was seen at contacts 14 – 16, 23, 24, 32, 40, covering the posterior/inferior part of the grid. Visual identification of the ictal onset zone suggested the anterior/superior perilesional cortex with some more distant sites being involved in seizure initialization. More than 70 of the habitual seizures



**Figure 4-5. Twenty seconds of ECoG recording in bipolar montage, with seizure onset represented by the red vertical line. Thirty-two channel pairs are shown.**

were captured, with > 90% of the seizures appearing to arise from contacts 27, 34 – 36, and 42. When seen, the ictal pattern consisted of a dramatic buildup of spikes at the onset of the clinical seizures. The remainder of the clinical seizures had indeterminate EEG onset. A 20-second segment of raw ECoG data in bipolar montage showing the ictal onset is given in figure 4-5.

A total of 150 min of ECoG data were extracted for HFO analysis (30 min immediately at the beginning of monitoring in the epilepsy monitoring unit (EMU), and then separately for 30 min during slow-wave sleep and awake states in each day over 2 days which were at least 4 h away from seizure activity). As a result, a total of 23,810 HFO events and 12,365 spikes were detected by the algorithm. For each segment, the

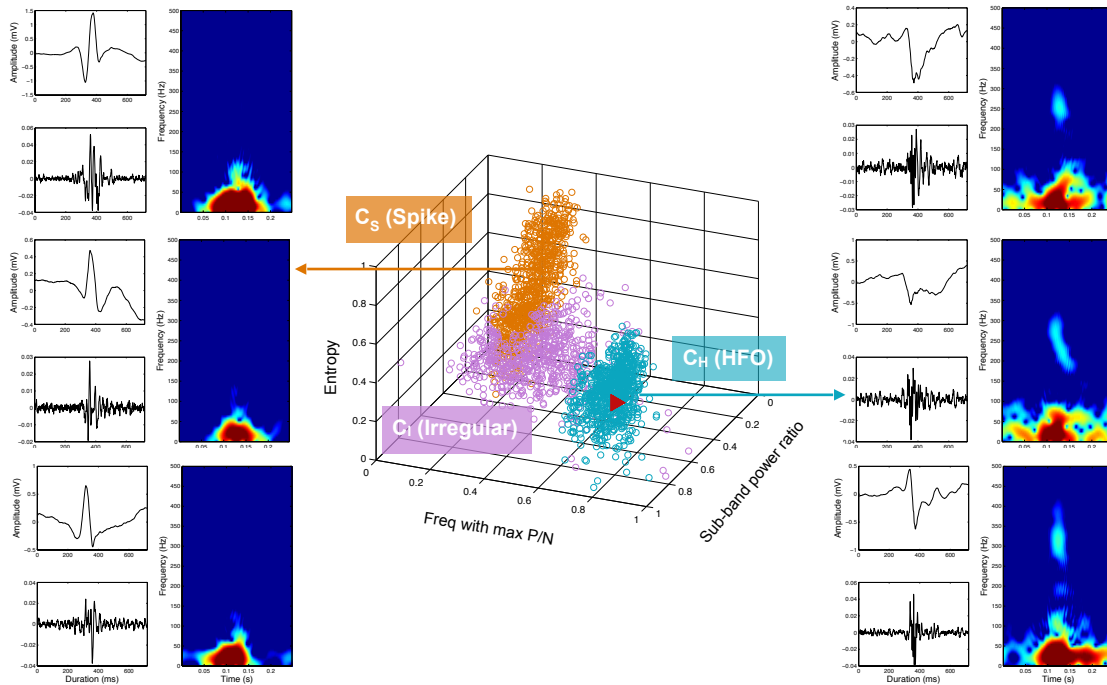


**Figure 4-6. Feature distribution of the three clusters calculated from the first 10 min of recording.  $C_H$ : HFOs,  $C_S$ : spikes,  $C_I$ : irregular waveforms. For  $C_H$  and  $C_S$ , three random sample events are shown.**

detected events were identified as three subgroups, as shown in figure 4-6. In general, one cluster ( $C_H$ ) was a mixture of ripple and FR, one cluster ( $C_S$ ) was composed of spikes, the rest ( $C_I$ ) was a group of irregular waveforms with noisy background. CH and CS were hereby used for the spatial analysis.

Consistently in all segments, the spatial maps indicated that most of the HFOs were generated from channels 28 – 29 located above the superior border of the cavernoma. Moreover, channels 35 – 36 and 37 – 38, representing the area superior to the lesion, were also involved as HFO-generating sites but with less consistency. Some less active locations responsive to HFO generation were found in channels 31 – 32, 39 – 40, and 41 – 42, covering the perilesional area and the posterior and anterior/superior parts of the electrode, especially in waking states (figure 4-7).

The HFO mapping results estimated from 30-min ECoG segments consistently highlighted the perilesional region, regardless of the day of recording. In particular, the HFO distribution was more compact and robust over days in sleep state, concentrating on channels 28 – 29 sitting immediately above the border of the CM. Remarkably, the HFO spatial map obtained from ECoG data of a short period recorded right after the electrode placement had also correlated with the CM and perilesional location. On the contrary, spikes were initially found in channels 17 – 18 – 19, covering Broca's area, along with channels 28 – 29 and 34 – 37, representing the CM and its anterior/superior region. During the monitoring period, spike channels shifted anteriorly and inferiorly surrounding the CM. The distribution also changed through the sleep-wake cycle, as shown in figure 4-7 (A) and (B).

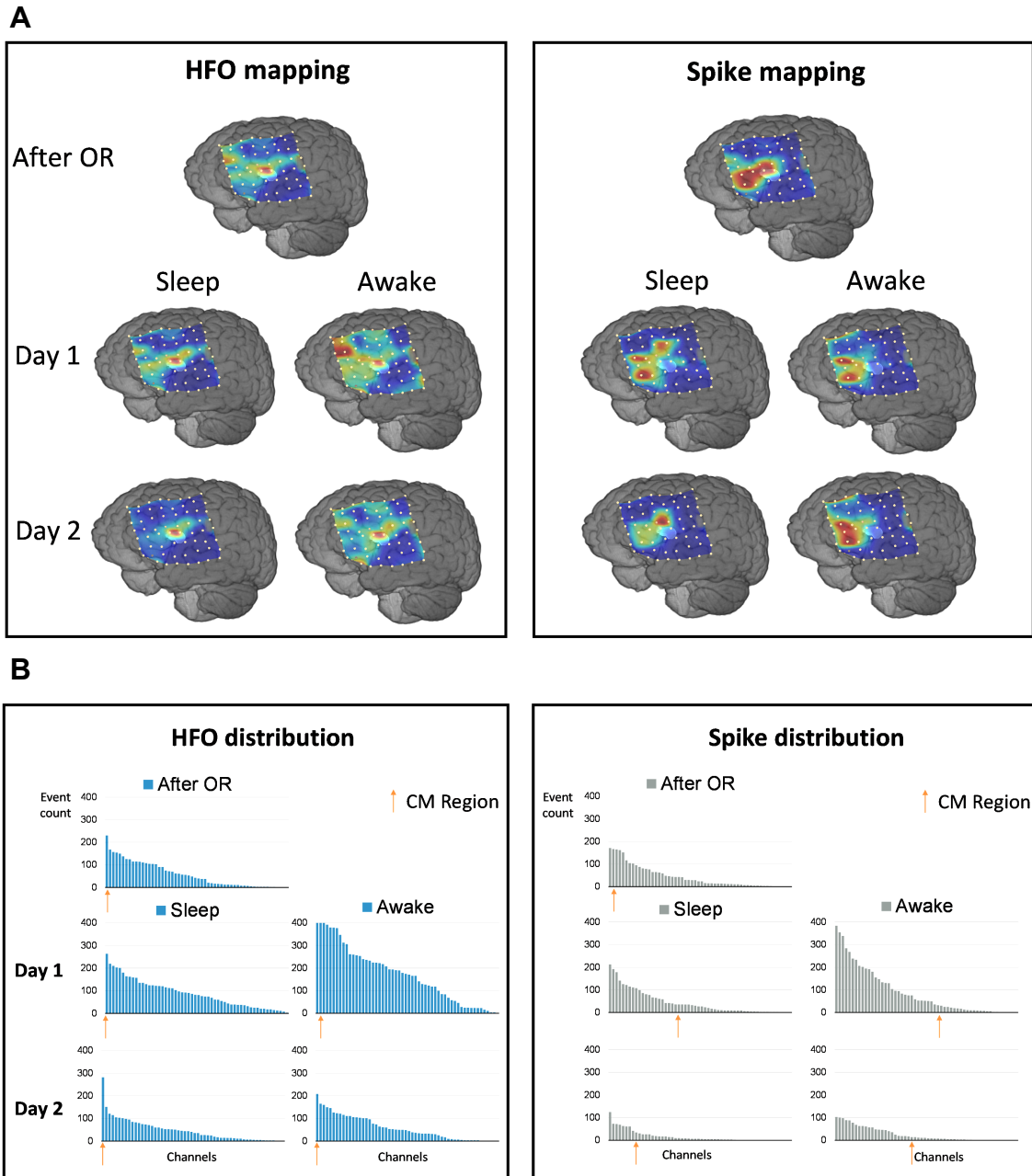


**Figure 4-7 (A) 3D rendering of the MRI with spatial distribution maps, with red representing the locations with most of the captured events. (B) Spatial distribution of HFOs and spikes in bar plot.**

Cavernous malformation does not contain neural parenchyma, thus the perilesional cortex, not the lesion itself, is always implicated in ictogenesis. The preictal spiking

patterns of ECoG data indicated a perilesional cortex anterior and superior to the CM as the SOZ. Taking into account the proximity of the nearly eloquent language regions, the neurologists decided to perform a cautious and conservative resection of the CM and adjacent hemosiderin-affected cortex only with plans to reevaluate for further resection if the seizures remained unaffected. Considering the associated risk, postsection intraoperative ECoG was not performed in this patient. As of today (February 2017), the patient remains seizure free with follow-up of 1 year.

#### **4.4 Case 2: HFOs in Extra-Temporal Lobe Epilepsy**

Ripples below 200 Hz have been historically linked to physiological events which plays an important role in memory consolidation (Girardeau and Zugaro, 2011; Kucewicz et al., 2014), however the discrimination between pathological or physiological HFOs cannot rely on the frequency distinctions alone. Studies have shown evidence that FR above 200 – 250 Hz can be absent in some cases, particularly in patients with neocortical epilepsy. Recent studies investigated different HFO patterns by visual inspection, where the investigators generally looked into features related to amplitude, duration, frequency and phase-coupling phenomenon (Matsumoto et al., 2013; Nonoda et al., 2016). Nevertheless, it is still challenging to reliably separate functional and pathological oscillations when recorded using macro-electrodes in clinical environment, particularly in the ripple range (Zijlmans et al., 2012). In this section a case where interictal ripples in 80 – 200 Hz range were automatically captured and identified as two sub-groups were presented. The detected HFOs were spatially correlated with seizure onset regions identified by neurologists, as well as the functional sites indicated by anatomical

landmarks or direct cortical stimulation. In addition, we investigated the classic features that had been used in literature, including mean frequency, amplitude, and duration of the oscillations. The group difference between clusters was quantified by performing two-sample student *t-test*.

#### **4.4.1. Case Presentation**

The 36 year-old female patient was referred to Capa Hospital of Istanbul University (Istanbul, Turkey) for drug resistant focal epilepsy with an aura of white vision and forced deviation to the left. There was no personal history of any neurological disorder. Neuropsychological evaluation showed non-pathological attention impairment. The patient had been treated with Carbamazepine (800 mg/day) and Levetiracetam (2000 mg/day) without resolution of seizures. Anatomical MRI showed normal result; PET scan showed hypometabolism on the right mesial temporal region.

The patient underwent electrode implantation after presurgical workup. Four surface/depth electrodes were placed to the possible irritative sites, including one  $6 \times 8$  grid to the right temporal-parietal region, one  $2 \times 8$  grid on the right temporal lobe, one 4-contact depth in the anterior insula, and one 6-contact depth in the posterior insula.

#### **4.4.2. Results**

Twenty-seconds of iEEG data showing a seizure onset is given in figure 4-8 (A). Most of the seizures (> 60%) arose from the parietal region covered by contacts 33 – 37 on the large grid, extending to all contacts on both grids. In figure 4-8 (B) we marked the SOZ contacts with different colors in accordance with their seizure frequency; contacts

with functional response are shown in the blue circle. The 3D reconstruction was obtained by co-registering the post-operative CT image with the patient's individual MRI.

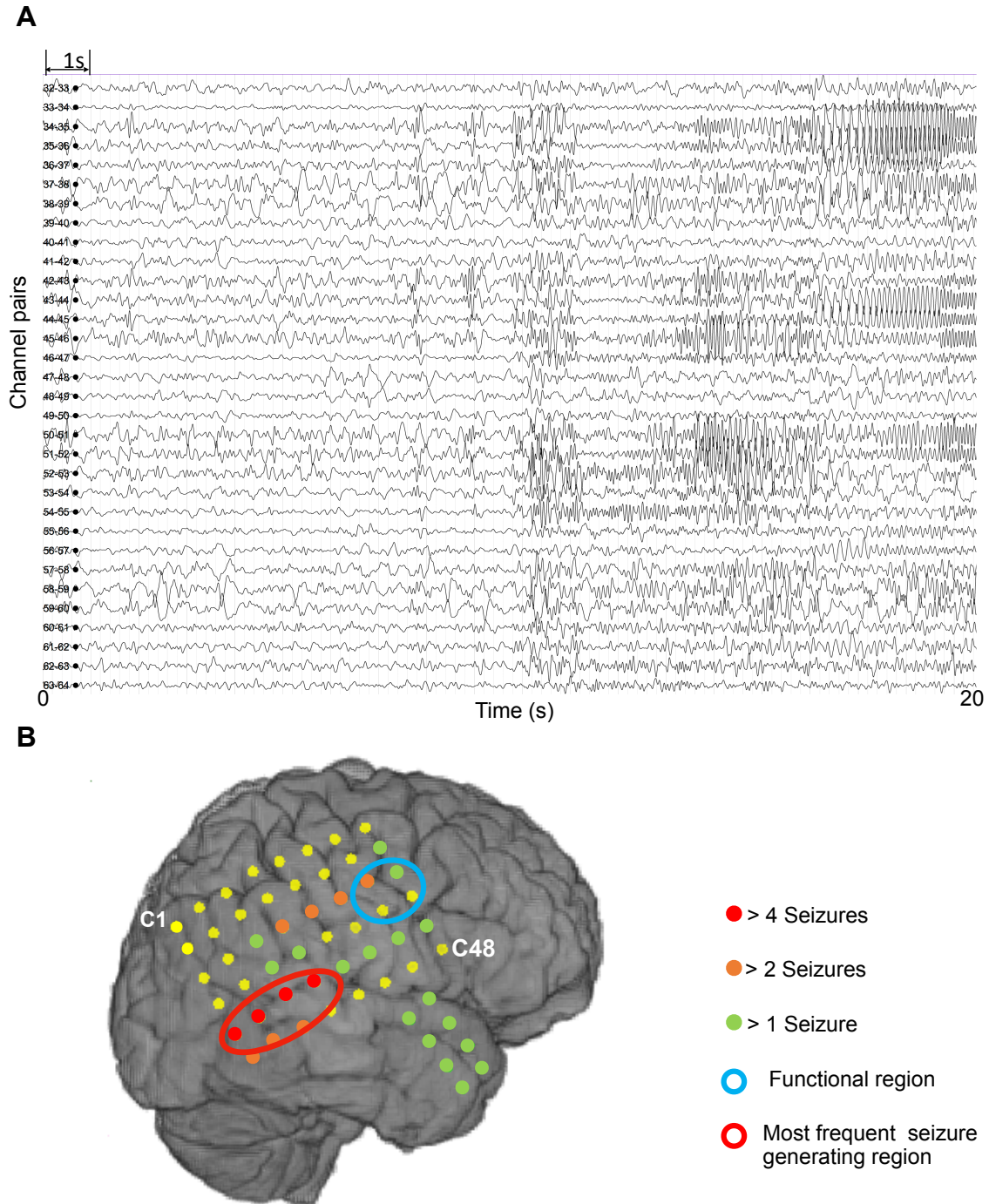


**Figure 4-8. (A) Twenty-seconds of iEEG data in bipolar montage showing the seizure onset. (B) Co-registration of pre-operative MRI and post-operative CT with SOZ information and functional zone.**

Cortical stimulation mapping for the patient was performed with a current amplitude of 15 mA, pulse width of 300  $\mu$ s, and duration of 0.2 s. The stimulation was conducted between each pair of contacts on the 6  $\times$  8 grid. The result revealed negative motor responses of the left mid finger on contacts 23 – 31, and the left index finger on contacts 24 – 32, as given in figure 4-8 (B). No other eloquent brain area was identified by the motor mapping.

A total of 60-minute waking baseline recording was pruned and used for HFO analysis, which was at least 4 hours away from a seizure. All 66 channels were used as the input. Consequently, 1,569 events were captured during initial detection. Surviving candidates were sub-classified into three clusters, with the spike group marked in green (n = 1096), one HFO group in orange (type 1 HFO, n = 183), and another HFO group in purple colors (type 2 HFO, n = 290). The feature distribution and 4 randomly selected sample events in both types of HFOs are given in figure 4-9 (A). For each HFO group, the time-frequency map averaged across 20 random samples is also provided in figure 4-9 (B). As we observed from the time-frequency representation, events in both HFO groups showed high-band spectral peaks in 80 – 200 Hz range, hence were deemed ripples. No fast ripple was detected in this data.

Figure 4-9 (C) illustrates the spatial distribution of type 1 and type 2 HFO. Transients from each group were seen in 30% and 58% of the total channels, respectively. The spatial maps implied that the majority (81%) of type 1 ripples were generated from contact 33 – 37 and the adjacent 25 – 28 (the posterior-inferior part on the large grid), which were also a subset of seizure onset channels with the highest seizure frequency. We

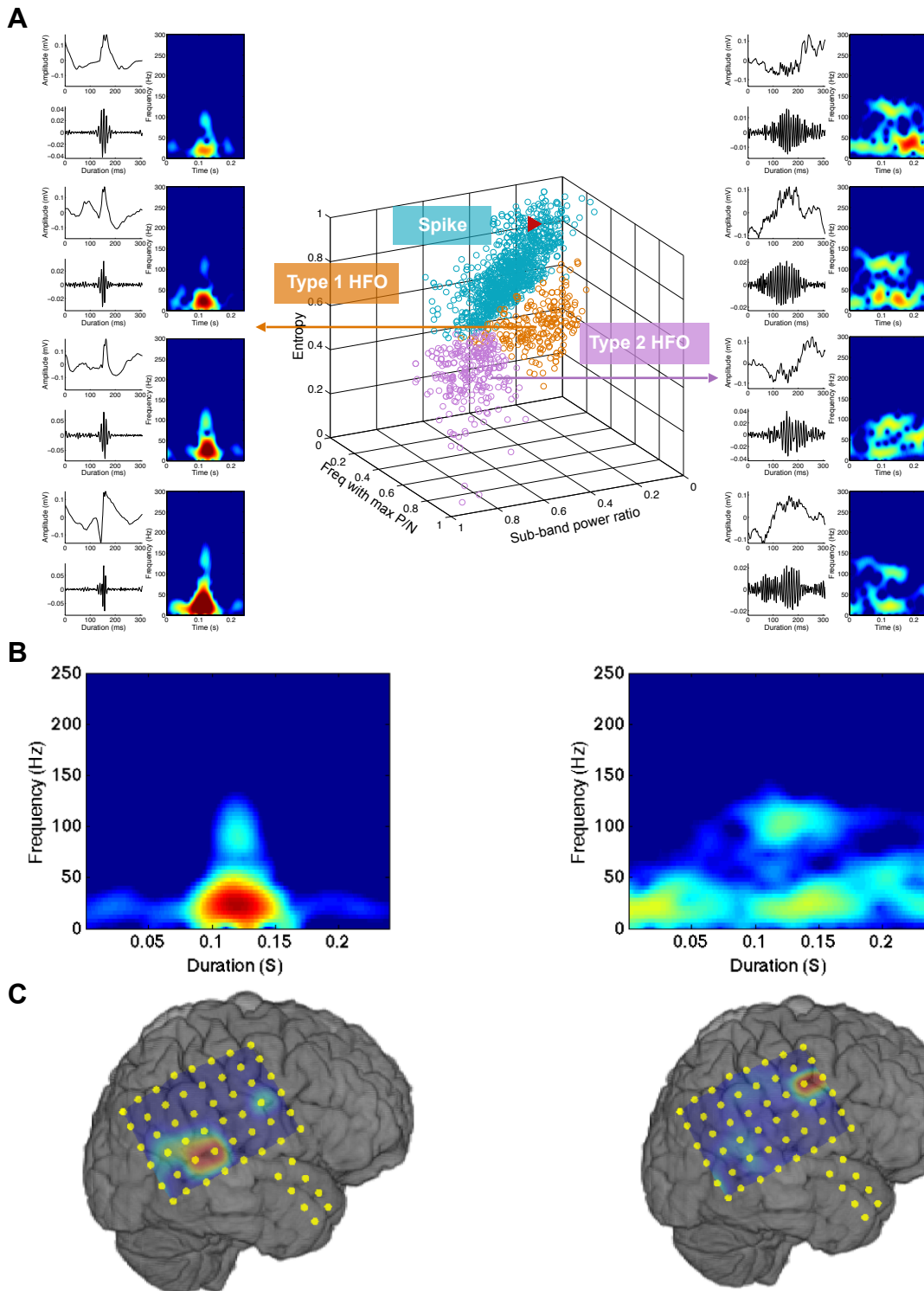


**Figure 4-9. (A) Feature distribution in 3D space. (B) Averaged time-frequency maps across 20 random samples in type 1 and type 2 HFO groups. (C) Spatial distribution of type 1 (left) and 2 HFO (right).**

assumed these were pathological HFOs (pHFOs). In contrast, most type 2 ripples were restricted to contacts 23, 24 and 31, 32, which were located outside the SOZ but overlapped with the functional motor area as delineated by electrical cortical stimulation, and hence were considered physiological/normal HFOs (nHFOs).

The 290 nHFOs generated from the motor cortex were compared with the 183 pHFOs. In the time domain, the average peak amplitude for pHFOs after high-pass filtered at 80 Hz was 51.9  $\mu\text{V}$ , significantly greater than nHFOs (21.2  $\mu\text{V}$ ,  $P < 10^{-10}$ ). pHFO exhibited shorter mean duration (62.6 ms) than nHFO (110.2 ms), with  $P < 10^{-3}$ . Compared to nHFOs, the mean frequency of pHFOs was also higher, with a small but significant difference ( $f_p = 122 \text{ Hz}$ ,  $f_n = 112 \text{ Hz}$ ,  $P < 10^{-3}$ ).

#### **4.5 Case 3: the Influence of Contact Size on HFO Detection**

In the current case we investigated the HFO characteristics in a patient with uncontrollable frontal lobe seizures. In particular, a customized surface electrode array was used which consisted of 113 contacts in two different sizes, to evaluate the effect of contact size on HFO recordings.

Epileptic HFOs were firstly recorded in human with temporal lobe epilepsy using microwires with 40 – 60  $\mu\text{m}$  in diameter (Bragin et al., 1999), and then were successfully recorded using commercially available macro-electrodes with contacts in various sizes (2.5 to 20  $\text{mm}^2$ ) (Akiyama et al., 2005; Worrell et al., 2008a, 2004a). Recent studies using microwires and macro-contact depth electrodes suggested an impact of contact size on the HFO detection rate in animal models and human patients (Bundy et al., 2014; Schevon et al., 2009a; Worrell et al., 2008a). Therefore, it is necessary to carry out

investigations into the methodology for optimized HFO recording in clinical environments. To our knowledge, the influence of contacts size on HFO recording ability using ECoG electrodes has not been documented. In this context, we evaluated the effect of contact size on HFO detection in ECoG recordings using a customized hybrid surface electrode array with macro-contacts in 1 mm and 2.7 mm diameters (0.8 mm<sup>2</sup> and 5.7 mm<sup>2</sup> surface areas). The clustered HFOs and spikes were spatially correlated with the resection border and postsurgical outcome, and then grouped based on the type of contacts by which they were recorded, in order to assess the influence of contact size on event detection. The rate of HFO and spike recorded by small contacts were compared in pair with the average of the neighboring four large contacts. In addition, the difference in signal amplitude, duration, high-band power, and mean frequency of HFOs were also discussed. A non-parametric Wilcoxon's Test was used for statistical analysis.

#### **4.5.1. Case Presentation**

The ECoG data were acquired from a 28-year-old male patient with brain tumor related epilepsy who underwent his first operation in 2012 for tumor resection in the left frontal lobe. The patient was admitted to the clinic at Capa Hospital of Istanbul University (Istanbul, Turkey) for new onsets of absence seizures resistant to antiepileptic drugs. The pre- and postoperative MRIs are provided in figure 4-10 (A). Neurological assessment showed no neurological deficit postoperatively.

A customized 113-channel hybrid ECoG grid (CorTec GmbH, Freiburg Germany) was implanted subdurally to map the eloquent functional area and to monitor the seizure activity. The electrode was positioned in a way to cover the border of the tumor and the

presumed seizure foci, and extended towards the primary motor area (M1) as shown in figure 4-10 (B). The grid consisted of 64 large contacts with 2.7-mm-diameter and 1 cm spacing, interlaced with 49 1-mm-diameter small contacts in 1 cm spacing (platinum-iridium alloy) embedded in medical grade silicon rubber substrate. The overall dimension of the electrode was 86 mm × 80 mm × 0.4 mm. A sketch of the electrode array is provided in figure 4-10 (C).

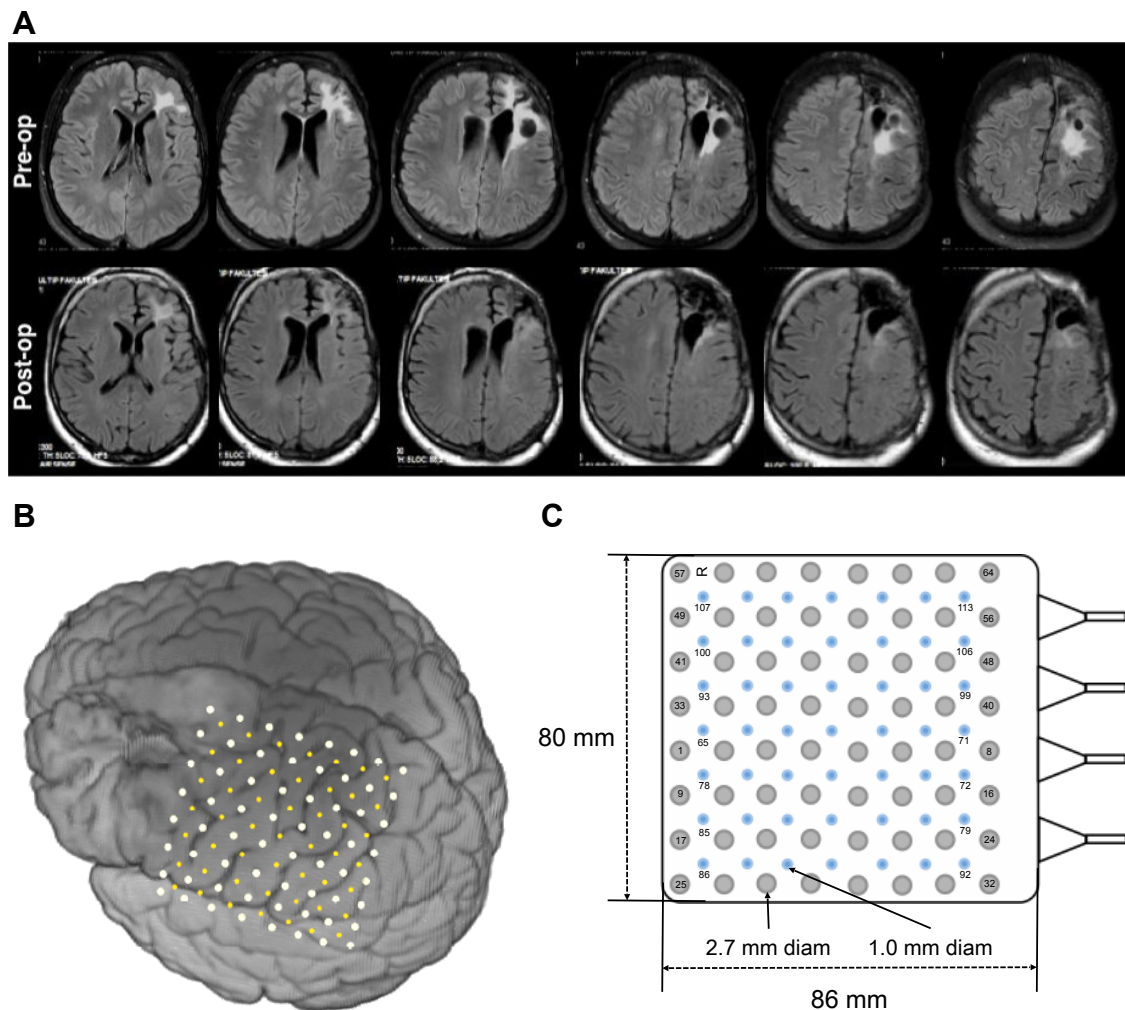


**Figure 4-10. (A) Preoperative image (upper) and postoperative MRI (lower). (B) Coregistration of the preoperative MRI and the intraoperative photos of the cortex. (C) The sketch of the hybrid electrode grid.**

#### 4.5.2. Results

Five hours of continuous ECoG data recorded during slow-wave sleep which was at least 4 hours always from seizures was analyzed for HFO detection. Without any channel pre-selection or artifact removal, the entire data segment was investigated using a previously published automated HFO detector.

A 30-second ECoG data segment showing an ictal onset with widespread propagation is given in figure 4-11 (A). A total of 7,583 events were identified by the detector, including 2,119 inter-ictal spikes and 5,464 HFOs. In general, we observed 3 clusters identified within the survived events, with one cluster consisting of HFO candidates in ripple frequency range, one cluster of spike activities, and another cluster of arbitrary noise or artifactual signal. Figure 4-11 (B) illustrates the 3-dimensional feature distribution of a subset of events containing 906 observations detected from one hour of recording. For each cluster, 8 random samples together with the averaged time-frequency maps are shown, to give a flavor of the cluster content.

Thirty-eight channels were identified as HFO-generating channels, accounting for 33% of the total channels. In 12 channels the rate of occurrence  $> 1$  HFO/min. Spikes were found originated from smaller regions involving 27 channels. HFOs were captured in 61% of these spike channels. In figure 4-12 we present the spatial distribution maps of HFO and spike computed from the entire ECoG data, as well as their relationship to the resection border. Notably, while 59.8% of the HFOs localized inside the area of resection, a considerable proportion of HFOs were discovered from a more distant area extending towards the motor, temporal, and parietal cortex as well. By contrast, most of the spikes



(81.0%) were located within the tumor area inside the resection border. Postsurgical evaluation indicated that the patient received limited improvement in seizure frequency (Engel Class III), although the majority of spike generating sites have been surgically removed, as presented in figure 4-12.

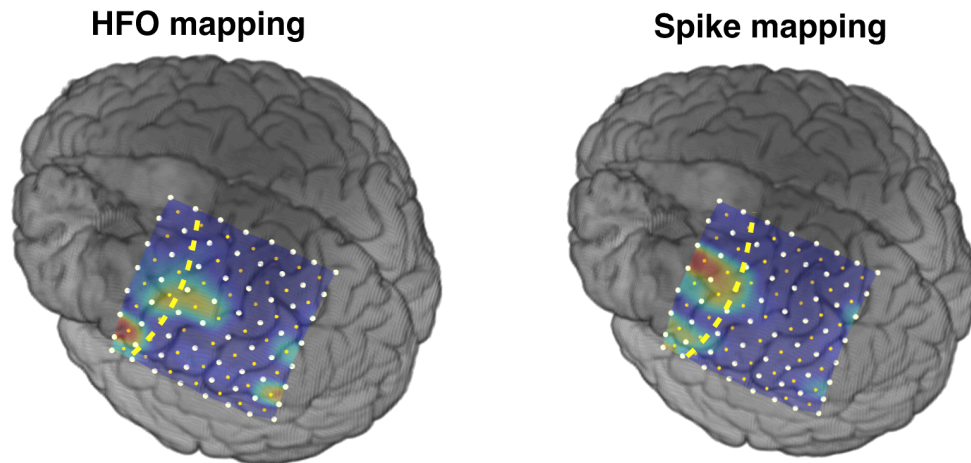


**Figure 4-12. Spatial distribution of HFO (left) and spike (right) projected to the individual MRI data, with the resection border given (yellow line).**

In figure 4-13 we show the total number of events captured by contacts in both sizes together with representative HFO and spike samples for each. Using 5-hour of continuous data, 3,975 HFOs were detected on the 1-mm contacts, whereas only 1,489 HFOs were detected on the 2.7-mm ones. Statistical analysis showed a significant advantage in ripple detection rate using small contacts compared to large ones (median = 13.3 vs. 5.0 HFOs/min,  $P = 0.001$ ). However, the performance in spike detection using small contacts was statistically comparable with the large ones (median = 3.7 vs. 3.2 spikes/min).

Overall, the HFOs shared similar appearance between groups, but differed in some other properties. The peak amplitude of HFOs (high-pass filtered by 80 Hz) recorded by 1-

mm contacts was larger than those detected by 2.7-mm contacts ( $P < 0.001$ ). Likewise, the mean frequency in small-contact group was higher, with a slight but significant difference compared to the other (median = 112.9 vs. 112.2 Hz,  $P = 0.03$ ). On the other hand, the HFOs in large-contact group possessed greater power in the high-band above 80 Hz ( $P < 0.001$ ). The duration of HFOs showed no statistical difference between small and large groups (median = 52.5 vs. 49.6 ms).

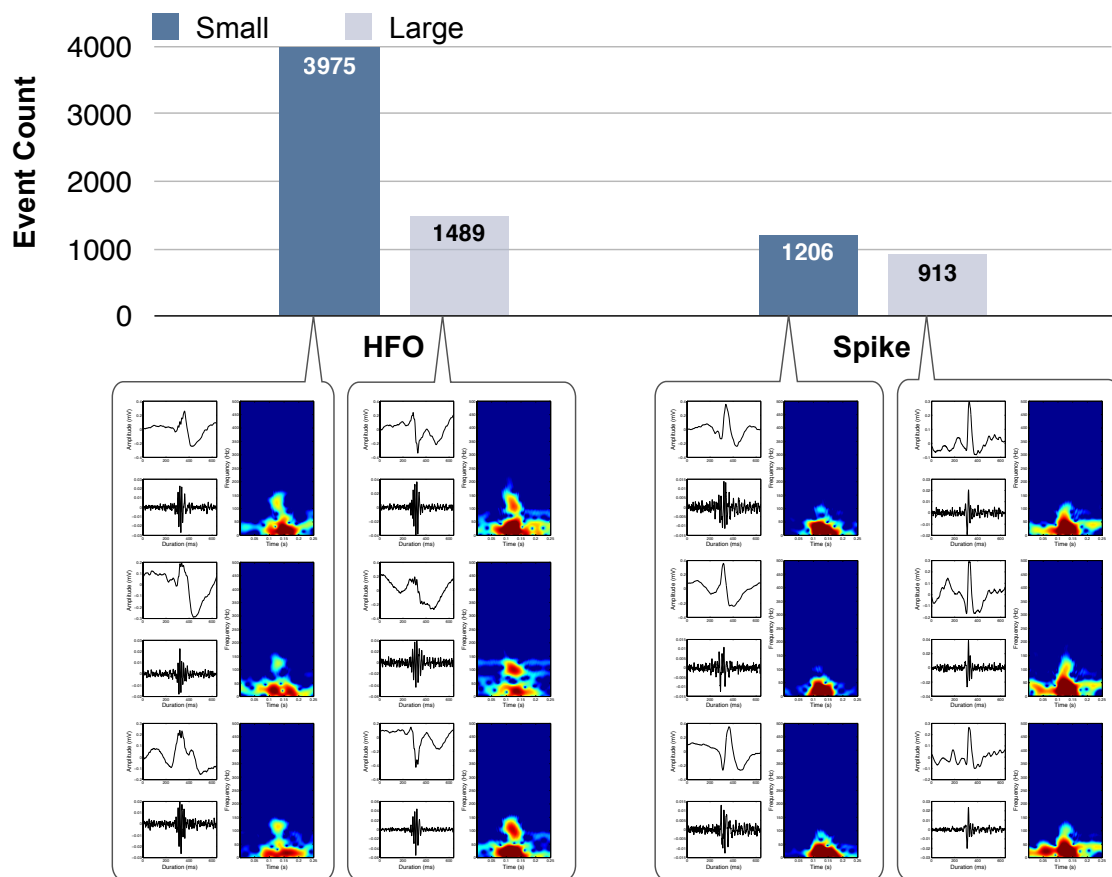


**Figure 4-13. Comparison of the event count between small and large contact groups for HFO and spike. For each group, three sample events are presented.**

The distribution maps of HFOs detected by two sized contacts were projected to the individual's brain image, for the comparison of spatial characteristics between groups. In both cases, most of the HFOs originated from the surrounding tissue of the tumor with 78% overlap. Pairwise comparison showed a significant correlation in HFO rate between small and large contacts ( $r = 0.58$ ,  $P < 0.001$ ), suggesting these two groups were spatially dependent. Nevertheless, the most active sites responsible for the generation of HFOs were located at the temporal-frontal region which was identified by the small contacts but could not be seen on the map of large contacts, as shown in figure 4-14.

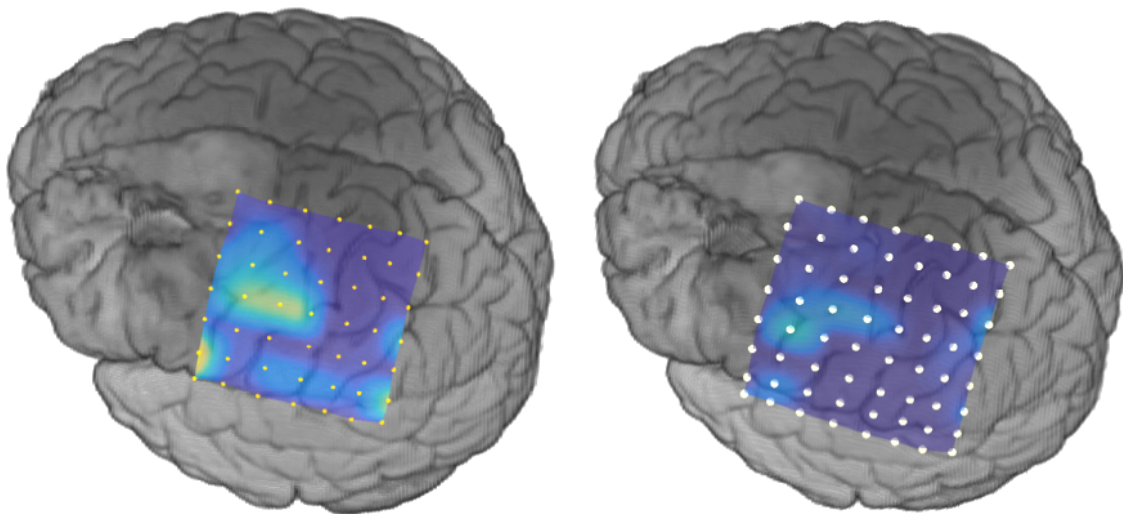


**Figure 4-14. Spatial maps of HFOs captured by small contacts (left) and large contacts (right).**

#### **4.6 Discussion**

We proposed signal representation methods that can be applied on the iEEG data of individual patients, and representative results were provided in this chapter.

In case 1 the spatial characteristics of HFOs and interictal spikes were investigated in a pediatric patient with CM-caused epilepsy. The clinical EEG evaluation results indicated a dramatic buildup of preictal spikes across channels located anterior/superior to the CM. The interictal epileptiform discharges extended far beyond the limits of the lesional area and furthermore extended to the majority of the grid. Interestingly, most of the HFOs were localized at channels 28 – 29 consistently over all awake and sleep states as well as in a brief 30-min recording right after the electrode implantation. We noted that both HFOs and spiking activity patterns at the seizure onset pointed to the superior/anterior perilesional cortex. However, compared to the ictal data, HFOs were more localized to the perilesional area superior to the CM. Based on the clinical evaluation, a conservative excision was limited to the resection of the CM and hemosiderin ring only, which correlated well with the HFO distribution and provided seizure freedom to the patient. Epileptic seizures are the most frequent symptom in patients with CM. During the presurgical evaluation, neurologists need to accurately define the resection territories in order to abolish the seizures. However, the precise identification of the seizure focus and resection border is cumbersome, because the epileptogenic zone is complex in most cases and could involve not only the perilesional region but also brain sites that are geographically distant from the lesion and functionally independent. Studies show that only 75% of patients with CM-caused epilepsy who undergo lesionectomy solely achieve postoperative seizure freedom because of the presence of independent epileptogenic regions, insufficient estimation of the planned resection area, or postoperative scar formation (Englot et al., 2011; Sevy et al., 2014). To identify the epileptogenic areas

more accurately, prolonged invasive monitoring is often required to guide a tailored resection for optimal seizure control (Schwartz 2010). Despite the potential benefits, the expense and risk of adverse events during intracranial monitoring have been documented, and the associated complications are significantly more common in pediatric patients (Arrington et al., 2013). There is an urgent demand for the investigation of reliable neurobiomarkers, which may potentially shorten the undefined monitoring period and assist presurgical planning. In our results, the HFO clustering results clearly pointed to the actual perilesion location consistently in all analyzed data segments. The brain sites with most of the HFOs were stably limited to two contacts, which were located immediately above the superior edge of the CM, and further linked to seizure-free outcome. We also observed that the HFO spatial distribution was more compact in sleep compared to in the waking state. Compared to the HFO maps, the spatial distribution of spikes was not robust because it varied over days as well as during the sleep-wake cycle. This is the first report describing HFOs in a pediatric patient with CM-caused epilepsy and shows their potential in identifying the seizure focus in an accurate and efficient manner, suggesting that the epileptic perilesional structure could be identified from the HFO spatial distribution estimated from 30-min ECoG data recorded immediately after the electrode placement.

In case 2 we reported our experience of automatically separating two types of HFOs by using the cluster based detection method. Type 1 HFO, as we assumed pathological, were generated from epileptic tissues and highly correlated with seizure-free outcome; type 2 HFO, deemed normal, were discovered from normal cerebral tissues distant from

the SOZ and from functional motor sites defined by electrical stimulation mapping. In this case we presented an example of applying time-frequency analysis with clustering technique in the detection and discrimination of normal and pathological HFOs. The results demonstrated that unsupervised clustering method with our current features had the potential to reliably and efficiently differentiate pHFOs from nHFOs, which is an essential step to utilize HFOs as valid clinical biomarkers in epilepsy surgical treatment. Interestingly, the HFOs analyzed in both cases were limited to the ripples-band. Early seminal observations supported the hypothesis that FRs were distinctly pathological transients associated with epileptic brain. However, later studies suggested that ripples within 80 – 200 Hz range might also have predictive power for the SOZ and they might actually have higher clinical values than fast ripples which can be difficult to detect in a substantial proportion of patients with neocortical epilepsy. Compared to fast ripples, ripples are commonly generated from a larger extent including both seizure foci and non-epileptic functional brain sites. This section provided preliminary evidences of simultaneously detecting and discriminating epileptic spikes, normal and pathological ripples using human iEEG according to their natural characteristics, without labeling the events which requires the existence of a yet unachievable precise definition for different HFO subtypes. Compared to nHFOs, we found the pHFO cluster presented higher frequency and amplitude but shorter duration, as described in other reports (Alkawadri et al., 2014; Nagasawa et al., 2012). The successful discrimination between pHFO and nHFO events may facilitate the accurate delineation of SOZ and avoid unwanted detection of functionally critical sites in the brain. In addition, by data inspection we

observed special waveform patterns in pHFO activities. We believe that the signal morphology and the relation between oscillation and signal baseline is a key feature for the interpretation of normal or pathological HFOs. In order to test this hypothesis, the current study was expanded with the details described in the Chapter 5.

In case 3 we executed automated HFO detection in continuous ECoG data recorded from an epilepsy patient with brain tumor using a hybrid high-density surface electrode array, and investigated whether HFOs were equally detectable using different sized ECoG contacts. Our results showed initial evidence that the detection efficacy of HFOs in the ripple range may be higher using small contacts, possibly due to the spatial averaging effect of the comparatively large surface area of the 2.7-mm contacts. Studies utilizing microwires or Utah arrays have demonstrated that HFOs are primarily generated by highly localized neuronal clusters in sub-millimeter scale (Bragin et al., 2002; Jefferys et al., 2012; Schevon et al., 2009b), which should theoretically be more effectively captured by smaller contacts that record from less volume of brain tissues. Since the contacts with 1-mm diameter had higher spatial specificity, this might provide an advantage in capturing focal HFO events which are generated by relatively small pathologic circuits. We observed that contact size significantly influenced HFO detection not only on the occurrence rate but also on signal characteristics including the amplitude, high-band power, and mean frequency, which is different from previous studies mainly suggesting similarities. A previous study using depth electrodes containing three sized macro-contacts (0.02, 0.05 and 0.09 mm<sup>2</sup>) suggested no significant difference in detection ability between contact sizes in a rat epilepsy model (Bragin et al., 2002). Another report

showed similar results in epilepsy patients by using electrodes with a surface area ranging from 0.2 – 5 mm<sup>2</sup> (Châtillon et al., 2011). The difference in our results might attribute to the distinct recording modalities (SEEG and ECoG), detection methods (human inspection and automatic detection), and subject population. The investigated HFOs in this study had a mean frequency of 112 Hz (85 – 198 Hz) and hence were deemed ripples. The overall rate, 14 HFOs/min, was comparable to other studies (Châtillon et al., 2011, 2013). The absence of fast ripples could partly be due to the decreased ability in HFO detection using macro-electrodes, especially in the higher frequency range above 200 Hz (Bundy et al., 2014). Despite the advantages, recordings using micro-electrodes require specialized equipment that do not allow for clinical data acquisition, which greatly limits its use in clinical practice. By contrast, intracranial recordings using macro-electrodes allows the direct application of HFO observations in SOZ prediction and presurgical planning, thus becoming more relevant to epilepsy diagnosis. For these reasons, the investigation of HFOs recorded using classical macro-contacts is of substantial importance for the utilization of HFO data in clinical practice. The macro-contacts used in this study were limited to two sizes. The influence of contact size on HFO detection in ECoG needs to be further explored in a larger population by increasing the size range. It is also noteworthy that after the removal of the presumed epileptogenic regions the patient received limited postsurgical improvement. In this case, over 40% of the HFO were generated from the cerebral tissues which were not resected during the surgery, we speculate that the existence of HFO generating areas outside of the resection region could be a possible cause of the poor seizure control. We therefore believe that

HFO spatial information might as well be taken into account for the delineation of the resection boundary to achieve a complete seizure-free outcome.

## **CHAPTER 5 DISCRIMINATION OF SEIZURE ONSET ZONES AND CRITICAL FUNCTIONAL REGIONS**

### **5.1 Introduction**

Resective surgical therapy targeting ictogenic cortex, clinically determined as the site with earliest detectable electrographic ictal discharges during habitual clinically evident seizures as the “seizure onset zone” (SOZ), has the potential to eliminate seizures in patients with medically intractable epilepsy. Long term monitoring of intracranial electroencephalogram (iEEG) is commonly utilized by epileptologists for the accurate localization of SOZ (Brna et al., 2015; Engel et al., 1990; Henry et al., 1999; So et al., 1989), where subdural grid or depth leads are surgically implanted into the presumed seizure focus. Accurate detection of an epileptogenic zone requires iEEG monitoring over an extended period of time and detailed visual inspection of collected data by medical experts. High frequency oscillations (HFOs, 80 – 500 Hz) recorded in iEEG have been proposed as promising neurobiomarkers for epileptogenic tissue. Studies over the last decade have shown that HFO transients are significantly correlated with epileptogenesis (Allen, Fish and Smith, 1992; Jirsch et al., 2006; Urrestarazu et al., 2006; Zijlmans et al., 2011), however, more recent reports indicate that HFOs can be generated not only by epileptic cerebral tissue but also by non-epileptic sites often including motor cortex, visual cortex and language areas (Kucewicz et al., 2014; Matsumoto et al., 2013; Nagasawa et al., 2012; Sinai et al., 2005), rising the question whether HFOs should be considered specific to epileptogenic tissue. The co-occurrence of pathological HFOs and physiological HFOs may interfere with the delineation of ictogenesis and increase the

risk of injury to functional area, as the spatial distribution of physiological HFOs can correlate with brain regions that are not responsible for seizure generation but functionally important and need to be preserved during resection.

Discrimination between physiological and pathological HFOs is not so straightforward. Spectral frequency alone is not a reliable differential feature (Bragin, Wilson and Engel, 2007; Köhling and Staley, 2011), as pathological HFOs may contain significant spectral power in the ripple-band (80 – 200 Hz), which had been historically linked to physiological activities. Further, fast ripples (FR, 200 – 500 Hz) could be observed in normal brain structures associated with visual perception which also complicates the clinical use of HFOs as valid biomarkers to guide epilepsy surgery (Dümpelmann et al., 2012; Jacobs et al., 2008b; Kerber et al., 2014; Wu et al., 2010). Currently, it is cumbersome to reliably separate functional and pathological HFOs when recorded using macro-electrodes in clinical environments, particularly in the ripple range (Zijlmans et al., 2012). To address this issue, several recent studies investigated the difference between HFOs discovered inside and outside the SOZ (Kerber et al., 2014; Melani et al., 2013); others compared pathological HFOs with oscillations induced by motor/visual tasks or cortical stimulation (Matsumoto et al., 2013; Nonoda et al., 2016). The investigators generally performed visual marking of HFOs in a pre-defined subset of data, then looked into features related to the rate of HFO occurrence, amplitude, duration, frequency, and their interaction with slow waves or baseline activities; some also attempted to differentiate between epileptic and non-epileptic HFOs using supervised classifiers based on the abovementioned features (Alkawadri et al., 2014; Burnos et al.,

2014; Nagasawa et al., 2012; Von Ellenrieder et al., 2016). Although some of the features presented group-wise statistical difference, little is known if the largely overlapped features can be employed to improve the process of clinical decision-making.

In Chapter 4 we reported a case where ripples below 200 Hz were generated by two distant cortical regions, one being epileptogenic and the other was involved in motor function. Based on initial visual inspection within the identified HFO clusters from this case, as well as other prior studies, we observed that HFOs generated from epileptogenic regions tended to be similar in wave shape, and repetitively occur throughout the recording. We hypothesized that pathological HFOs occur in a repetitive fashion with a similar waveform morphology that specifically indicate seizure onset zones. Here we expanded our previous method and by using a pipeline of unsupervised machine learning techniques we captured recurrent stereotyped HFO waveforms in large iEEG recordings automatically. We investigated these “clones” of HFO waveforms in 13 patients with focal epilepsy and five control patients with brain tumor but no epilepsy, where subdural ECoG grids are implanted for the mapping of the eloquent brain regions. In particular, we aimed to clarify whether the recurrence of similar HFO waveforms is exclusively linked to seizure focus, such that it can be used to facilitate the discrimination between SOZ and other functional regions. We believe our methods and results will provide a new pathway towards the separation of pathological and physiological HFOs, and assist in the accurate delineation of SOZ as well distinguish them from eloquent areas to assist surgical therapy of epilepsy.

## **5.2 Materials and Methods**

### **5.2.1. Patient Population**

Eighteen subjects were included in the study (12 females), including 13 patients with intractable temporal lobe or neocortex epilepsy (P1 – P13), and five control subjects with brain tumor but no epilepsy who went through intraoperative functional mapping in an awake surgery (C1 – C5). The inclusion criteria for epilepsy cohort consisted of the following: patients with intractable temporal lobe or neocortex epilepsy who went through iEEG monitoring with video after the implantation of subdural grid or depth electrodes in University of Minnesota (UMN, Minneapolis, Minnesota), Capa Hospital of Istanbul University (IU, Istanbul, Turkey), and Texas Children’s Hospital (TCH, Houston, Texas). This yielded a total of 13 patients, including 10 adults (ages 30 – 53) and three pediatric patients (ages 3 – 18). Additional data was collected using the same recording system at Istanbul University and MD Anderson Cancer Center (MDA, Houston, Texas) from five control subjects with brain tumor but no epilepsy history who underwent intraoperative cortical stimulation to identify the functional cortex. These subjects were involved for the investigation of non-epileptic HFOs originating from functional regions. Data collection and scientific workup have been approved by the Institutional Review Board of each institution.

### **5.2.2. Electrode Placement and Intracranial EEG Recording**

Electrode implantation was performed after presurgical workup. In the 13 patients with epilepsy, a combination of surface and depth electrodes were implanted to the

possible irritative sites for the accurate delineation of SOZ. Subdural grid arrays were placed over the functional region in 10 subjects to give a sufficient coverage of the eloquent cortex (P9 – P13 and C1 – C5). Post-implantation MRI/CT or intraoperative photos were taken to determine the electrode locations in all subjects.

Multichannel iEEG data was obtained with 2 kHz (at UMN) or 2.4 kHz (at IU, TCH and MDA) sampling frequency and 24 bit A/D resolution using g.HIamp system (g.tec Medical Engineering, Austria) with an anti-aliasing filter set to 600 Hz. For P1 – P13, continuous iEEG signal was recorded for 2 – 4 days in the EMU simultaneously with video monitoring throughout the period. For C1 – C5, data was recorded intraoperatively in awake state for 40 – 50 minutes.

### **5.2.3. Delineation of SOZ and Functional Regions**

For the epilepsy cohort, the seizure onset channels with earliest ictal discharges were visually determined by neurologists based on the long-term video iEEG monitoring. Functional mapping was performed in 10 subjects as a part of clinical routine, including five patients with epilepsy where the implanted grid electrodes covered the motor/language areas, and five control subjects without history of epilepsy. Direct cortical stimulation (DCS) was conducted between each pair of contacts row- and column-wise on the grid, shifting from the first to the last contact, with a current amplitude ranging from 3 – 15 mA, pulse width of 200 – 300  $\mu$ s, and duration of 0.2 s, according to the patient's individual tolerance. Contacts with motor responses were defined at which the stimulation reproducibly induced sensory changes or body movement.

#### 5.2.4. Data Selection and HFO Detection

All data was de-identified and transferred to University of Houston for the offline analysis in Matlab environment (Mathworks, MA, USA). For P1 – P13 who underwent prolonged recording in the EMU, 60 minutes of iEEG data in the waking baseline (at least 4 hours away from seizures) was used per patient to obtain a sufficient number of HFO events. For C1 – C5, the entire intraoperative recording was used for the analysis.

Detection of HFOs and their waveform patterns was performed by using a pipeline of unsupervised machine learning techniques which is provided in figure 5-1. HFOs were automatically identified in all recorded channels using our previously validated detector (Liu et al., 2016) with modifications. In brief, raw iEEG data firstly went through an amplitude-based detector after band-pass filtering within 80 – 500 Hz range. Short-time Fourier transform (STFT) was then performed on the original signal in each remained candidate, followed by a denoising step to eliminate minor background activities on the time-frequency map. The denoising level, detection threshold and other parameters were consistent with our previous studies (Liu et al., 2015, 2016). For all surviving events, the entire iEEG bandwidth was explored, where three time-frequency features were extracted and used with Gaussian Mixture Model (GMM) clustering with  $k$ -medoids initialization (Kaufman and Rousseeuw, 1987) to isolate HFOs from spikes and other arbitrary events. The cluster number was determined based on the elbow method (Ketchen and Shook, 1996).

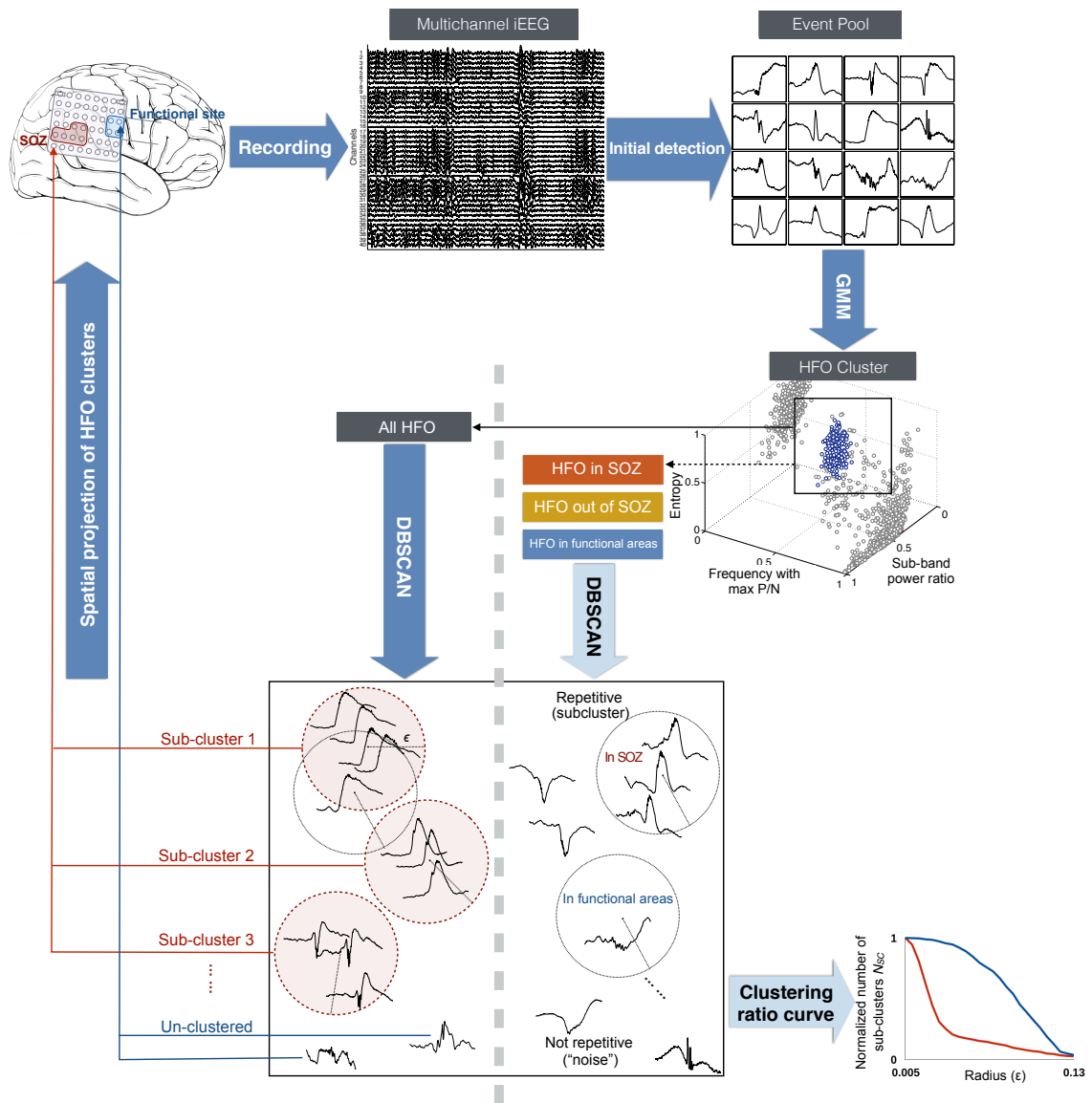


**Figure 5-1. Data analysis workflow. The HFO clusters were first categorized by their spatial origins for a group-wise comparison. Next, the detection of stereotyped HFOs was blindly performed in the entire HFO pool.**

After generating a pool of HFOs, we categorized them according to their spatial origin and group comparison was performed among HFOs inside the SOZ (sHFO), outside the SOZ (oHFO), and inside the functional areas (fHFO) across patients. Classic

HFO features including mean frequency and rate of occurrence were also inspected. The detection of recurrent HFO subclusters within sHFO, oHFO and fHFO was implemented using the procedures described in the section below.

### 5.2.5 Detection of Stereotyped HFOs

Following a visual inspection of HFOs in a few subjects, we observed that HFOs originated from epileptic tissues tended to occur repeatedly with similar waveform morphology, raising a presumption that pathological HFOs might produce compact subclusters in the high-dimensional native space, with each of the subcluster being a group of events that shared the same waveform pattern. In comparison, HFO members detected in non-SOZ areas were assumed to present irregular wave shapes with relatively large intra-cluster distance in native space. To uncover this underlying pattern in an objective and unbiased manner, we performed the detection using the density-based spatial clustering of applications with noise (DBSCAN) approach (Ester et al., 1996). As it is explained in figure 5-2, the original algorithm was designed to identify dense regions in a dataset by grouping data points neighboring a “core point” within a certain radius *Epsilon* ( $\epsilon$ ). The radius also represents the distance between two events (measure of dissimilarity). The “core point” is defined as a point with its neighbor count exceeding a user-specified threshold *MinPts*. After isolating the HFO events with GMM method, we executed DBSCAN algorithm to capture subclusters of stereotyped HFO waveforms. Specifically, we implemented the algorithm in different HFO groups (sHFO, oHFO and fHFO) with an increasing sequence of  $\epsilon$ , computed the corresponding number of subcluster ( $N_{SC}$ ), and visualized the estimation result by plotting the curves of clustering

ratio ( $N_{SC}$  vs.  $\epsilon$ ), which is the change in the number of detected subclusters within each HFO group for different distance values. The initial  $\epsilon$  was assigned to 0, with  $MinPts$  of 1, such that each HFO event in the group was taken as an individual subcluster at the first place. Given that closely spaced points would be merged instantly as the cluster radius  $\epsilon$  expanded, we expected to observe an immediate drop in the  $N_{SC}$  value in sHFO datasets with repetitive waveform patterns (figure 5-1). Thus, the difference in waveform patterns among sHFO, oHFO and fHFO groups can be quantified by comparing the area under curve (AUC) between groups. The estimation was executed in HFO data after removing the low-band component below 4 Hz. The dissimilarity of the signals was computed using Euclidean distance metric after aligning the HFO observations by maximizing the absolute cross-correlation ( $\pm 10$  ms lags) between each pair of events.

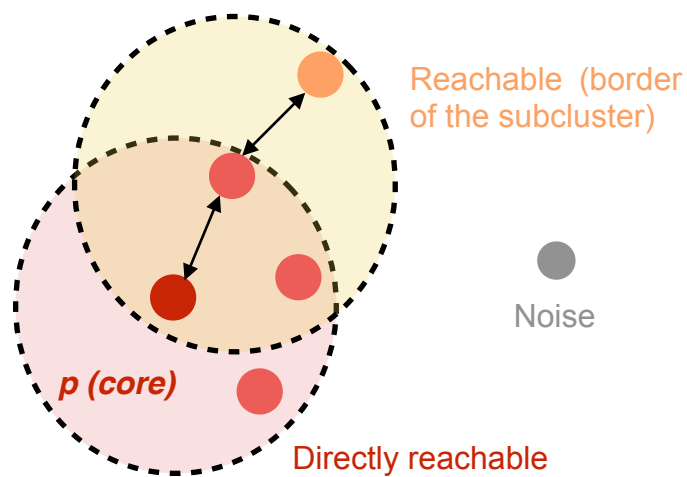


**Figure 5-2. DBSCAN clustering algorithm. A core point has neighboring points more than a specified number ( $MinPts$ ) within distance  $\epsilon$ ; a noise point is any point that is not a core point or a border point.**

### 5.2.6. Identification of SOZ Using Stereotyped HFOs

In this stage, we investigated if stereotyped HFO waveform patterns could be employed in the discrimination of SOZ and eloquent areas in a blinded fashion. This was done by executing DBSCAN in all HFOs recorded from each patient without grouping them according to their origins, and quantifying the change in spatial distribution of HFOs when the degree of signal dissimilarity increased.

After employing the GMM clustering in 3D feature space on the entire candidate event population and forming the HFO pool, we identified repetitive HFO waveforms in P1 – P11, using an increasing value of  $\epsilon$  from 0.05 to 1 and a fixed *MinPts* of 3. At each  $\epsilon$  level, the algorithm discovered subclusters of stereotypical HFO waveforms with intra-cluster distance smaller than the current  $\epsilon$ . We computed the proportion of clustered HFOs inside the SOZ, inspected the spatial distribution of HFOs with and without a repetitive waveform pattern, and discussed their correlation with SOZ and functional regions. For each patient, the spatial maps of HFOs were projected to a 3D model of the brain which was generated after the coregistration of post-implantation CT image and the individual's MRI. Finally, we sought to clarify whether the highly correlated HFOs (i.e., clustered by DBSCAN using a small radius) give specific information about epileptogenic location, and evaluated the predictive performance when these HFOs were used for SOZ localization. More precisely, we determined the number of channels with repetitive HFO patterns ( $CH_R$ ) and without a repetitive pattern ( $CH_{NoR}$ ), and then evaluated their relationship with SOZ channels by calculating the sensitivity, specificity and accuracy which were defined as:

$$\text{Sensitivity} = \frac{CH_R \text{ in SOZ}}{CH_R \text{ in SOZ} + CH_{NoR} \text{ in SOZ}}, \quad (5-1)$$

$$\text{Specificity} = \frac{CH_{NoR} \text{ not in SOZ}}{CH_{NoR} \text{ not in SOZ} + CH_R \text{ not in SOZ}}, \text{ and} \quad (5-2)$$

$$\text{Accuracy} = \frac{CH_R \text{ in SOZ} + CH_{NoR} \text{ not in SOZ}}{\text{Number of total Channels}}. \quad (5-3)$$

### 5.2.7. Statistical Analysis

We compared the HFO rates, mean frequency, the minimum clustering radius and area under the clustering ratio curve inside and outside the SOZ using a two-tailed non-parametric Wilcoxon signed rank test with a confidence interval of 95%. A Wilcoxon rank sum test was carried out to compare the signal characteristics between fHFO and the other two groups across patients. The same test was also applied for the comparison between epilepsy and control cohorts.

## 5.3 Results

### 5.3.1. SOZ Identification and Functional Mapping Results

Demographic and clinical information for all subjects is provided in table 5-1. In each individual subject 28 – 120 channels were implanted. SOZ was visually identified by neurologists in 11 patients (P1 – P11) after electrode placement and the following long-term video EEG monitoring. In each patient, 2 – 14 channels where the earliest clear electroencephalographic discharges started were determined by the neurologists and marked as the SOZ. As a result, 92 out of 1,309 channels were defined as the SOZ,

accounting for 15% of the channels in P1 – P11, and 7% of the total recorded channels. After 12 – 24 months of follow-up, as of May 2017 all patients received significant seizure reduction with Engel class I or II outcome (Engel 1987). In P12 and P13 the SOZ could not be identified after initial implantation. In these cases the grid electrodes covered eloquent areas of the brain, and the data was used for functional HFO analysis only. Direct cortical stimulation (DCS) were performed in five patients with epilepsy (P9 – P13) and all control subjects (C1 – C5) intraoperatively to map the eloquent cortex. The total number of channels with functional response was 138, accounting for 11% of the recorded channels, with 2 – 34 contacts being identified per subject.

**Table 5-1 Patient demographic data**

ID	Age	Gender	Seizure type <sup>a</sup>	MRI <sup>b</sup>	Electrode type	Channel Number	SOZ <sup>c</sup>	Surgical outcome <sup>d</sup>
P1	30	M	FAS	RMTS	Depth, strip	28	RAH	I
P2	32	F	FAS	Normal	Depth, strip	56	LA, LAH, LPH, RA, RAH, RPH	I
P3	37	M	FIAS	LMTS	Depth, grid	54	LA, LAT	I
P4	15	F	FAS	TS	Depth	74	AMF, PMF	II
P5	18	F	FAS	LMTS	Depth	64	LPH, left uncus, left occipital-temporal	I
P6	35	F	FIAS	Left temporal grey matter heterotopia	Grid, strip	64	LST	I
P7	32	M	FIAS	RMTS	Grid, strip	48	Right temporal, LST, LLT, RAST, RPST	I

**Table 5-1 Patient demographic data (continue)**

P8	53	F	FAS	Normal	Grid, strip	40	LAT, LST, RAT, RPT	II*
P9	36	F	FAS	Normal	Grid	66	Left parietal- temporal	I
P10	3	M	FAS	CM	Grid	64	LA, LAH, LPH, RA, RAH, RPH	I
P11	36	F	FIAS	RMTS	Grid, strip	72	AST, PST	I
P12	49	F	FAS	Normal	Grid	54	Left cingulate gyrus	/
P13	36	F	FAS	Normal	Grid	120	Left temporal	/
C1	53	M	/	Right parietal LGG	Grid	32	/	/
C2	30	M	/	Left posterior frontal LGG	Grid	113	/	/
C3	40	F	/	Left frontal LGG	Grid	120	/	/
C4	42	F	/	Right frontal LGG	Grid	120	/	/
C5	45	F	/	Right posterior frontal LGG	Grid	120	/	/

<sup>a</sup> FAS: focal aware seizure, previously known as simple focal seizure; FIAS: focal impaired awareness seizure, previously known as complex focal seizure.

<sup>b</sup> L/RMTS: left/right mesial temporal sclerosis; TS: tuberous sclerosis; CM: cavernous malformation; LGG: low-grade glioma.

<sup>c</sup> L/RA: left/right amygdala; L/RAH: left/right anterior hippocampus; L/RPH: left/right posterior hippocampus; L/RAT: left/right anterior temporal; L/RPT: left/right posterior

temporal; A/PMF: anterior/posterior middle frontal gyrus; L/RST: left/right sub-temporal; A/PST: anterior/posterior sub-temporal.

<sup>d</sup> Surgical outcome is measured by Engel Classification. Class I: free from disabling seizures. Class II: Rare disabling seizures (almost “seizure-free”).

\* P8 has been treated with responsive neural stimulation system. The patient has received a significant reduction of seizure frequency since the device implantation.

### **5.3.2. Unsupervised HFO detection**

Across 18 subjects, a total of 28,832 events were captured in the 16.5 hours of recording during the amplitude-based detection stage, generating the initial pool of candidates. In each patient, the events in candidate pool were categorized into 2 – 4 clusters in 3D feature space using GMM method, which generally consisted of one-or-two clusters of HFOs, while other clusters turned out to be mixtures of irregular waveforms or artifacts. In the epilepsy group, one additional cluster of spikes was identified consistently per patient. This step helped us to successfully isolate HFOs from spikes and other events. The scatter plots of two representative patients (P3 and P9) showing the distribution of detected events in 3D feature space are given in figure 5-3. For each HFO cluster, four random event members and their filtered signal above 80 Hz are displayed together with the t-f maps, to give a flavor of the cluster content. For each patient, the spatial extent of HFO cluster is presented on the electrode sketch in the last column. Higher HFO rate is represented by darker shades. Although majority of the HFOs are located in the SOZ in P3, the large portion of HFOs recorded from the

functional area in P9 evidences that HFO rate alone will not be sufficient to identify the SOZ in certain cases.

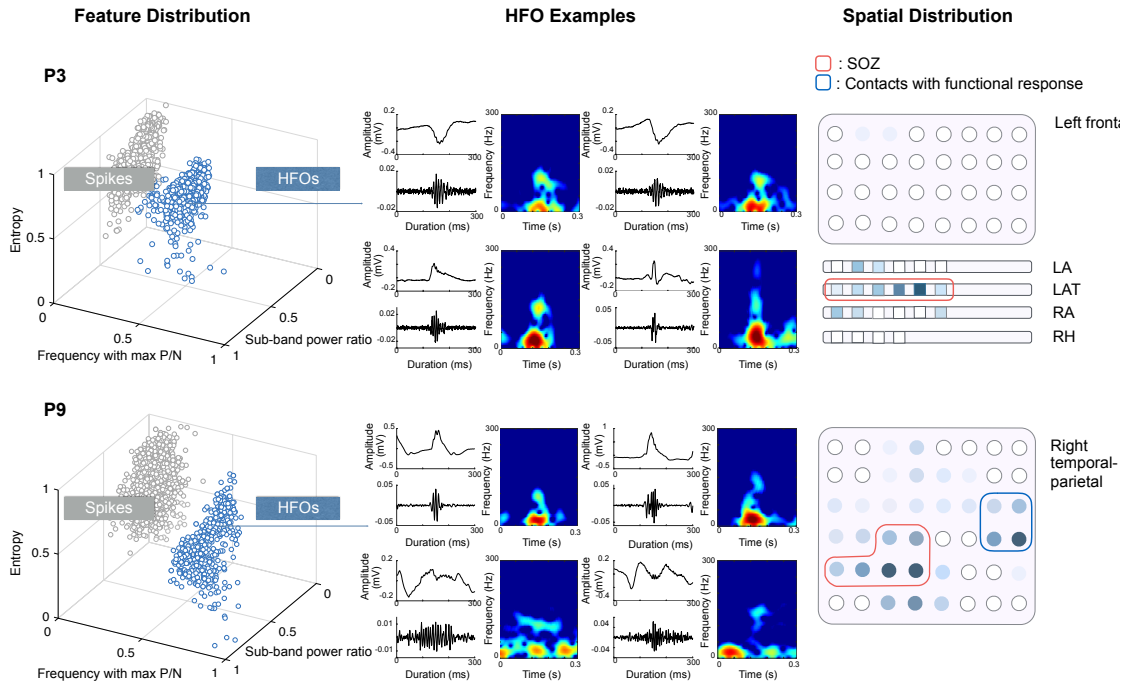


**Figure 5-3. Three-dimensional distribution of HFO and spikes identified by GMM clustering in 2 patients. In P9, the HFOs were generated from both SOZ (red line) and functional area (blue line).**

### 5.3.3. Comparison of HFOs Originating From Different Locations

In total, 13,011 HFOs were isolated by the unsupervised detection based on GMM and were investigated in the subsequent analysis. The number of HFO-generating channels in each patient ranged from 9 to 77. In epilepsy patients with clear SOZ definition (P1 – P11), HFOs were found in 60% of the channels. In P12, P13 and the control subjects (C1 – C5) where the electrode covered the functional cortex only, the HFOs were located in 38% of the recorded channels. Based on the SOZ delineation and

functional mapping results, the HFO candidates were first grouped according to their spatial locations. Overall, 41% HFOs were detected from the seizure onset channels in P1 – P11 and were named as sHFO. In these same patients, 32% percent of HFOs were detected from other brain regions excluding the SOZ and functional regions. These HFOs were denoted as oHFO. Finally, 19% of the HFOs were recorded from the functional regions such as motor or language cortex in 10 subjects where functional mapping was performed, and hence were labeled as fHFO.

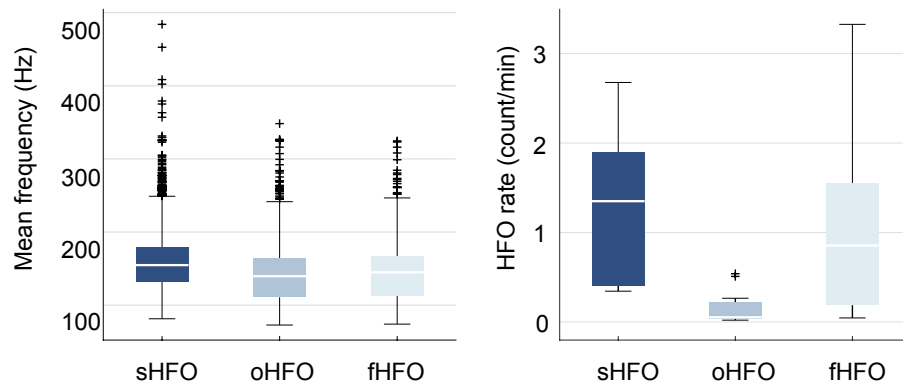


**Figure 5-4. Group comparison of sHFO, oHFO and fHFO. The mean frequency for sHFO was higher than oHFO and fHFO events. The rate for sHFO was higher compared to oHFO but not to fHFO events.**

In figure 5-4 we provide the boxplots showing the comparison among sHFO, oHFO and fHFO groups in terms of mean frequency and the rate of occurrence. The sHFO events possessed higher mean frequency compared to the other two HFO types (sHFO = 154 Hz, oHFO = 146 Hz, fHFO = 150 Hz,  $P < 10^{-3}$ ), with substantial overlaps across groups. The average rate per channel for sHFO = 1.2/min, which was significantly higher

than oHFO (0.2/min,  $P < 10^{-3}$ ) but comparable to fHFO events (1.0/min,  $P = 0.4$ ). The rate of fHFO was also significantly higher compared to oHFO ( $P < 0.01$ ).

#### **5.3.4. Stereotyped HFO Waveform Patterns**

We executed DBSCAN clustering in sHFO, oHFO and fHFO groups in each patient to identify subclusters of repetitive HFOs with similar morphometric waveform patterns, without prior knowledge on the shape of the raw signal. Highly stereotyped HFO waveforms in varying shapes were observed from single or multiple sources in individual patients. In figure 5-5 we present examples of repetitive HFO waveform subclusters and HFOs without a repetitive pattern in 5 patients. For each type of HFO, four individual samples and the pile plot of events in the same subcluster are shown along with the averaged t-f map. The origin of the presented HFOs are marked on the electrode contacts in red color if it's inside the SOZ, yellow if it's outside the SOZ, or blue if it's located inside the functional area. In P1, repetitive HFOs in different forms were generated by epileptic hippocampal structure. In P2, repetitive HFOs were generated by posterior hippocampus and amygdala, both of which appeared to be epileptogenic. In P3, highly similar ripples were found in the temporal lobe. These repetitive HFOs recorded from a subset of SOZ channels commonly associated with stereotyped waveform patterns in the form of slow waves, spikes or sharp waves resigning in the low band. In P9 and P10, while recurrent HFO patterns were seen in the SOZ (temporo-parietal and frontal region), the irregular HFOs were mostly seen in the functional motor cortex appearing more frequently with oscillating background activities and not correlated with the SOZ.

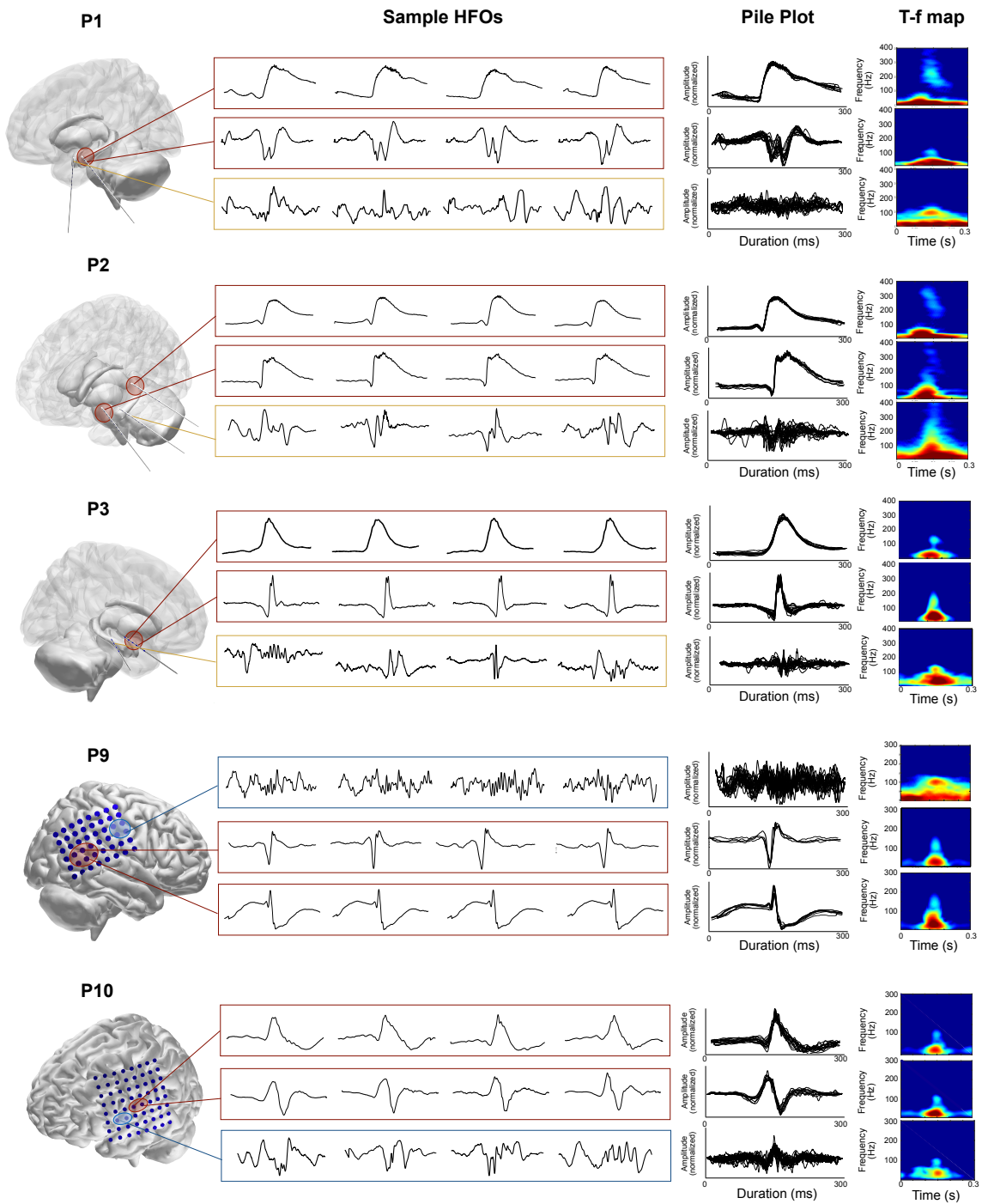


**Figure 5-5. Examples of HFO subclusters and their spatial locations in five patients. For each pattern, 4 sample events and the pile plot of the events in the same subcluster are shown with the averaged t-f map.**

In order to give more insight into these stereotypical waveform structures, we visualized the distance matrix of HFOs by plotting a circular network for each HFO group. In figure 5-6 (A), we first provide the results obtained from 13 HFO samples which were manually selected based on their waveform morphology. In the network, each node represents a HFO observation, which is connected to other samples by edges in different shades indicating the strength of the relevant connection. In our case, a strong connection provides smaller Euclidean distance demonstrating higher similarity between two HFO candidates. HFOs with very similar waveforms provide linkage in darker shades. The connectivity of subsets of events in one representative patient (P9) is shown in figure 5-6 (B), where HFOs were detected inside the SOZ, out of the SOZ, and from the functional sites of this patient, respectively. The result suggested a much stronger correlation between events in the sHFO group compared to oHFO and fHFO groups. The “gap” in the network graph indicates that at least two distinct patterns exist among the presented sHFO candidates, each of which shared compact intra-subgroup connectivity but barely correlated with the other pattern. Quite weak connectivity was observed in the fHFO network compared to the other two groups. These results suggested that with different distance thresholds SOZ could be distinguished from functional and other regions by investigating the HFO waveform similarity between the captured events.

Figure 5-7 (A) displays the curve of clustering ratio ( $N_{SC}$  vs.  $\epsilon$ ) for 3 representative patients. The number of subclusters ( $N_{SC}$ ) is normalized to the total number of events in each HFO group. For a distance  $\epsilon = 0$ , where the constraint is to have identical waveforms, the number of subclusters is equal to the number of events. As the  $\epsilon$  or the

radius of possible subclusters increased, the  $N_{SC}$  values started to decrease for all groups but dramatically faster for sHFO events, where we consistently observed subclusters of recurrent HFO waveforms for moderate distance values ( $\epsilon < 0.5$ ).

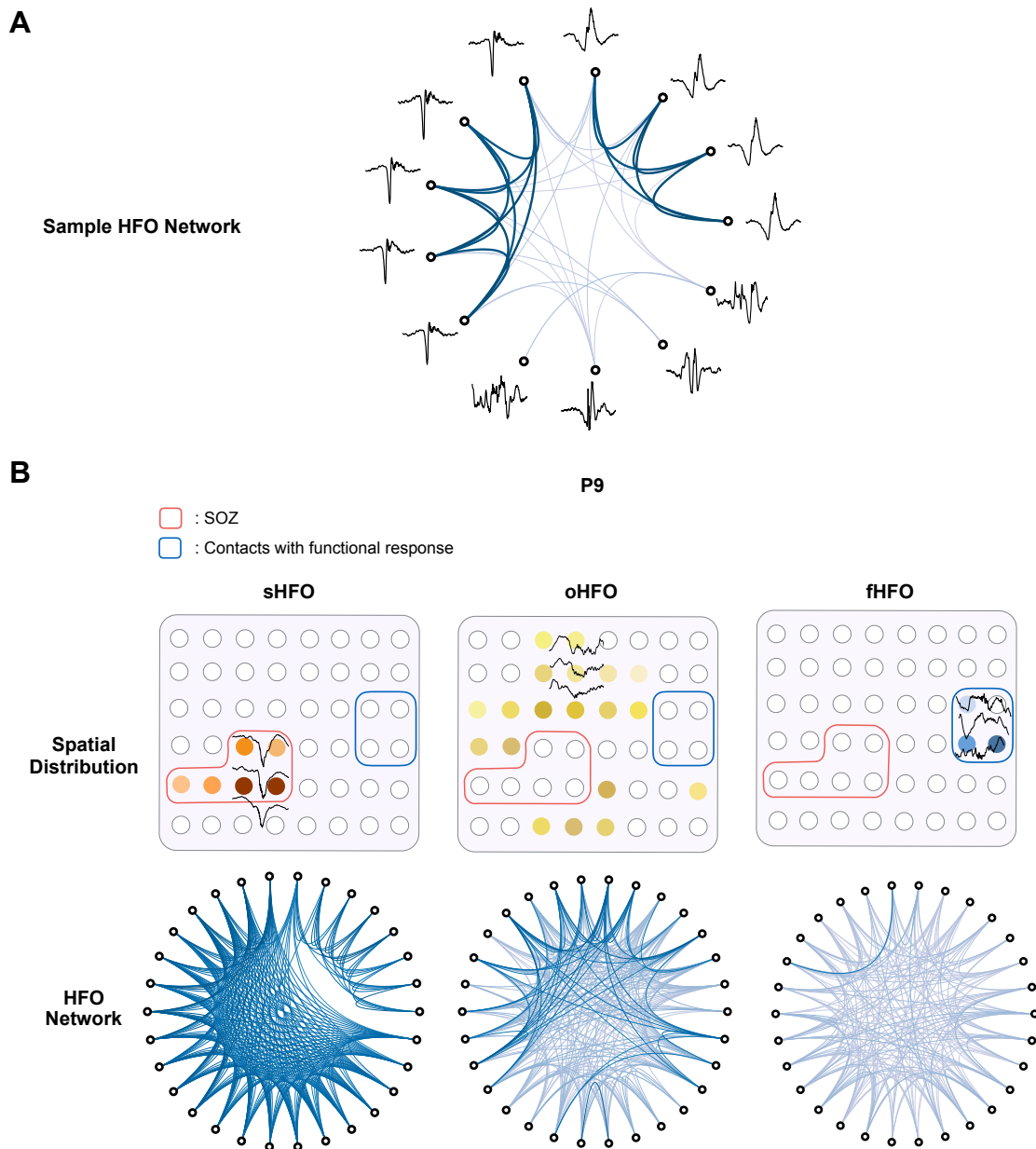


**Figure 5-6. (A) Circular network visualizing the distance matrix in 13 HFO samples. (B) Network plots in 3 groups, each being composed of 30 HFOs inside the SOZ, outside SOZ, and inside the motor area in P9.**

The averaged plots in figure 5-7 (B) were computed from sHFO and oHFO groups in 11 patients, and fHFOs in 10 subjects with functional mapping. We noted that, in all cases the  $N_{SC}$  values for sHFO exhibited a sharper decline as soon as the cluster radius reached a relatively small value ( $\approx 0.1$ ). For oHFO and fHFO groups, by contrast, the initial  $\epsilon$  where individual observations started to merge were significantly larger, as with the area under curve (AUC) ( $P < 0.01$ ), as shown in figure 5-7 (C). The difference was more evident between sHFO and fHFO groups ( $P < 10^{-3}$ ). The initial “plateau” in the curves of fHFO group implied a relatively large and uniform spacing of the members, which then gradually fell to the bottom. The comparison of initial clustering radius  $\epsilon$  between oHFO and fHFO also showed significant difference ( $P < 0.05$ ), suggesting that fHFO events may exhibit greater variability in signal shapes. These results indicate that epileptogenic brain regions tend to produce stereotypical HFOs with quite repetitive waveform morphology whereas the HFOs occurring in functional areas are relatively irregular in their wave shapes.

### **5.3.5. Comparison of HFOs in Epilepsy Patients and the Control Group**

We sought to determine whether the functional HFOs recorded from controls also followed the same irregular waveform characteristic with those recorded from patients with epilepsy. A total of 3,207 HFOs were recorded from the five control subjects and 73% of these HFOs were detected from the contact locations identified by DCS, whereas the remaining 27% of events were located at the surrounding cortical regions. The fHFOs recorded in control subjects were compared with the sHFOs in 11 epilepsy patients, as well as the other fHFOs recorded from the motor and language cortex of the five epilepsy

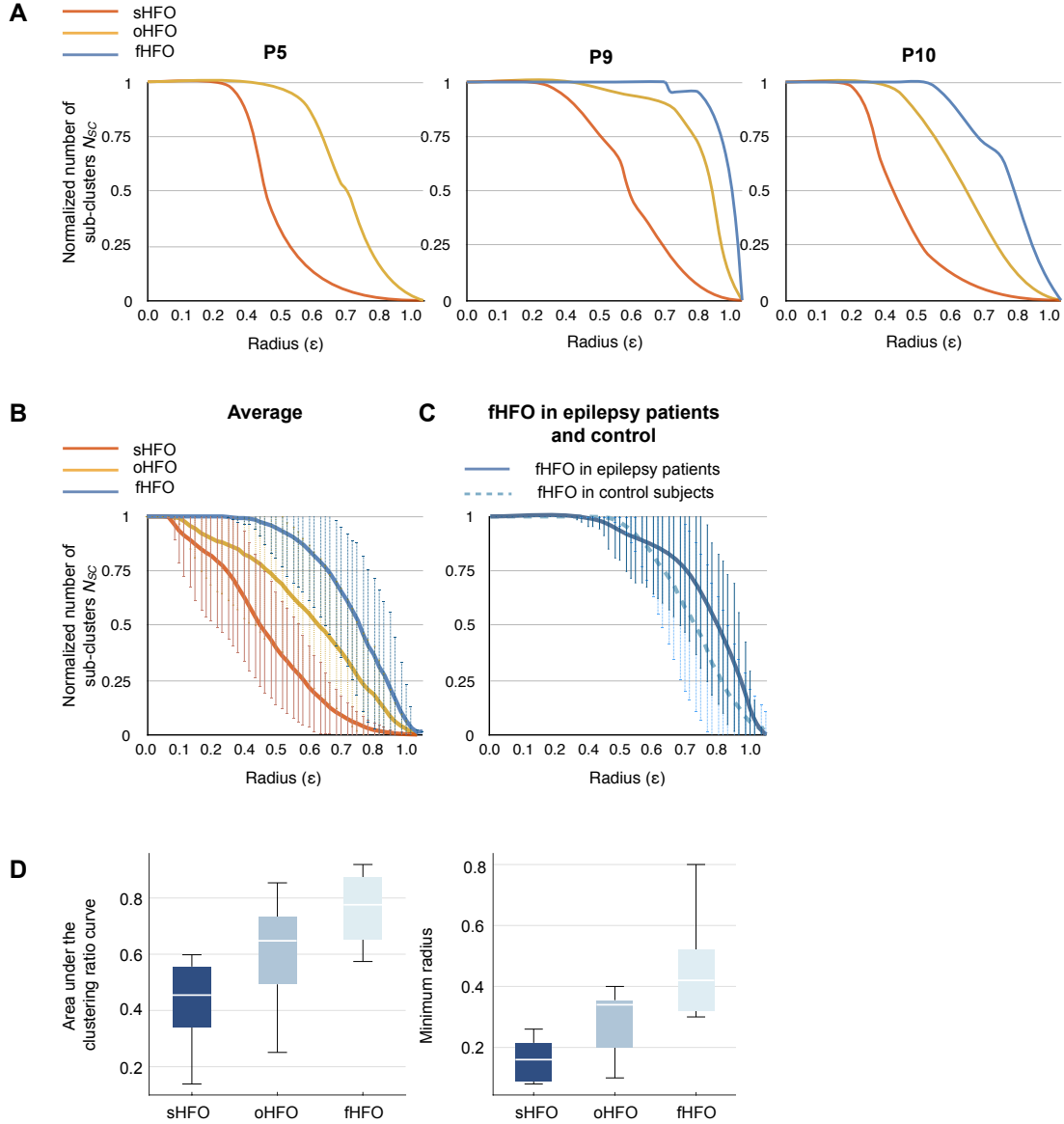


**Figure 5-7. (A) Clustering ratio curves for three representative patients. (B) The average clustering ratio plots. (C) The curves in fHFOs of epilepsy patients and controls. (D) Group differences in the AUC and minimum  $\epsilon$  to generate sub-clusters.**

patients. Figure 5-7 (C) demonstrates the clustering ratio curves of fHFO in epilepsy and control cohorts. The AUC and minimum clustering rate for fHFO in control cohort were comparable to that of the epilepsy cohort, both of which were significantly larger than

sHFOs ( $P < 10^{-3}$ ). Similar to the fHFO events of epilepsy patients, the fHFOs of control subjects did not build subclusters at low distances suggesting that their waveforms were random and non-repeating. These results indicated that fHFOs generated by the motor cortex in controls possessed similar characteristics with fHFOs of epilepsy cohort and could be differentiated from sHFOs by using the clustering ratio analysis.

### **5.3.6. Spatial Correlation of HFO Waveform Patterns with SOZ and Eloquent Cortex**

In order to explore whether the HFOs with repetitive patterns could distinguish the SOZ from functional regions, we identified stereotyped HFO waveforms within the entire HFO pool in those cases where the electrodes also covered the eloquent cortex. Based on the clustering rates given in figure 5-7 (B), at a radius of 0.5 we noted around 70% of sHFOs had been merged with other similar events forming subclusters, whereas 92% – 95% of fHFOs remained un-clustered. Consequently, we set the radius  $\epsilon$  to 0.5 and visually inspected the spatial distribution of clustered events and those ones which had not been assigned to any subcluster using  $\epsilon = 0.5$ .

Figure 5-8 provides representative data showing HFO distribution in those cases where the grid electrode covered SOZ and functional areas (P9 and P10) or functional areas only (P12 and C1). In the two patients where both SOZ and eloquent cortex were included, while the channels dominated by repetitive HFOs were found restricted to SOZ, the random shaped HFOs showed distinct spatial distribution suggesting a considerable portion of HFO activities located in the motor and language function areas, as well as the

- : SOZ
- : Contacts with function response
- : Central sulcus

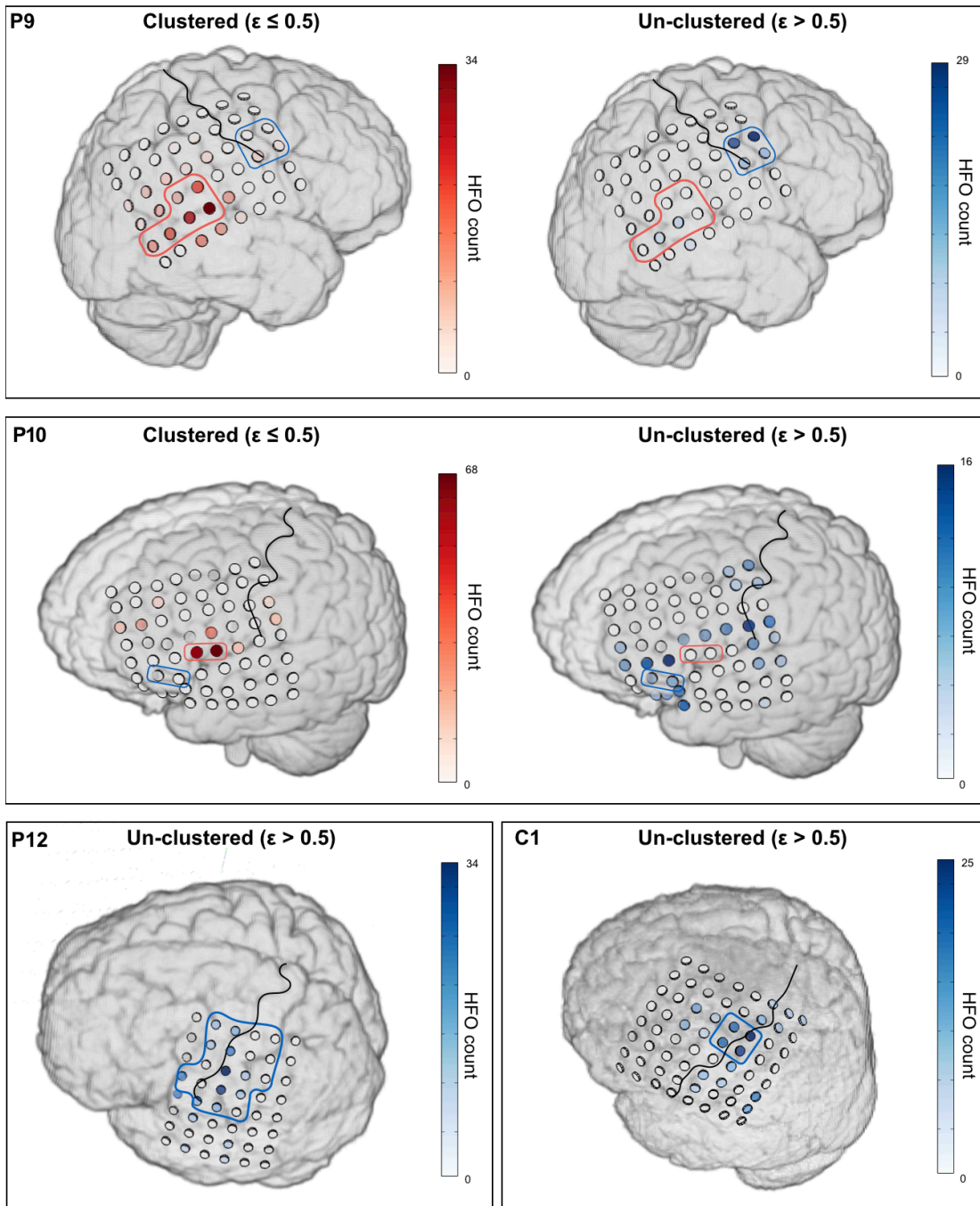


**Figure 5-8. Spatial projection of repetitive and non-repetitive HFOs in four patients. Using radius of 0.5, The un-clustered HFOs are spatially localized at functional cortex or brain regions distinct from the SOZ.**

surrounding eloquent regions. In P12 and C1, the spatial maps of un-clustered HFOs also pointed the functional motor areas identified by DCS.

Overall, the results indicated that at a radius of 0.5, the percentage of un-clustered HFOs originated from outside the SOZ was significantly higher than that of the clustered HFOs (56% vs. 32%,  $P < 0.01$ ). In P12, P13, and C1 – C5, where repetitive HFOs were rarely observed (less than 3%,  $\epsilon = 0.5$ ), the non-repetitive HFOs were concentrated around the motor cortex with majority of them falling into the functional regions defined by DCS mapping.

### **5.3.7. Localizing the SOZ Using Stereotyped HFO Waveforms.**

We observed an association between the degree of HFO signal similarity and ictogeneity, as events clustered by a smaller  $\epsilon$  generally pinpointed those channels with higher seizure frequency. Figure 5-9 illustrates an example of HFO subcluster automatically identified by using different radius (0.15, 0.3 and 0.5) in P9. The SOZ is represented by red dashed lines, while contacts locations generating most of the seizures are marked with red solid lines. Interestingly, the spatial distribution of highly repetitive HFOs clustered by a smaller radius also reflected the epileptic brain structures generating most of the seizures.

To investigate to what extent the identification of repetitive HFOs can contribute to the accurate delineation of the SOZ, we detected the stereotypical HFOs for each patient (with SOZ definition) at varying cluster radius (similarity levels). By using the channels involving stereotyped waveforms, the sensitivity, specificity and accuracy were computed

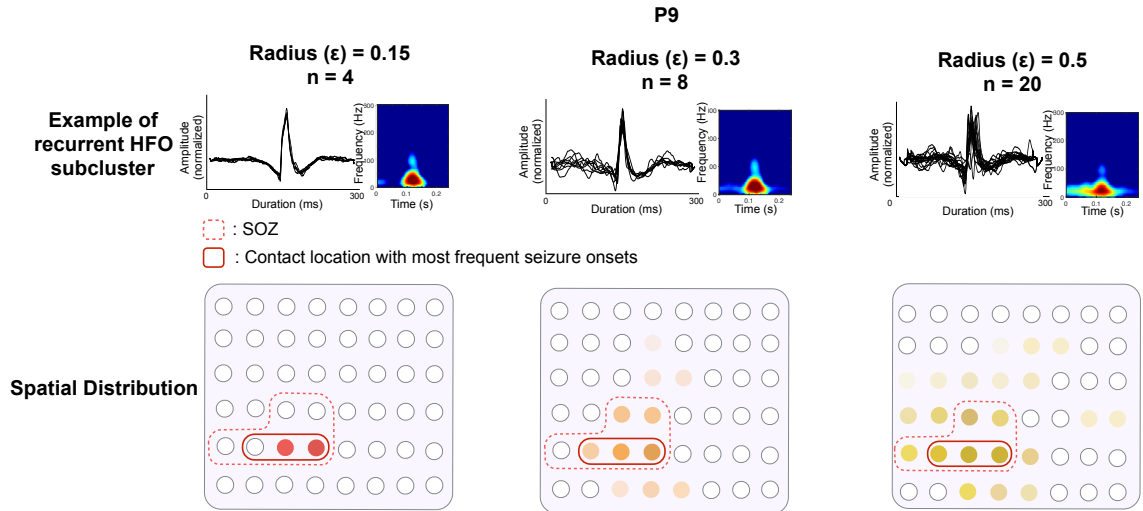


**Figure 5-9. Spatial association of “cloned” HFO waveforms and the SOZ. As the intra-cluster similarity decreases, the clustered HFO provides a larger spatial expansion that extends beyond the SOZ.**

at each radius for SOZ identification. In figure 5-10 we give the results of specificity, accuracy, and the proportion of repetitive HFOs occurring inside the SOZ at each  $\epsilon$  in P1 – P11. Consistently in all patients, the spatial distribution of stereotyped HFOs presented agreement with clinician defined SOZ. A specificity of 100% and an accuracy of 86% was achieved when the “most compact” HFO subclusters were used for the SOZ prediction. In other words, all of the HFOs firstly being clustered were generated by the seizure onset regions. The averaged sensitivity was low in this case (24%, ranging from 11% to 100%), as expected, because the initially identified HFO patterns consisted of small number of events spatially concentrated to 1% – 5% of the total channels, making up 0.1% – 1% of the entire HFO pool (3 – 7 events per subcluster). Nevertheless, the origin of HFO subclusters with smallest diameter precisely pointed the locations responsible for the initiation of most seizures. As the cluster radius increased to 0.5, the proportion of HFO inside the SOZ decreased by 10% – 87% per patient, leading to an

overall specificity of 63% (20% – 87%), a sensitivity of 85% (38% – 100 %) and an accuracy of 65% (25% – 80%). Further increase in the radius caused significant drop in the accuracy, especially in P6 where the HFOs were predominantly originated from left inferior frontal region independent from the SOZ (left mesial temporal lobe), and in P9 – P11 where the electrodes covered both SOZ and functional regions. Using  $\epsilon = 1$ , as the entire HFO pool was taken into consideration for SOZ localization, the specificity and accuracy reduced to 44% and 52%, respectively. These results suggested that the radius to detect stereotyped HFO waveforms had to be adapted to each case for the accurate prediction of the SOZ.

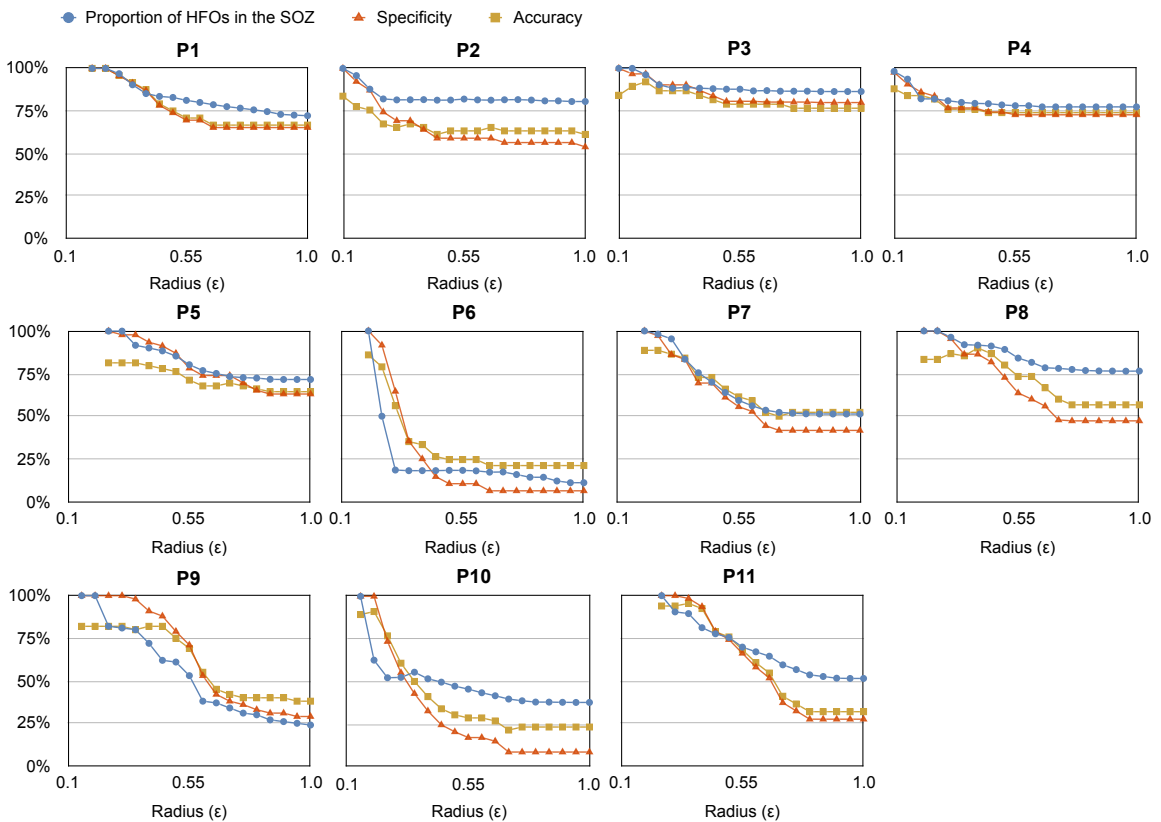


**Figure 5-10. SOZ identification performance using HFOs clustered by using radius ( $\epsilon$ ) ranging from 0.05 to 1. As the radius increases to 1, the overall specificity and accuracy decrease considerably.**

### 5.3.8. Stereotyped Ripple and Fast Ripple Oscillations

Finally, we explored the spectral content of HFOs clustered by DBSCAN in all subjects, in order to characterize the rate of repetitive HFOs in ripple and FR ranges. Fig. 8 summarizes the proportion of stereotyped ripples versus FRs clustered by using radius ranging from 0.1 to 0.4. Further increase in the radius resulted in the mixing of ripple and FR events and hence was not investigated. At each  $\epsilon$ , the clustered HFO events were visually inspected by an expert and then were assigned to ripple or FR category based on the t-f maps showing their spectral peaks in the high-band. Using  $\epsilon \leq 0.4$ , the algorithm identified 683 stereotyped FRs in four patients. The initial subclusters identified by the algorithm were comprised mostly of HFOs above 200 Hz, suggesting that FRs represented the most stereotypical HFO patterns in these patients. As the cluster radius gradually increased, the number of clustered ripples started to grow and eventually dominated the repetitive HFO category. These results indicated that compared to ripples, the presence of repetition in FRs were more evident in these patients, as majority of the

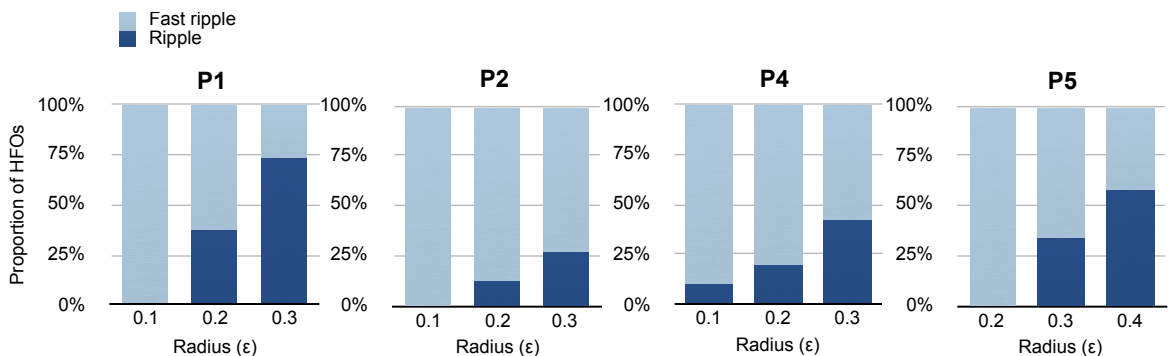


**Figure 5-11. Proportion of stereotyped FR versus ripple clustered by different radius. FRs were recorded in four patients, and consistently presented a higher degree of signal similarity compared to ripples.**

FRs formed sub-groups with small radius that were identified by the algorithm at the first place.

#### **5.4 Discussion**

As many of the previous studies have shown, the brain regions with high rate of HFO activity often correlate with epileptogenesis (Bragin et al., 1999; Jacobs et al., 2008a; Worrell et al., 2008a), and a complete resection of HFO-generative sites is likely to provide favorable surgical outcomes (Cho et al., 2014; Jacobs et al., 2010; Wu et al., 2010). Nevertheless, not all kinds of HFOs were specifically linked to epileptogenicity, since they can be recorded from normal (Buzsáki and Silva, 2012) or functional areas (Bragin et al., 2007; Girardeau and Zugaro, 2011; Köhling and Staley, 2011; Staba et al., 2002). The fact that channels with the highest HFO rate may correspond to non-epileptic functional areas increases the complexity of HFO application in epilepsy presurgical planning. Because injury to the eloquent regions may cause irreversible neurologic impairment to the patient, it is paramount to develop methods that could efficiently and reliably identify pathological HFOs specific to the epileptogenic zones.

In the present study, we investigated HFOs automatically detected from 13 patients with focal epilepsy and five control subjects without epilepsy. HFOs were simultaneously detected from inside and outside the SOZ as well as the functional regions. HFOs were firstly categorized into three groups based on their spatial origins. Events in sHFO group were generated from epileptogenic zone identified by neurologists through intracranial video EEG monitoring. The other two groups, namely oHFO and fHFO, were extracted from regions outside the SOZ and from functional sites as defined by direct cortical

stimulation respectively. We explored the characteristics of these three groups of HFOs in terms of their traditional features such as frequency and rate of occurrence. The results were concordant with previous studies pointing out that sHFOs had higher frequency than those detected from outside the SOZ (Matsumoto et al., 2013). However, the fact that there are substantial overlaps observed across these groups supported the view that spectral frequency is not a prominent feature to determine the pathological nature of HFOs (Engel et al., 2009), or to assist in the discrimination between SOZ and eloquent cortex. Previous modeling works suggested that both epileptic and physiologic processes can produce HFOs with identical peak frequencies (Stacey, Krieger and Litt, 2011). Mixed events recorded using micro- and macro-electrodes also suggested that epileptic HFOs might overlap with physiological HFOs in both ripple and FR bands (Blanco et al., 2011; Le Van Quyen et al., 2010; Worrell et al., 2008a, 2004b). Therefore, restricting the peak frequency of HFOs alone is not sufficient to assure that they are specific to SOZ. On the other hand, in our data the HFO rate presented significant difference between sHFO and oHFO groups, which was consistent with previous studies demonstrating a strong correlation between HFO rate and the SOZ (Allen et al., 1992; Jirsch et al., 2006; Urrestarazu et al., 2006; Zijlmans et al., 2011). Nonetheless, the difference in event rate between sHFO and fHFO groups showed no statistical significance, demonstrating that the rate alone may not be an accurate indicator to distinguish between SOZ and eloquent regions. It has been addressed, that the use of HFOs in brain structures such as mesial temporal lobe is limited by the inability to separate pathological HFOs from physiological activities generated over the same areas. Thus, an area with high HFO rate

may not only represent an active epileptogenic region but also indicate active memory processing, which makes the current use of interictal HFOs for clinical decision premature (Jacobs et al., 2012). Consequently, any process to utilize HFOs for clinical decision making must account for this fact that there will always be a channel with the highest HFO rate, even if the recording site does not include the SOZ. Besides the spectral peak and rate of the event, other properties such as signal amplitude and duration have also been investigated in studies, but the significantly overlapped distribution highlighted the fact that the use of conventional features was not adequate to separate pathological and physiological HFOs.

Recently, several studies suggested to distinguish pathological HFOs from different perspectives by looking into the interaction between high-band and low-band components of the signal. The investigators showed evidence that pathological HFOs commonly occurred before the peak of “down” stage of slow waves (Von Ellenrieder et al., 2016), or modulated by slow activities within 3 – 4 Hz (Nonoda et al., 2016). Yet these studies are limited by the restriction of the patients’ states (NREM sleep) as well as the HFO identification process (visual review). In the current study we detected “clones” of HFO events by applying a density-based aggregated clustering method without presumption of any specific waveform pattern, and presented evidences that sHFO group included small subclusters of stereotypical waveforms whereas the fHFO waveforms were more irregular. The stereotyped patterns in sHFO were identified in all patients with SOZ regardless of the disease phenotype or implantation modalities. These results suggested that HFOs generated by epileptic tissues may present in a variety of morphological

patterns such as on top of slow/sharp waves or spikes but tended to be re-occur constantly throughout the recording. The oligomorphic waveform distribution of epileptic HFOs makes them distinguishable from non-epileptic HFOs, as the values of minimum radius necessary for detecting repetitive event subclusters and the areas under the clustering ratio curve in sHFO and fHFO groups showed very limited overlap. Examining the waveform patterns in the time domain enabled the separation of time-series data with morphological distinctions, which might otherwise overlap in the frequency or time-frequency domains. Our results did not rule out the possibility that a random HFO pattern may still associate with epileptic network, however it is conceivable that HFOs associated with a stereotypical pattern is more likely to be introduced by pathological circuits. Our observations also offered practical implications into the clinical utilization of HFOs to guide the epilepsy surgery. The unsupervised identification of repetitive HFO waveforms can be applied as a universal method without the aid of prior knowledge of any specific wave shape, which makes the approach more robust to interpatient variation. These findings, when combined with appropriate methodologies, can provide an excellent tool for one to efficiently locate the “core” HFOs that are highly indicative of the SOZ and separate them from eloquent cortexes and other non-SOZ regions.

On the other hand, the most heterogeneous HFO patterns were seen in fHFO groups where the events were detected from functional structures distinct and distant from the SOZ (P9 – P13), as well as in the control subjects without seizure history (C1 – C5). The inclusion of the control group provides important data regarding the spatial distribution of HFOs in patients without epilepsy. We note that, the clustering rate for fHFOs in control

cohort was very similar to the epilepsy cohort indicating that the nature of physiological HFOs are similar in these groups and repetitive waveforms barely originate from functional areas detected in these subjects.

By blindly detecting stereotypical waveforms among all HFO candidates, we demonstrated that HFOs with repetitive waveform patterns were specifically associated with epileptogenicity. When used for SOZ localization, the highly stereotyped HFO waveforms provided direct information of ictogenesis with a specificity of 100%. More importantly, we showed that the spatial origin of the most compact stereotypical HFO subclusters consistently linked to SOZ also in difficult cases where multiple HFO generating sites were covered by electrodes, and where the HFO rate estimated from the entire pool was not a good discriminator for SOZ and other areas of the cortex. For instance, we noted that in those cases (P9 – P11) where the electrodes covered both SOZ and functional regions, the detection of stereotyped HFO events with highest degree of similarity made more significant difference in the accuracy of SOZ identification compared to those cases (P1 – P5) where the electrodes were sitting in deep brain structures and the surrounding areas.

Our data showed that the rate and compactness of repetitive HFO waveforms is also related to the spectral content of the event. In particular, our method detected FRs in four patients, where we consistently observed a higher degree of waveform similarity compared to ripples, supporting the view that FRs might be better indicators for epileptogenesis (Bikson, Fox and Jefferys, 2003; Jacobs et al., 2010; Köhling and Staley, 2011). Early observations raised the hypothesis that FRs were distinctly pathological

transients associated with epileptic brain (Bragin et al., 1999). From a cellular perspective, each pathological HFO event appears to represent co-firing of small groups of principal cells, which are pathologically interconnected (Bragin et al., 2007; Foffani et al., 2007). Previous studies showed evidence that ripples were associated with rhythmic firing of presumed interneurons whereas FRs were believed to reflect abnormal synchronous burst firing of small independent neuronal clusters of principal neurons in areas of seizure onset. It has been demonstrated that FRs are generated by the bursting activity of hyperexcitable principal cells whereas larger networks contribute the generation of ripples other than FRs. We speculate that the higher rate of stereotypical waveforms with more compact structure in FRs could be due to involvement of small clusters of neurons and related bursting patterns. The larger networks involved in ripple generation might increase the randomness in waveform structure. Compared to FRs, ripples are less preferred as clinical biomarkers because they are commonly generated from a larger area including both seizure foci and non-epileptic functional brain sites (Engel et al., 2009; Grenier, Timofeev and Steriade, 2003). It is likely that these physiological ripples will interfere with the HFO interpretation, and most of the proposed clinical studies, particularly the ones with automatic HFO detectors applied, investigated a mixture of both physiological and pathological activities (Kerber et al., 2014). It is noteworthy that in our results the highly repetitive waveforms did not exist solely in FR but also in ripple oscillations. We therefore speculate the repetition in HFO is associated with enhanced pathological synchronization in neuronal populations, thus may reflect the underlying neuronal substrates of epileptogenesis. This finding may introduce new

avenues to describe pathological and physiological HFOs other than the current spectral-based characterization.

Our analysis of the multichannel iEEG data was executed using all recorded channels in a fully-automatic fashion, which differs from most of the previous studies where the investigators commonly use retrospective visual review to select HFOs from limited datasets (Worrell and Gotman, 2011). While recognizing that there is no clear demarcation between “pathological” and “physiological”, so as the “ripple” and “fast ripple” HFOs, we sought to uncover the distinction between presumed HFO subclasses by utilizing unsupervised clustering technique to “let the data speak”. It is expected that the characterization of “cloned” signal patterns can give additional clues toward the detection and discrimination of multiple types of signature neuronal activities in human iEEG without manual labeling process which might potentially put bias towards the examination. The method may benefit from the use of an extended length of recording, and need to be validated with larger patient cohort.

# **CHAPTER 6 TEMPORAL CHARACTERIZATION OF HFO AND EARLY PREDICTION OF THE SEIZURE ONSET ZONE IN TEMPORAL LOBE EPILEPSY**

## **6.1 Introduction**

Surgical resection of epileptogenic zone, defined as the cerebral tissues responsible for the generation of ictal activity, has the potential to eliminate seizures and produce seizure freedom in patients with drug-resistant epilepsy. The successful localization of seizure onset zone (SOZ) can be achieved by intensive visual inspection of intracranial EEG (iEEG) recordings obtained during video-iEEG monitoring of an prolonged period of time to ensure that numbers of habitual clinical seizures have been recorded. The time of hospitalization in the epilepsy monitoring unit (EMU) is often undefined, which adds to the risk of complications, increases the cost and places a high demand on the clinical service (Nagarajan et al., 2015). It is an essential need to conduct research involving translational biomarkers for the fast and accurate identification of seizure generating zone to reduce the associated medical risks and expenses.

The increasing number of high frequency oscillation (HFO) studies using macro-electrode recordings allow the correlation of clinical EEG events with HFOs recorded from the same locations, and potentially facilitates the SOZ delineation based on HFO findings. However, the visual identification of HFO has been impeded by the transient appearance and narrow-band nature of the signal. For this reason, majority of the past research primarily investigated HFO activities using iEEG data of relatively short length

(1 – 10 minutes per patient) to reduce the highly intensive labor work (Andrew et al., 2007; Jacobs et al., 2008a; Schevon et al., 2009b; Staba et al., 2002, 2004; Urrestarazu et al., 2006; Zelmann et al., 2012). Data collected during non-rapid eye movement (NREM) sleep is preferentially used, as prior studies analyzing HFOs detected in 10-minute data segments pointed out the HFO rates during sleep appeared to be higher compared to waking states (Staba et al., 2004). These studies successfully demonstrated the advantage of using HFOs as a spatial markers that are specific to SOZ, but methodological challenge in large scale data processing has limited the progress in the temporal characterization of these standalone signature events.

Early seminal research using data in vitro suggested a significant increase in both ripple and FR rates before seizures (Khosravani et al., 2005). Similarly, several studies investigating HFO temporal changes in human subjects also observed increased high-band power 8 – 10 seconds before the seizure onset (Khosravani et al., 2009), supporting the hypothesis that HFOs are highly associated with ictogenesis. On the other hand, later studies investigating HFO temporal distribution using data of 15-30 min showed highly variable changes in all patients where no clear systematic trends could be demonstrated (Blanco et al., 2011; Dümpelmann et al., 2015; Pearce et al., 2013). There have been very few studies evaluating the temporal stability of HFO using prolonged data segments of multiple hours. Elucidation of the long-term dynamics of HFOs is still one of the biggest challenge that need to be resolved (Jiruska et al., 2017).

In the current study we investigated the spatiotemporal properties of HFO by conducting automatic HFO detection using long-term continuous iEEG data collected in

6 patients with mesial temporal lobe epilepsy, with particular intentions to clarify whether HFOs can be used prospectively as a screening technique to predict seizure and thus shortening the undefined invasive monitoring period. Based on prior studies of individual cases and preliminary observation of the data, we developed our hypotheses that i) HFO rates present variability across time and exhibit changes during the transition of baseline to pre- and postictal status, ii) using iEEG data of longer intervals gain advantages over 10-minute segments in terms of HFO detection, and iii) HFOs detected in hours of data collected at the beginning of EMU monitoring provide critical information and can be used for SOZ early prediction.

## **6.2 Materials and Methods**

### **6.2.1. Data Description**

Multi-channel iEEG data was collected from 6 patients (P1 – P6, 4 females, ages 28 – 34) with temporal lobe epilepsy refractory to anti-epilepsy drugs from University of Minnesota (MN, USA). All patients underwent intracranial EEG monitoring simultaneously with video monitoring in the context of presurgical workup. In each patient, 4 – 8 depth electrodes consisting of 4 – 10 stainless steel contacts with 5 mm spacing (Ad-Tech, Racine, WI, USA) were implanted bilaterally to the medial temporal structures where the neurologist speculated to be ictogenetic, with 28 – 72 channels being recorded per patient. The sleep stage was visually annotated by neurologists based on the combined information of EEG and video recording. Data acquisition was conducted by University of Minnesota using XLTEK EMU128FS (Natus Medical Inc, CA) with 2 kHz

sampling frequency and an anti-aliasing filter set to 1 kHz. Data collection and scientific workup was approved by the University of Minnesota Institution Review Board. The description of demographical information, seizure types and SOZ are given in table 6-1.

**Table 6-1. Patient demographic data**

ID	Sex	Age	Seizure types <sup>a</sup>	SOZ <sup>b</sup>	MRI	No. of Sz	Day of monitoring	Day of 1st Sz	Surgery Outcome <sup>c</sup>
P1	M	30	FAS	RHA	Right mesial temporal sclerosis	6	6	Day 4	Engel class I
P2	F	32	FAS	LA, LAH, LPH, RA, RAH, RPH	Foci of cortical thinning in the LFO and LT	6	5	Day 3	Significant reduction of seizure frequency*
P3	F	28	FAS	LA, LAH, LPH	Left mesial temporal sclerosis	4	7	Day 5	Engel class I
P4	F	28	FIAS	LAT, LMT, RMT	Normal	11	9	Day 4	Engel class I
P5	M	33	GTC	RMT, RAT	Normal	3	7	Day 6	Engel class I
P6	F	34	FIAS	RAH, RPH, RPT	Normal	7	8	Day 6	Engel class I

\*P2 has been implanted with responsive neural stimulation system because of bilateral temporal onset seizures. Post-surgery outcome based on clinical report and follow up of the patient. <sup>a, b, c</sup> See table 3-1.

### 6.2.2 Delineation of the Seizure Onset Zone

All patients involved in this study went through 6 – 9 days of intracranial EEG monitoring. For each individual patient, 3 – 11 clinical and subclinical seizures were recorded during the EMU monitoring period. In all patients, the first seizure generally

occurred after 3 – 6 days of monitoring. Data were retrospectively analyzed after the detailed review and determination of the SOZ performed independently by two neurologists. The ictal iEEG onset of a seizure was defined as the time of the earliest iEEG signal change (a clear electrographic seizure discharge) as annotated by the clinicians, and the corresponding electrode contacts were thereby determined as the SOZ.

### **6.2.3 HFO Detection**

The HFO detection was implemented using an unsupervised clustering based approach depicted in Chapter 3. To concisely summarize, after converting the raw iEEG signal to bipolar montage by subtracting the data from adjacent contacts, in the first stage all anomalies were detected and extracted through an amplitude-based initial detector and sieved according to a set of HFO selective criteria which were established upon the broadly accepted definition of an HFO, namely, an oscillatory neuronal activity possessing a minimum of 4 oscillatory cycles that are clearly distinct from background activities, with a duration of approximately 20 – 100 ms. In the next stage, all accepted event candidates went through the feature extraction step and were passed to the final clustering step in order to separate HFOs of interest, recognized as an isolated energy “blob” concentrated in the high-band beyond 80 Hz in the time-frequency representations, from other activities such as inter-ictal spikes and arbitrary waveforms or artifacts. The method is capable of simultaneously grouping spikes, ripples and fast ripples in an automated fashion. The algorithm has been validated for the accurate and efficient quantitative detection of HFOs (Liu et al. 2016). All data analysis procedures are implemented in Matlab environment (Mathwork, MA) using a self-developed

software package dedicated for data exploration, event navigation and the three-stage detection.

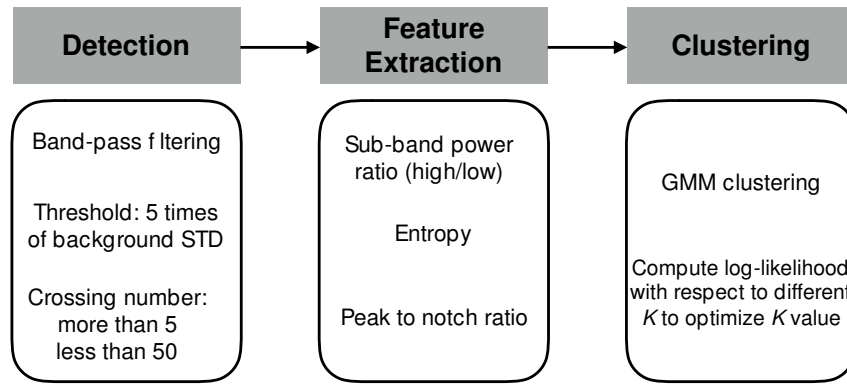


**Figure 6-1. Schematic diagram of the HFO detection algorithm.**

#### 6.2.4. Temporal Characterization of HFO

In each patient, two successive hours of iEEG data segment recorded at the immediate beginning of the intracranial monitoring were extracted as “initial baseline” (IB). In addition, we used two hours of data recorded during NREM sleep on the first day of monitoring, as well as 60 minutes before and after each seizure, defining them as sleep baseline (SB), preictal, and postictal states, separately. Data of extended length (2 hours) was used as baselines for the purpose of examining the HFO temporal progression in a longer period of time after the surgical implantation of intracranial electrodes and during sleep. Data of a shorter interval (1 hour) was chosen for pre- and postictal analysis to avoid any overlap in time between two seizures.

After executing the unsupervised detection algorithm, temporal variation of the events was computed from the clustering results in terms of detections per bipolar

channel-pair and the corresponding time stamp for each detected event. Considering that most of the past studies have recommended the use of 10-min data epochs for HFO analysis, for each 2-hour baseline segment we computed the total numbers of FR, ripple and spike recorded from all regions, as well as the number of events detected in the SOZ channels only, using 10-minute window bins. Same estimation was conducted for pre- and postictal states of each seizure in all patients, to study the temporal changes in the presence of HFO and spike activities after electrode implantation, during sleep, and during the interictal-to-ictal transition.

#### **6.2.5. Early Prediction of the SOZ**

Given the observed variability in the temporal distribution of HFOs, we speculate that the localization of SOZ may benefit from HFO analysis using a prolonged iEEG data epoch rather than a randomly selected 10-minute data chunk, either during awake or sleep states. We therefore computed the SOZ localization accuracy using FR, ripple and spikes captured during the 120 minutes of IB (i.e. the first two hours of EMU monitoring) for each patient. In order to answer if there is noticeable improvement in the performance of SOZ localization compared to the use of data in discrete windows, the localization accuracy was computed in a cumulative fashion based on the spatial distribution of detected events aggregated every 10 minutes.

Specifically, in each individual patient, information regarding the contact locations where seizures were believed to originate were provided by epileptologists, and were defined as seizure onset channels. For all types of events (i.e., FR, ripple, and spike), we used bipolar channel pairs introducing majority of the events as HFO/spike generative

channels (positives), and cumulatively computed the overlapping rate of the predicted channels with the SOZ channels using 10-minute discrete windows. We hypothesized that studying the iEEG data recorded during the beginning 1 – 2 hours of EMU monitoring should be sufficient for the investigation of HFO (especially for FR) and thereby provide substantial evidence for the localization of SOZ.

### 6.2.6. Statistical Analysis

To evaluate the performance of the SOZ prediction using FRs, ripples and spikes, we computed the accuracy (ACC) and Matthew correlation coefficient (MCC) (Matthews 1975) over each inspected epoch. Channels generating less than 5% of the total number of accumulated events were disregarded. The prediction was considered true positive if it was in agreement with the seizure onset location, or false positive if it lied outside of the SOZ. The ACC and MCC are defined as:

$$ACC = \frac{TP + TN}{P + N} \text{ and} \quad (6-1)$$

$$MCC = \frac{TP \times TN - FP \times FN}{\sqrt{(TP + FP) \times (TP + FN) \times (FP + TN) \times (TN + FN)}} . \quad (6-2)$$

In this equation, TP stands for true positive, TN for true negative, FP for false positive, and FN for false negative. Both ACC and MCC take benefit of all the information in the contingency table (confusion matrix) and as such are more representative and comprehensive in terms of performance evaluation. In particular, the MCC value ranges from -1 to 1, with the minimum value of -1 representing a negative correlation, 0 a random prediction and 1 a perfect correlation. The MCC was computed in

addition to the ACC because it is generally regarded as a good measure when the two classes (i.e., SOZ and non-SOZ channels) are largely imbalanced (Powers 2011).

The non-parametric Mann–Whitney U-test was taken for the group comparison between the HFOs rates in IB and SB, as well as pre- and postictal periods of each seizure in each patient. Same test was performed to evaluate the cumulative prediction improvements using data of 10 – 120 min in IB, with significance level  $P < 0.05$ .

## **6.3 Results**

### **6.3.1. Automatic Detection of HFO and Spike**

Overall, 98 hours of multichannel iEEG data was used for the automatic detection of HFO and spikes, consisting of 24 hours of baseline data (including SB and IB) recorded on the first day of monitoring, 37 hours of pre-ictal, and 37 hours of post-ictal data for each seizure. The total number of electrode channels being involved in this study was 310, the average number of recorded channel per patient was 52.

Over 150,000 event candidates were accepted after the initial detection and sieving stages and were clustered in the final phase. In each patient, the algorithm successfully isolated one or two HFO clusters from spikes and other arbitrary events. As a result, the automatic detection algorithm identified 16,572 FRs, 49,964 ripples and 45,550 spikes in 6 patients, making up 11%, 33% and 30% of the entire candidate pool respectively, with the rest 25% being clusters of irrelevant noise/artifacts.

### 6.3.2. Spatial Characterization of Detected Events

In each patient, 2 to 9 channels were determined as SOZ, accounting for 10% of the total recorded channels. As a result, 91% of the detected FRs, 45% of the ripples, and 50% of the spikes were located inside the SOZ. In figure 6-2 we present boxplots demonstrating the proportion of FR, ripple and spike inside the SOZ in IB, SB, pre- and postictal periods. Regardless of the different states, the percentage of FR locating inside the SOZ was significantly higher than both ripple and spike populations ( $P < 0.001$ ).

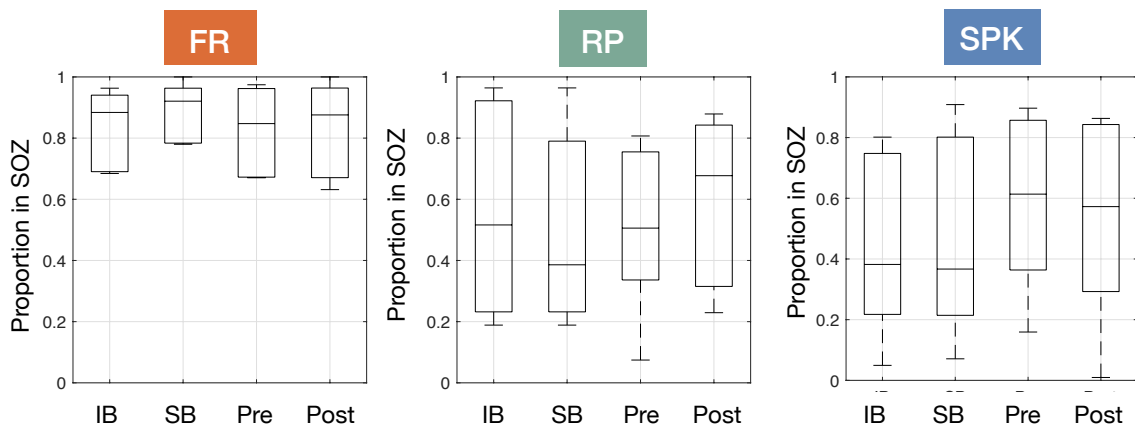


**Figure 6-2. Spatial distribution of FR, ripple and spike in different states. Compared to ripples and spikes, majority of the FRs were detected inside of the SOZ .**

### 6.3.3. Comparing the Event Rates In Different States

Temporal distribution of HFO and spike was evaluated for each individual patient using iEEG data during the 2-hour baselines, 1-hour data prior to each electrographic seizure onsets, and 1-hour after seizure termination. All data were used as the input, without manual selection of corrupted channels (if any). In figure 6-3 we provide the rates of FR, ripple and spike captured in four states computed from all patients. Across 6

patients, the mean FR rate during IB was 4.7/min (ranging from 1.3 to 12.2/min) which was comparable with the results derived from SB (4.3/min, ranging from 1.1 to 9.3/min). Interestingly, we observed reduction in FR rate during the pre- and postictal epochs (mean = 2.9/min and 1.6/min, respectively;  $P < 0.05$ ), suggesting that FR rates both before and after seizures were significantly different compared to baselines in all patients. This suppression in rate of occurrence was not observed for ripples. As it is shown in figure 6-3, both ripple and spike activities presented similar firing frequency with large inter-patient variations, whether or not being close to a seizure. The mean rates for ripples were 8.5/min in IB (0.7 – 15.0/min), 7.1/min in SB (1.7 – 16.5/min), 7.3/min for preictal (0.8 – 16.7/min), and 10.2/min for postictal (1.1 – 19.0/min). Similar to ripple activities, the spike rates exhibited large variation across patients. The average rates were 10.3/min for IB (1.3 – 36.0/min), 8.4/min for SB (1.3 – 32.6/min), 3.8/min for preictal (0.8 – 8.7/min), and 9.4/min for postictal (0.4 – 41.0/min), respectively.

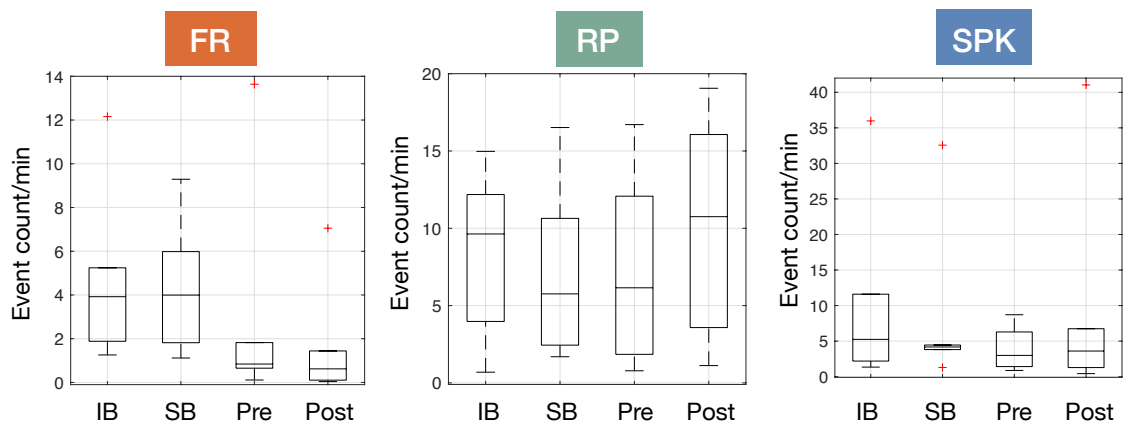


**Figure 6-3. Event rates for FR, ripple and spike in different states. FR rates were significantly lower in pre- and postictal periods compared to IB and SB.**

#### 6.3.4. Temporal Dynamics of Events In Different States

Using discrete time windows we inspected the event count in each 10-minute epoch for all detected HFOs/spikes and those detected in SOZ channels only. In figure 6-4 (A) we give the results regarding the number of event captured during IB and SB states in one patient (P4), with the overall results presented in figure 6-4 (B). As it is seen in the figure, in P4 the number of FR captured in each 10-min window varied dramatically, spanning from no detections at all to over 30 events per window. The fluctuation in FR rate coincided during both IB and SB in all patients, of which four had time periods with absent or minimal FR events lasting for 10 – 30 min, raising the question that a random pick of 10-min epoch may fail to catch the proper segment where FR activity is more frequent. The variation also existed in ripple and spike groups where the temporal changes occurred both inside and outside the SOZ, most of the time independent from FRs.

The results for preictal temporal distribution of FR, ripple or spike did not show systematic change across patients. Furthermore, we found intra-individual variation in terms of FR temporal trend in all patients. While the FR rate during postictal periods behaved rather consistently, we noted multiple patterns of FR temporal distribution existed preictally within the same patient, which can be summarized as following: i) none-to-very low FR rate throughout the investigated 60-min preictal period; ii) general decrease in FR rate, iii) general increase in FR rate, and iv) a sudden increase before a seizure emerges. Pattern ii) and iii) might be accompanied by rate fluctuations. Pattern iv)

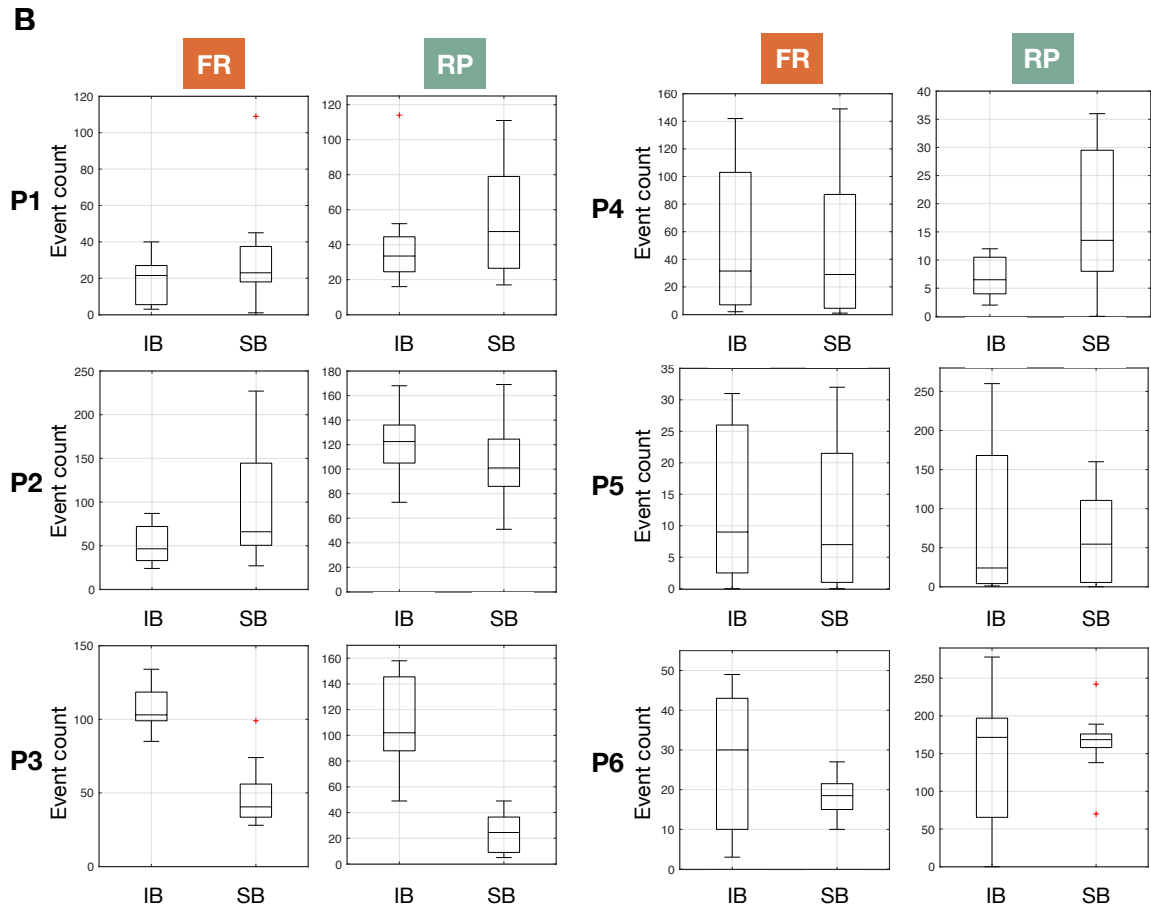
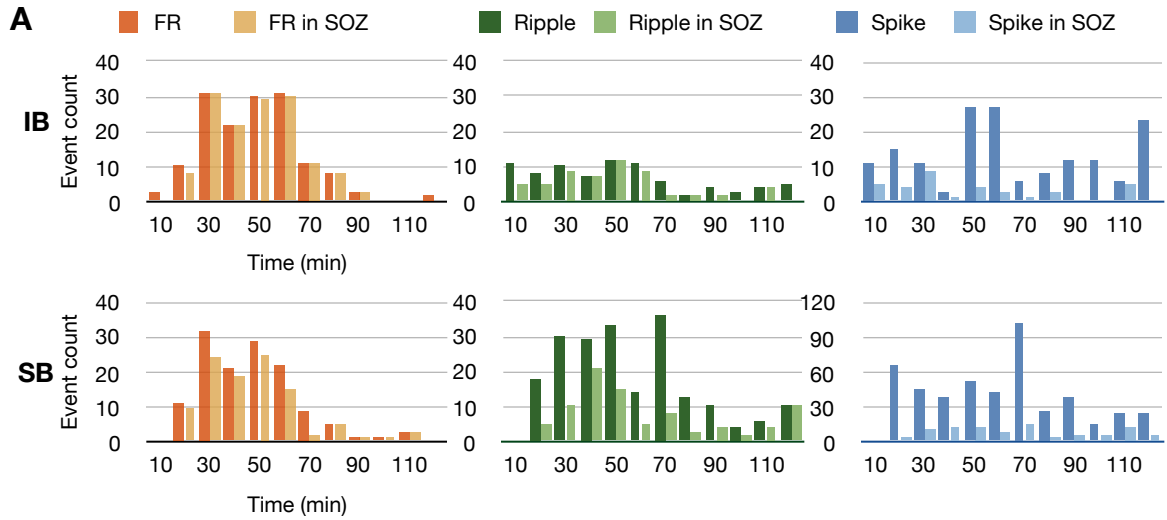


**Figure 6-4. (A) The number of FR, ripple and spike captured during IB and SB states in P4. (B) The FR and ripple temporal variation in each 10-min window in baseline segments for 6 patients.**

were observed in 3 patients where we speculated might attribute to the actual ictal onset, considering the fact that it is challenging to precisely identify a electrographic seizure onset (Khosravani et al., 2009). We therefore examined the FR firing patterns in those preictal segments where dramatic FR increase was seen in the last 10-min preictal window. Results indicated that the rising in FR rate occurred 30 s – 10 min before these seizures, making it unlikely that the increased firing rate was due to an inaccurate annotation of seizure onset.

In figure 6-5 we provide the pre- and postictal HFO temporal distribution results in 3 seizures derived from a representative patient (P6) where preictal temporal patterns i), ii) and iii) were observed. For two seizures we also plotted the FR distribution in the first 10-minute after the seizure termination to show the recovery activity. All of the three presented seizures in this patient were complex partial seizures emerged from right mesial anterior hippocampus, followed by ictal propagation involving the posterior temporal and frontal-occipital lobes. In this patient, ripple and spike (not shown) activities presented similar patterns of temporal progression compared to FR, with significant postictal increase in ripple and spike rates both in- and out of the SOZ ( $P < 0.05$ ).

To illustratively evaluate any seizure associated pre- and postictal changes, we plotted the event count of FR and ripple inside the SOZ in each 10-min bin, computed from each seizure in each patient, the results are given in figure 6-6. We noticed distinct patient-specific trends in the evolution of FR rates before impending seizures. More specifically, In three of the patients (P1, P3, and P4), the number of FR as well as its variance was relatively low as seizures were approaching. More pronounced variability in

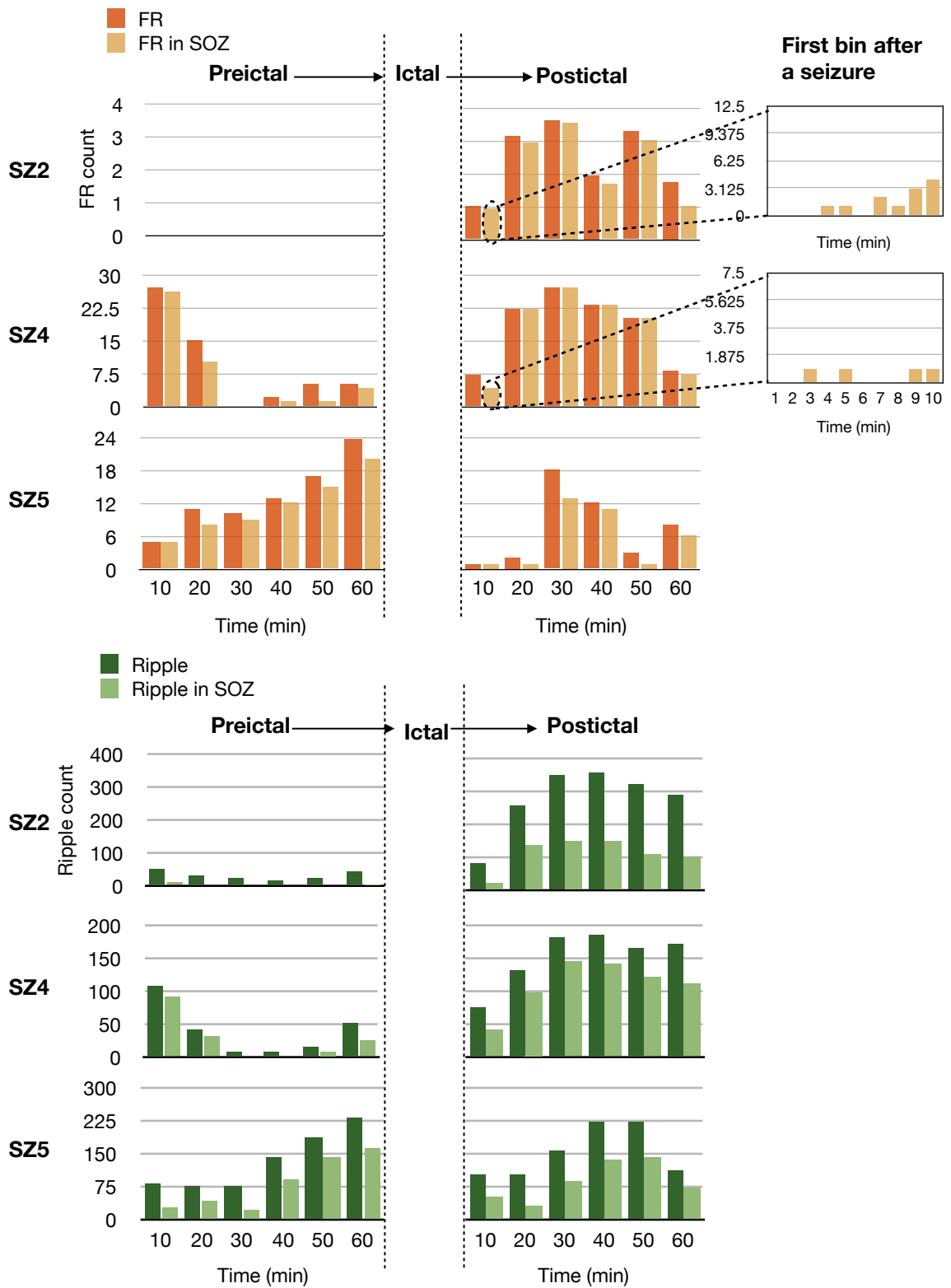


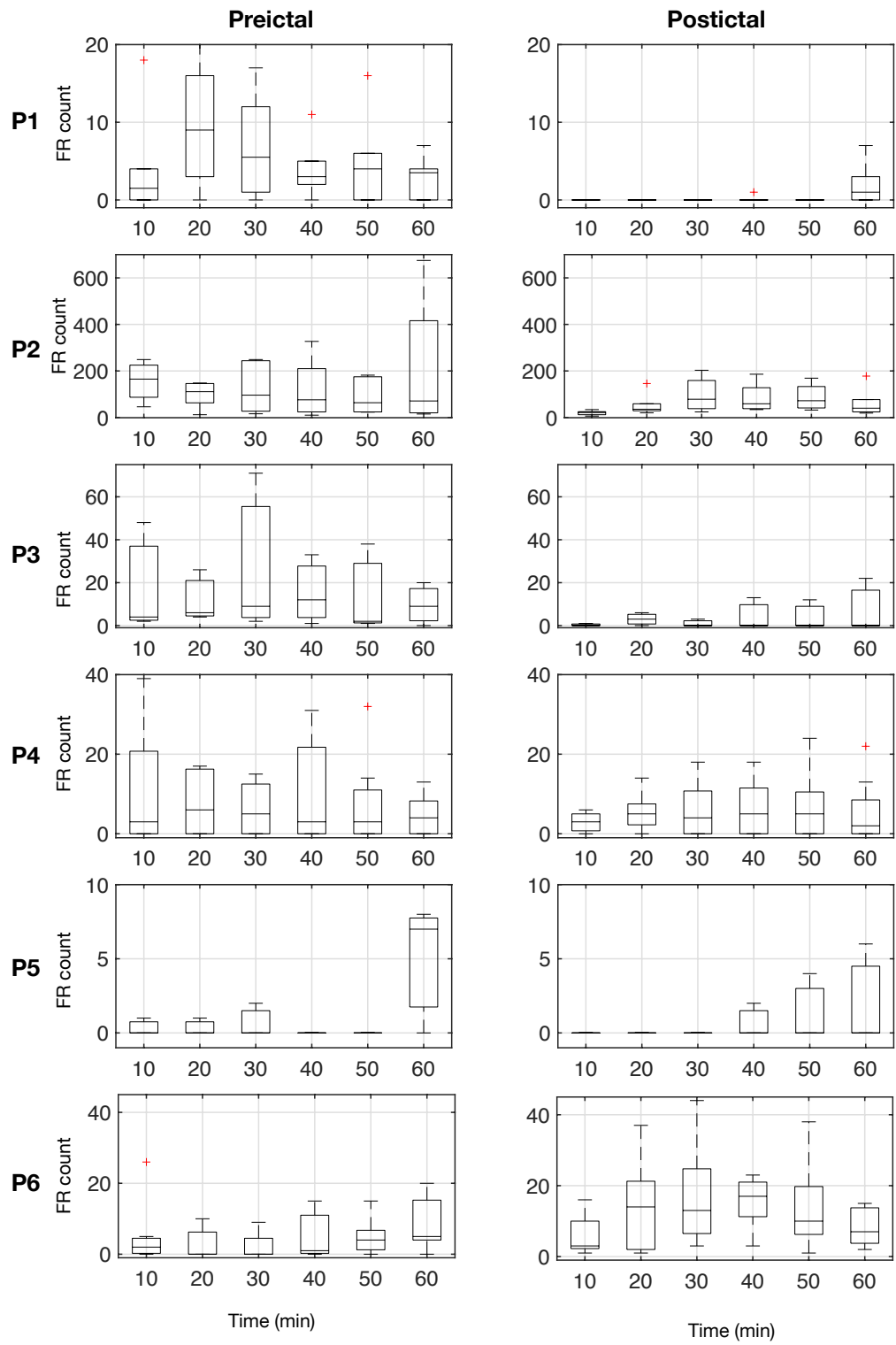
**Figure 6-5. Pre- and postictal HFO temporal distribution results in 3 seizures derived from P6 where three preictal patterns were observed for FR.**

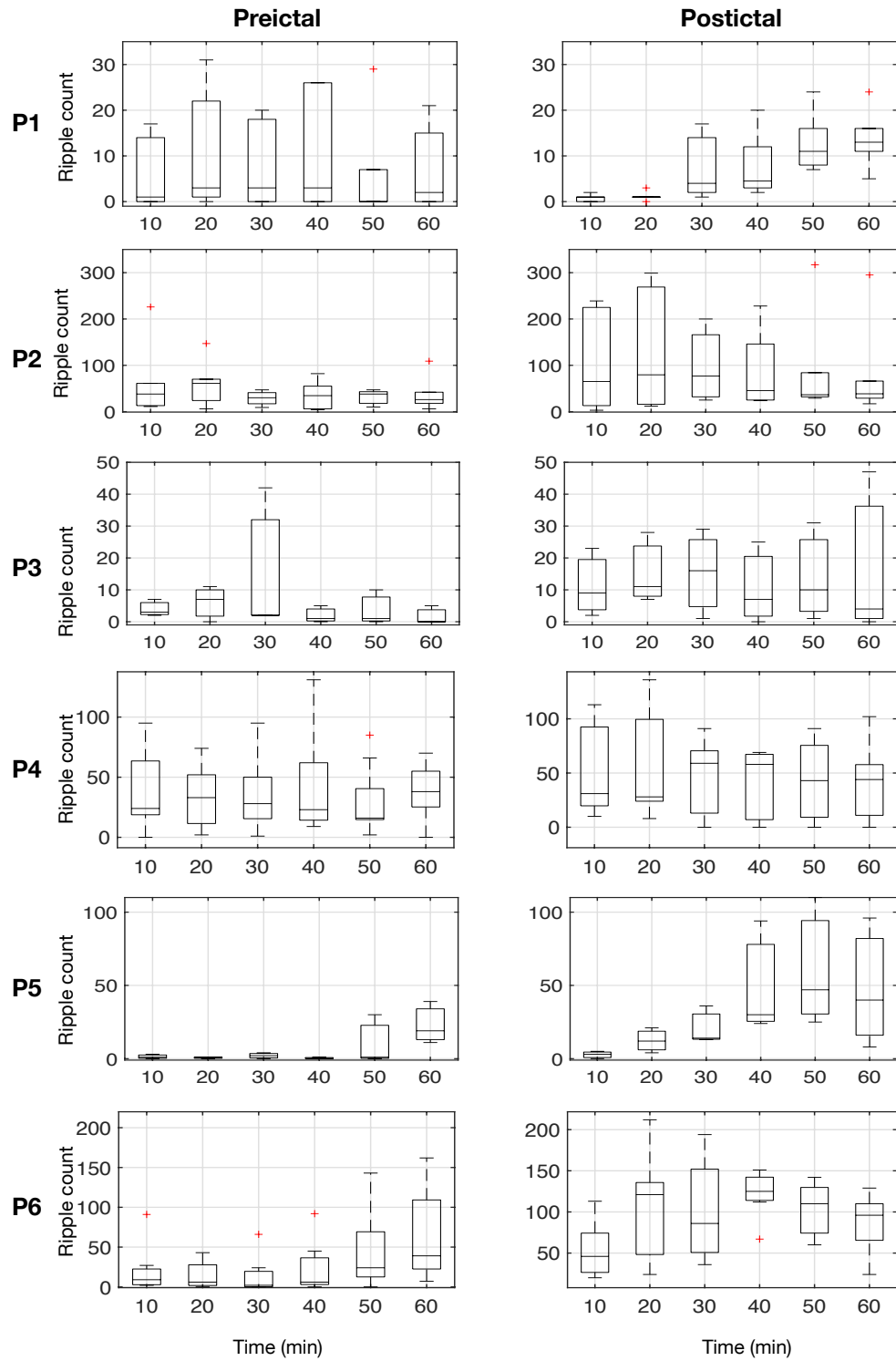
FR rate was found in P2, P5 and P6 where the boxplots of the last 10-min widow bin suggested sudden FR increase in some of the seizures in these three patients. The individual temporal changes in ripple, however, behaved quite differently in P2 (ripple stayed inactive while FR rate boosted during the last 10 minutes before seizures). In P3, P5 and P6 the ripple rates exhibited same preictal patterns as FR, whereas in P1 and P4 no clear firing pattern was observed.

Considering each individual patient, pairwise comparison showed a trend of overall decrease in FR rate postictally compared to the preictal stage, but the difference was not significant, due to the contradicting behavior in FR in one patient (P6). We noted that P6 was the only patient with neocortical onset seizures, and majority of the postictal FRs were generated from the neocortex. Despite the exception, the averaged postictal temporal trend for FRs fit into the linear regression model with  $P < 0.01$ . On the contrary, we observed overall predominance of ripples in postictal states in all patients. Ripples in the SOZ appeared to be more active after seizure termination ( $P < 0.05$ ), and their temporal distribution showed distinctions compared to FRs (non-linear trends). These findings demonstrated the strong temporal relationships FRs had with ictal activities, the existence of diverse mechanisms underlying FR and ripple generation in epileptogenic structures, as well as the disparate patterns found in different patients.

### **6.3.5. Early Prediction of the SOZ**

By showing the temporal dynamics in each patient, we observed drastic changes in the rate of events, particularly in FRs. The spatial locations of FRs, when found, was rather stable and consistent compared to ripples or spikes, with the premise that a “right”

**A****FR**

**B****RP**

**Figure 6-6. (A) Event count of FRs and (B) ripples inside the SOZ in each 10-min bin, computed from each seizure in each patient.**

data segment introducing sufficient number of FR was selected (figure 6-7). It was then expected that FR detection and SOZ localization would benefit from examining iEEG of extended length. To determine the amount of time required for robust detection as well as the interpretation of HFOs, we performed SOZ prediction based on the spatial attributes of FR, ripple and spike events cumulatively captured in 10 – 120 minutes at the beginning of EMU monitoring. Channels contributing to > 90% of the total events were taken into account for SOZ prediction.

In figure 6-8 we present the prediction specificity, ACC and MCC results for FRs, ripples and spikes in each patient as well as the average cumulative prediction curves. Unlike spikes or ripples, FRs were well localized in a few channels from the very beginning of recording which showed consistency with SOZ indicated by neurologists,

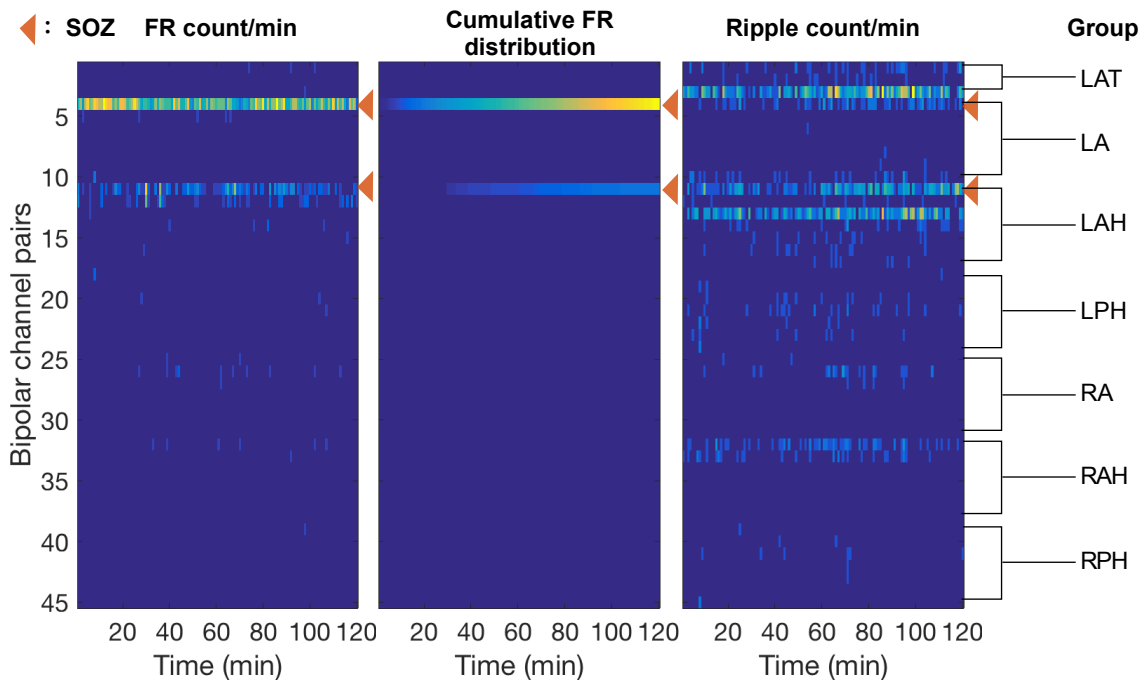


**Figure 6-7. Left: spatiotemporal distribution for FRs in 1-min discrete windows throughout the 2-hour IB recording in P3. Middle: cumulative FRs distribution. Right: spatiotemporal distribution for ripples.**

resulting in a high average specificity of 95.0% (82.6% – 100%) starting from the first 10-minute recording. The ACC in this case was 88.2% (80.0% – 95.6%), with initial MCC of 0.29 (-0.10 – 0.63). The performance of the detection improved significantly after 30 minutes of cumulative detection in terms of ACC and MCC (ACC = 92.4%, MCC = 0.39,  $P < 0.05$ ), both of which continued the rising trend till the 6<sup>th</sup> window bin representing 1 hour of recording (ACC = 94.5%, MCC = 0.67). After this point, the cumulative prediction curves reached the plateau with subtle rise and falls but no significant difference was seen. At the end of the 120-min recording we were able to achieve an overall ACC of 94.4% and MCC of 0.71, representing a very strong positive relationship between FR distribution and SOZ information (Powers et al., 2011).

The initial ACC for ripple prediction was 85.9% (80.0% – 95.9%), with an average MCC of 0.25 (-0.12 – 0.61). The prediction performance using ripples showed a significant improvement after 40 minutes of recording when both ACC and MCC values reached their peaks (ACC = 91.6%, MCC = 0.54,  $P < 0.05$ ). Further recordings, however, did not provide informative input towards the SOZ prediction and the final result for ACC (= 89.3%) and MCC (= 0.44) did not show statistical difference compared to the results acquired from the first 10-min window. Similarly, no significant advantage was seen using spikes collected from 120-min data (ACC = 87.6%, MCC = 0.31) comparing to the use of 10-min data segment (ACC = 87.0%, MCC = 0.36).

## **6.4 Discussion**

In the current study we investigated the spatial and temporal characteristics of HFOs and spikes during 120-min preictal-ictal-postictal transition periods in 6 patients with

temporal lobe epilepsy which has not been explored previously. Inter- and intra-patient variability was observed in terms of HFO temporal progression during 60-min preictal periods. Although no consistent changes were noted, we observed significant reduction in

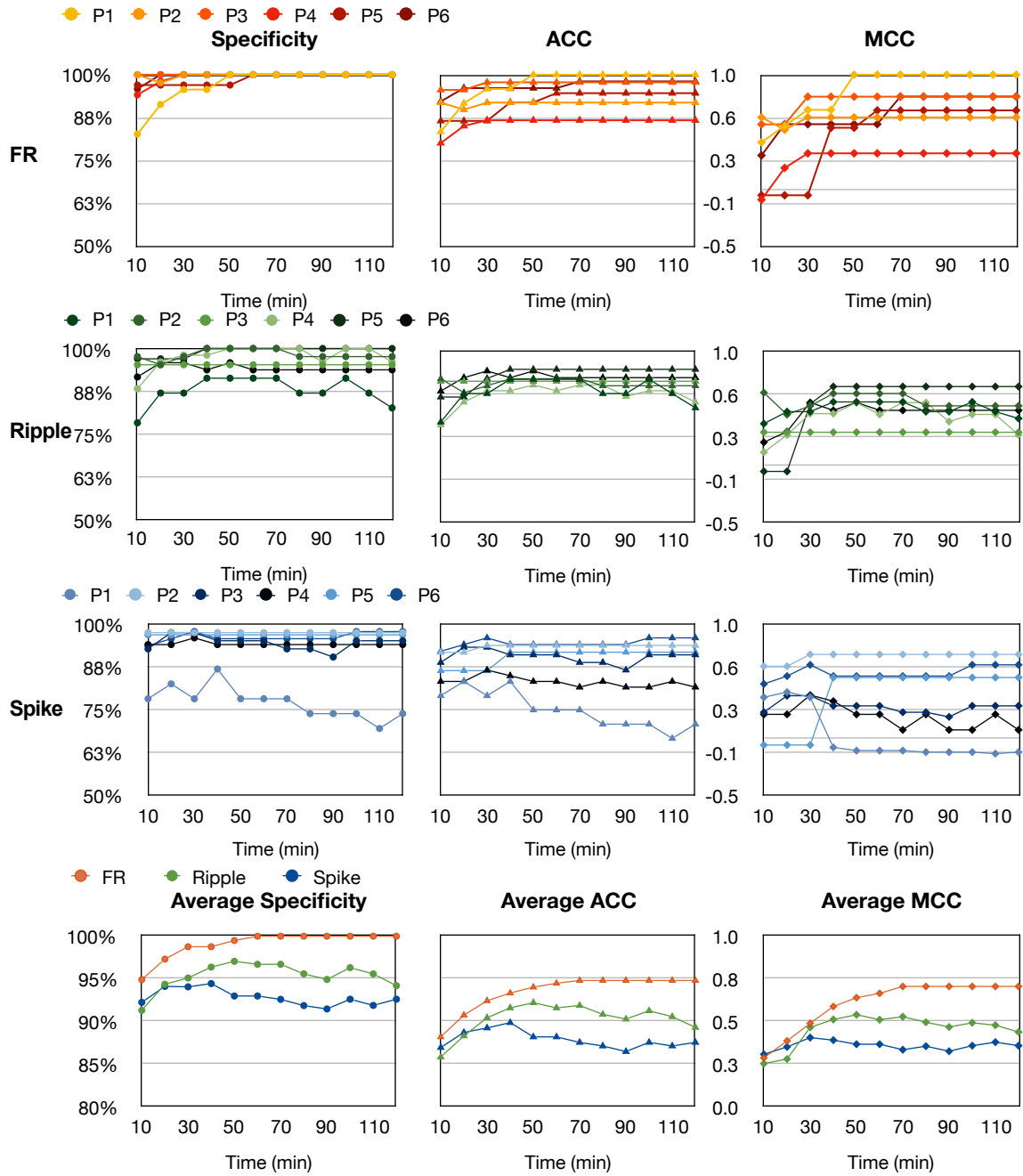


Figure 6-8. Cumulative prediction results for FR, ripple and spikes.

HFO rates 1 hour before and after seizures compared to baseline segments. This suppression was exclusively observed in the fast ripple group (above 200 Hz) but not in ripples or spikes, suggesting the specific association between FR and epileptogenesis. In addition, we explored the temporal dynamics of different subtypes of HFOs in different baseline states of multiple hours, with specific consideration to the HFO progression at the beginning of intracranial monitoring after implantation surgery. By performing cumulative SOZ prediction using FRs detected from initial baseline data collected at the beginning 2 hours in the EMU we achieved an overall prediction accuracy of 92% after 30 minutes of monitoring, which later increased to 95% and reached a plateau after approximately 1 hour of monitoring. This is the first report emphasizing the benefit of using extended iEEG recording for HFO analysis and its potential application for SOZ early prediction.

Up till present, majority of the existing research focusing on HFO detection and evaluation was conducted using iEEG data of short length (Andrew et al., 2007; Dümpelmann et al., 2012; Melani et al., 2013; Staba et al., 2002). More recent studies utilizing advanced machine learning techniques showed capability of detecting HFOs in longer intervals (Blanco et al., 2010b). Nevertheless, few of the reports capitalized the use of automatically detected HFOs in clinical application or validated the predictive value of HFO as a specific SOZ indicator to serve presurgical evaluation. Here for the first time we investigated the HFO temporal distribution during prolonged baseline data as well as expanded pre- and postictal periods in 6 patients, with an average of 16 hours of data being analyzed per patient. By computing the aggregation for HFOs and spikes

using 10-min time windows, we found considerable variations in the rate of FR, ripple and spike during baseline and preictal stages. A previous study looking into HFO rate during sleep/waking cycles demonstrated great temporal variation in ripple ( $< 250$  Hz) generation (Dümpelmann et al., 2015). In the present study we showed evidence that FR temporal distribution also varied dramatically, suggesting that the brain network responsible for FR generation does not activate evenly across time in sleep or vigilance states, resulting in the absence in FR during certain time intervals. This temporal variation in HFO generation may leave substantial influence on HFO detection, putting into question if analysis based on the selection of tens of minutes of interictal data during sleep or awake states can be regarded as reliable and robust.

Multiple studies have reviewed the change in HFO activity before an impending seizure. Still, researchers barely look at HFO dynamics anytime earlier than 30-min before a seizure emerges, and generally pay less attention to HFO activity after seizures. In this study we tried to determine whether HFO firing rate presents distinct temporal trends before and after seizures. We observed different patterns preictally across patients and across seizures within the same patient. Typical patterns include a total “silence” or extensive suppression of FR in the SOZ, a decreasing/increasing trend, as well as a rapid increase 30 s to 5 min immediately before a seizure. These findings are in agreement with other studies inspecting preictal HFO properties in a shorter period of time. Although there is evidence showing preictal power increase in the HF band using very short data segments (30 s) (Khosravani et al., 2007), no consistent and systematic trend was documented when analyzing preictal epochs by several minutes (Jacobs et al., 2009;

Pearce et al., 2013). It has been proved that the HFO increase during seizure onset is associated with seizure types. For instance, ictal HFOs were found increasing right before the onset of spam but not other types of seizures (Zijlmans et al., 2011, 2009a). Our results suggest that FR activities close to seizure generation may be modulated by individual's unique pathological network or mechanism of the disease, and therefore must be evaluated individually for HFO interpretation. Further, in this study we observed an overall decrease in FR rate 60 minutes before and after seizures which was not seen in ripples or spikes, supporting the view that fast ripples are more specifically associated with epileptogenesis. Due to the temporal fluctuation, it remains unclear if the decrease in FR rate can be reliably used as a discriminative feature to monitor seizure activity. Additional studies are needed to test whether this information can be employed in a predictable manner.

Our results showed that postictal recovery for FR could take up to one hour after seizure termination in patients with mesial temporal lobe seizure onsets. On the contrary, ripple rates after seizure increased significantly inside and outside the SOZ, suggesting different mechanisms underneath these two HFO subtypes. Studies showed that spike frequency increased postictally in widespread regions that might or might not correspond to SOZ (Gotman and Koffler, 1989; Gotman and Marciani, 1985), which was also observed in this study. Nonetheless, reports related to HFO post-seizure activity is sparse. The aftermath of a seizure gives clue of altered brain function, and therefore their biological significance need to be investigated (So and Blume, 2010).

One prior HFO study with human-screening suggested that HFO distribution was stable across multiple days when only 1 minute of data was scored each night (Zijlmans et al., 2009b). We argue that, although spatially consistent, the temporal variation will affect the detectability of FRs and interfere with the interpretation. By contrast, we observed that both temporal and spatial distributions changed considerably over time for ripple events. The most frequent ripple generative regions shifted across the long-term time window, suggesting the co-existence of pathological ripples and physiological ones generated from non-epileptic regions. This is the supporting evidence for previous research demonstrating the necessity of separating epileptic and non-epileptic HFOs, particularly in the frequency range below 250 Hz.

By executing cumulative SOZ prediction using 10 – 120 minutes of initial baseline in 6 patients we confirmed that HFO detection and SOZ identification could profit from prolonged iEEG recording of 30 – 60 minutes compared to the conventionally used 10-min data segment. In particular, SOZ prediction performance using FR information showed significant improvement after 30 minutes of detection, and stabilized at the level of 95% after 1 hour of monitoring. There are evidence that epileptic FRs are generated by small clusters of desynchronous firing cells (Demont-Guignard et al., 2012), making them spatially sparse in nature, which further links to high specificity when used for channel prediction (i.e., tends to assign most of the channels to negatives). One may argue that such imbalanced class sizes (numbers of SOZ and non-SOZ channels) make it difficult to evaluate the classification, and that prediction accuracy may not be sufficient to reflect the actual performance of the prediction. However, from a practical standpoint,

it would still be helpful if the HFO generative region always indicated a subset of the critical epileptic network. In addition, to overcome the bias towards prediction specificity we used another descriptor, MCC, to assess the prediction results. The cumulative MCC showed prominent increase from 3.5 to 7.1, reflecting a very strong association between FR channels and SOZ location (Davenport Jr and El-Sanhurry, 1991). Due to the larger spatial extent and variability of ripples and spikes,

It is noteworthy that in current study the early prediction of SOZ was achieved by using the first hour of EMU recording after electrode implantation. Considering the clinical utility of HFOs as markers of epileptogenicity always arises the question of whether to analyze HFOs during awake, sleep, or preictal, periods (Jacobs et al., 2012). Earlier HFO study using limited length of data is in favor of detecting HFO during NREM sleep, however it is important that a valid neurobiomarker for epileptogenic regions being independent from patient's states, thus providing additional advantage that neurologists would not be relying on a specific condition, or waiting for multiple spontaneous seizures to occur during the intracranial EEG investigation. Here by executing the cumulative FR detection we present evidence that SOZ prediction can be achieved within the initial two hours of monitoring with high accuracy of 94%. Further study is required to answer whether HFOs are better predictors of disease activity and epilepsy remission than the traditional hall mark, known as the interictal spikes.

## **CHAPTER 7 SIGNIFICANCE AND CONCLUSION**

### **7.1 Major Contributions**

HFOs are complex dynamic phenomena that are difficult to identify by visual inspection. In this thesis we introduced a series of new method for automatically detecting and characterizing high frequency field potential oscillations within 80 – 500 Hz range in continuous intracranial electroencephalographic recordings collected in realistic clinical environment without channel pre-exclusion. Instead of limiting the analysis to 80 – 500 Hz range, we explored the raw iEEG data of the entire frequency band. The automatized detection showed capability of identifying HFO and spikes using iEEG data collected from multiple centers. It is important to point out that this thesis is not merely about new theoretical advancement in signal processing or machine learning techniques, but how this proposed algorithm can be utilized as a unique tool to solve the problem of HFO detection and spatial approximation of the SOZ using clinical data which are more prone to signal artifacts compared to data collected in an experimental setting.

First, in Chapter 3 we reported the methodological contributions of the thesis, where a novel algorithm integrating the amplitude-based detection, time-frequency analysis and unsupervised clustering is introduced to automatically separate HFO activities with other false detections such as interictal spikes and arbitrary events, based on the concept of learning from the data. By using novel features extracted after time-frequency analysis, we investigated the correlation of possible HFO clusters and clinician-determined SOZ in patients with epilepsy in sleep, awake, and pre-ictal states. The algorithm successfully

localized SOZ in all patients but one whose postoperative outcome reported unfavorable results, achieving its highest sensitivity in the sleep state. Comparing to existing SOZ approximation method, the algorithm provided significantly better performance. Our results indicate that unsupervised clustering methods exploring the time-frequency content of HFOs in the available full band can efficiently be used to localize the epileptogenic zone in clinical practice.

In Chapter 4, we described how the proposed detection method can be applied in real clinical cases where the seizure onset patterns are not robust nor clear, and where the patients had extra-temporal onset that is generally considered more challenging in terms of HFO interpretation due to the inclusion of functional cerebral cortex. By running unsupervised HFO detection in patients with extra-temporal lobe onset epilepsy we showed that the spatial location of automatically detected HFOs correlated well with the epileptogenic zone as well as the postsurgical outcome in all investigated cases. In addition, we explored the spatial attribute of HFOs by executing automated HFO detection in continuous ECoG data using a hybrid high-density surface electrode array, and examined whether HFOs were equally detectable using different sized ECoG contacts. Our results provide initial evidence that the detection efficacy of HFOs in the ripple range may be higher using small contacts possibly due to the spatial averaging effect.

Chapter 5 describes a critical finding where we observed a novel pattern in HFO waveforms originating from pathological structures that were rarely seen in the eloquent brain regions responsible for the generation of physiological oscillations. Such patterns

can be automatically identified using unsupervised machine learning approaches and thus being efficiently employed to localize the SOZ and avoid unwanted detections of the functional areas. Most importantly, the highly stereotypical HFO waveform patterns described in this chapter are observed exclusively in SOZ, yielding a new possibility to describe HFOs instead of the current frequency-based characterization. The outcomes of this study adds to our understanding of the electrophysiological basis of HFOs as well as the epileptogenic networks, and provide new avenues for the interpretation of HFOs that can be efficiently applied to distinguish SOZ from functional cortical structures that need to be preserved during the resection surgery, which is a critical step towards the translation of HFOs to valid clinical biomarkers. It is expected that the identification of stereotyped signal patterns can give additional clues toward the detection and discrimination of multiple types of signature neuronal activities in human iEEG without manual labeling process which might potentially put bias towards the examination.

In Chapter 6 we further investigate the temporal variation of HFOs during awake and sleep, as well as the temporal distribution of HFOs before and after seizures. To explore the temporal characteristics of HFO, our analysis was executed using all recorded channels over ninety hours of multichannel iEEG data in a fully-automatic fashion, which differs from most of the previous studies where the investigators commonly use retrospective visual review to select HFOs from limited datasets. On top of this, we sought to answer whether SOZ can be predicted earlier than the first clinical seizure observed during prolonged monitoring, which may potentially reduce the time frame and cost of the invasive monitoring. The results of this study present the spatial stability and

temporal variability of FRs, which was confirmed by the cumulative SOZ detection accuracy. It is possible that using FR information, SOZ prediction can be achieved after the initial 60 to 120 min of EMU recording, which may reduce the potential risk associated with long-term invasive monitoring.

## **7.2 Future Directions**

Even though emerging studies are showing strong evidences that HFOs are of high clinical significance and should be used as a guide to assist in the presurgical evaluation, these studies are derived from relatively small patient cohorts. Therefore, in future it is necessary to conduct properly designed, randomized multichannel trials that provide strong statistical power to assess the validity of HFOs as clinical indicators. One of the most exciting aspects of future work would be to map the epileptogenic brain regions and monitor the ictal activity based on HFOs information and other epileptic hallmarks, for instance, interictal spikes. It is possible that the real-time detection of these signature activities will open the door to intraoperative localization of SOZ, and thus eliminating the need for prolonged invasive monitoring and the associated medical complication risk and expenses.

Another possible future direction of HFO studies would be the application of HFO in neuromodulation therapies, for example, in open- and close-loop neurostimulation treatments. Neurostimulation is a new option for epilepsy treatment which is flexible and reversible. Its efficacy and safety has been proved by pivotal clinical trials. Both deep-brain stimulation (DBS) and responsive neurostimulation (RNS) devices have programmable settings to control its output by adjusting the current, pulse width, frequency and polarity, which will also determine the stimulation effect on neuronal

tissue. The efficacy of therapeutic stimulation depends critically on the targeted site of effect and on the exact nature (parameters) of the stimulus, which have been empirically derived by trial and error, and the mechanisms by which electrical stimulation might benefit patients with epilepsy are still poorly understood. Stimulation technology and protocols are usually adapted from approaches to treat disparate conditions such as movement disorders. Study reporting the HFO dynamics related to direct brain stimulation is rare. Considering the association of HFO and epileptogenic network, it would be interesting to carry out studies to explore the role of HFO as a biomarker to predict the efficacy of neurostimulation therapy, which may also help us understand the exact mechanism of action and the best parameters used during electrical stimulation.

## REFERENCES

- Akiyama, T., Otsubo, H., Ochi, A., Ishiguro, T., Kadokura, G., Ramachandranair, R., Weiss, S. K., Rutka, J. T., and Carter Snead, O. (2005). Focal Cortical High-frequency Oscillations Trigger Epileptic Spasms: Confirmation by Digital Video Subdural EEG. *Clinical Neurophysiology : Official Journal of the International Federation of Clinical Neurophysiology*, 116(12), 2819-2825.
- Alkawadri, R., Gaspard, N., Goncharova, I. I., Spencer, D. D., Gerrard, J. L., Zaveri, H., Duckrow, R. B., Blumenfeld, H., and Hirsch, L. J. (2014). The Spatial and Signal Characteristics of Physiologic High Frequency Oscillations. *Epilepsia*, 55(12), 1986-1995.
- Allen, P. J., Fish, D. R., and Smith, S. J. (1992). Very High-Frequency Rhythmic Activity During SEEG Suppression In Frontal Lobe Epilepsy. *Electroencephalography and Clinical Neurophysiology*, 82(2), 155-159.
- Alonso-Vanegas, M. A., Cisneros-Franco, J. M., and Otsuki, T. (2012). Surgical Management of Cavernous Malformations Presenting with Drug-Resistant Epilepsy. *Frontiers in Neurology*, 2, 1-6.
- Andrade-Valença, L., Mari, F., Jacobs, J., Zijlmans, M., Olivier, A., Gotman, J., and Dubeau, F. (2012). Interictal High Frequency Oscillations (HFOs) in Patients with Focal Epilepsy and Normal MRI. *Clinical Neurophysiology : Official Journal of the International Federation of Clinical Neurophysiology*, 123(1), 100-105.

- Andrew, B. G., Greg A, W., Eric, M., Dennis, D., and Brian, L. (2007). Human and Automated Detection of High-frequency Oscillations in Clinical Intracranial EEG Recordings. *Clin Neurophysiol.*, 118(5), 1134-1143.
- Arrington, D. K., Ng, Y. T., Troester, M. M., Kerrigan, J. F., and Chapman, K. E. (2013). Utility and Safety of Prolonged Video-EEG Monitoring in a Tertiary Pediatric Epilepsy Monitoring Unit. *Epilepsy and Behavior*, 27(2), 346-350.
- Arthur, D., And Vassilvitskii, S. (2007). K-Means++: The Advantages of Careful Seeding. In *Proceedings of the eighteenth annual ACM-SIAM symposium on discrete algorithms* (pp. 1027-1035).
- Arya, R., Mangano, F. T., Horn, P. S., Holland, K. D., Rose, D. F., And Glauser, T. A. (2013). Adverse Events Related to Extraoperative Invasive EEG Monitoring with Subdural Grid Electrodes: A Systematic Review and Meta-Analysis. *Epilepsia*, 54(5), 828-839.
- Asano, E., Brown, E. C., and Juhász, C. (2013). How to establish causality in epilepsy surgery. *Brain & Development*, 35(8), 706-720. doi:10.1016/j.braindev.2013.04.004
- Baghdadi, T. S., and Najjar, M. W. (2010). Evaluation of Intractable Epilepsy. Invasive Monitoring. *Neurosciences (Riyadh, Saudi Arabia)*, 15(2), 71-78.
- Ball, T., Kern, M., Mutschler, I., Aertsen, A., and Schulze-Bonhage, A. (2009). Signal Quality of Simultaneously Recorded Invasive and Non-Invasive EEG. *NeuroImage*, 46(3), 708-716.
- Baumann, C. R., Acciarri, N., Bertalanffy, H., Devinsky, O., Elger, C. E., Lo Russo, G., Cossu, M., Sure, U., Singh, A., Stefan, H., Hammen, T., Georgiadis, D., Baumgartner,

- R. W., Andermann, F., and Siegel, A. M. (2007). Seizure Outcome After Resection of Supratentorial Cavernous Malformations: A Study of 168 Patients. *Epilepsia*, 48(3), 559-563.
- Belluscio, M. A., Mizuseki, K., Schmidt, R., Kempter, R., and Buzsáki, G. (2012). Cross-Frequency Phase-Phase Coupling Between and Oscillations in The Hippocampus. *The Journal of Neuroscience : The Official Journal of the Society for Neuroscience*, 32(2), 423-435.
- Berg, A. T., and Scheffer, I. E. (2011). New Concepts in Classification of The Epilepsies: Entering The 21St Century. *Epilepsia*, 52(6), 1058-1062.
- Bénar, C. G., Chauvière, L., Bartolomei, F., and Wendling, F. (2010). Pitfalls Of High-Pass Filtering for Detecting Epileptic Oscillations: A Technical Note on “False” Ripples. *Clinical Neurophysiology : Official Journal of the International Federation of Clinical Neurophysiology*, 121(3), 301-310.
- Bikson, M., Fox, J. E., and Jefferys, J. G. (2003). Neuronal Aggregate Formation Underlies Spatiotemporal Dynamics of Nonsynaptic Seizure Initiation. *Journal of Neurophysiology*, 89(4), 2330-2333.
- Biot, G., Kachenoura, A., Albera, L., Bénar, C., and Wendling, F. (2013). Automatic Detection of Fast Ripples. *Journal Of Neuroscience Methods*, 213(2), 236-249.
- Blanco, J. A., Stead, M., Krieger, A., Stacey, W., Maus, D., Marsh, E., Viventi, J., Lee, K. H., Marsh, R., Litt, B., and Worrell, G. A. (2011). Data Mining Neocortical High-frequency Oscillations in Epilepsy and Controls. *Brain : A Journal of Neurology*, 134(Pt 10), 2948-2959.

- Blanco, J. A., Stead, M., Krieger, A., Viventi, J., Marsh, W. R., Lee, K. H., Worrell, G. A., and Litt, B. (2010b). Unsupervised Classification of High-frequency Oscillations in Human Neocortical Epilepsy and Control Patients. *Journal of Neurophysiology*, *104*(5), 2900-2912.
- Bourgeois, M., Di Rocco, F., and Sainte-Rose, C. (2006). Lesionectomy in The Pediatric Age. *Child's Nervous System*, *22*(8), 931-935.
- Bragin, A., Engel, J., Wilson, C. L., Fried, I., and Mathern, G. W. (1999). Hippocampal and Entorhinal Cortex High-frequency Oscillations (100-500 Hz) in Human Epileptic Brain and in Kainic Acid-Treated Rats with Chronic Seizures. *Epilepsia*, *40*(2), 127-37.
- Bragin, A., Mody, I., Wilson, C. L., and Engel, J. (2002). Local Generation of Fast Ripples in Epileptic Brain. *The Journal of Neuroscience : The Official Journal of the Society for Neuroscience*, *22*(5), 2012-2021.
- Bragin, A., Wilson, C. L., and Engel, J. (2007). Voltage Depth Profiles of High-frequency Oscillations After Kainic Acid-Induced Status Epilepticus. *Epilepsia*, *48*(s5), 35-40.
- Bragin, A., Benassi, S. K., Kheiri, F., and Engel, J. (2011). Further Evidence That Pathologic High-frequency Oscillations Are Bursts of Population Spikes Derived From Recordings of Identified Cells in Dentate Gyrus. *Epilepsia*, *52*(1), 45-52.
- Brna, P., Duchowny, M., Resnick, T., Dunoyer, C., Bhatia, S., and Jayakar, P. (2015). The Diagnostic Utility of Intracranial EEG Monitoring for Epilepsy Surgery in Children. *Epilepsia*, *56*(7), 1065-1070.

- Bundy, D. T., Zellmer, E., Gaona, C. M., Sharma, M., Szrama, N., Hacker, C.,  
Freudenburg, Z. V., Daitch, A., Moran, D. W., and Leuthardt, E. C. (2014).  
Characterization of The Effects of The Human Dura on Macro- And Micro-  
Electrocorticographic Recordings. *J. Neural Eng.*, *11*(1), 16006.
- Burnos, S., Hilfiker, P., Sürücü, O., Scholkmann, F., Krayenbühl, N., Grunwald, T., and  
Sarnthein, J. (2014). Human Intracranial High Frequency Oscillations (Hfos)  
Detected By Automatic Time-frequency Analysis. *PloS One*, *9*(4), e94381.
- Buzsáki, G., Horvath, Z., Urioste, R., Hetke, J., and Wise, K. (1992). High-frequency  
Network Oscillation in The Hippocampus. *Science*, *256*(5059), 1025-1027
- Buzsáki, G., and Silva, F. L. D. (2012). High Frequency Oscillations in The Intact Brain.  
*Progress in neurobiology*, *98*(3), 241-249.
- Chaibi, S., Sakka, Z., Lajnef, T., Samet, M., and Kachouri, A. (2013). Automated  
Detection and Classification of High Frequency Oscillations in Human Intracerebral  
EEG. *Biomedical Signal Processing and Control*, *8*(6), 927-934.
- Châtillon, C. E., Zemann, R., Hall, J. A., Olivier, A., Dubeau, F., and Gotman, J. (2013).  
Influence of Contact Size on The Detection of HFOs in Human Intracerebral EEG  
Recordings. *Clinical Neurophysiology : Official Journal of the International  
Federation of Clinical Neurophysiology*, *124*(8), 1541-1546.
- Châtillon, C. -É., Zemann, R., Bortel, A., Avoli, M., and Gotman, J. (2011). Contact Size  
Does Not Affect High Frequency Oscillation Detection in Intracerebral EEG  
Recordings in A Rat Epilepsy Model. *Clinical Neurophysiology*, *122*(9), 1701-1705.

- Chen, C., Ibekwe-SanJuan, F., and Hou, J. (2010). The Structure and Dynamics of Cocitation Clusters: A Multiple-Perspective Cocitation Analysis. *Journal of the American Society for Information Science and Technology*, 61(7), 1386-1409.
- Cho, J. R., Koo, D. L., Joo, E. Y., Seo, D. W., Hong, S. C., Jiruska, P., and Hong, S. B. (2014). Resection of Individually Identified High-Rate High-frequency Oscillations Region is Associated with Favorable Outcome in Neocortical Epilepsy. *Epilepsia*, 55(11), 1872-1883.
- Cosgrove, G. R. (1999). Occult Vascular Malformations and Seizures. *Neurosurg Clin N.Am.*, 10(3), 527-535.
- Crépon, B., Navarro, V., Hasboun, D., Clemenceau, S., Martinerie, J., Baulac, M., Adam, C., and Le Van Quyen, M. (2010). Mapping Interictal Oscillations Greater Than 200 Hz Recorded with Intracranial Macroelectrodes in Human Epilepsy. *Brain : A Journal of Neurology*, 133(Pt 1), 33-45.
- Davenport Jr, E. C., and El-Sanhurry, N. A. (1991). Phi/phimax: Review and Synthesis. *Educational and Psychological Measurement*, 51(4), 821-828.
- Demont-Guignard, S., Benquet, P., Gerber, U., Biraben, A., Martin, B., and Wendling, F. (2012). Distinct Hyperexcitability Mechanisms Underlie Fast Ripples and Epileptic Spikes. *Annals of Neurology*, 71(3), 342-352.
- Dempster, A. P., Laird, N. M., and Rubin, D. B. (1977). Maximum Likelihood From Incomplete Data Via The EM Algorithm. *Journal of the Royal Statistical Society. Series B (methodological)*, 1-38.

- Dümpelmann, M., Jacobs, J., and Schulze-Bonhage, A. (2015). Temporal and Spatial Characteristics of High Frequency Oscillations As A New Biomarker in Epilepsy. *Epilepsia*, 56(2), 197-206.
- Dümpelmann, M., Jacobs, J., Kerber, K., and Schulze-Bonhage, A. (2012). Automatic 80-250 Hz "Ripple" High Frequency Oscillation Detection in Invasive Subdural Grid and Strip Recordings in Epilepsy By A Radial Basis Function Neural Network. *Clinical Neurophysiology : Official Journal of the International Federation of Clinical Neurophysiology*, 123(9), 1721-1731.
- Engel, J. (1987). *Surgical treatment of the epilepsies*. New York.
- Engel, J., Bragin, A., Staba, R., and Mody, I. (2009). High-frequency Oscillations: What Is Normal and What Is Not? *Epilepsia*, 50(4), 598-604.
- Engel, J., Pitkänen, A., Loeb, J. A., Edward Dudek, F., Bertram, E. H., Cole, A. J., Moshe, S. L., Wiebe, S., Jensen, F. E., and Mody, I. (2013). Epilepsy Biomarkers. *Epilepsia*, 54(s4), 61-69.
- Engel, J. J., Henry, T. R., Risinger, M. W., Mazziotta, J. C., Sutherling, W. W., Levesque, M. F., and Phelps, M. E. (1990). Presurgical Evaluation For Partial Epilepsy: Relative Contributions of Chronic Depth-Electrode Recordings. Relative Contributions of Chronic Depth-Electrode Recordings Versus Fdg-Pet and Scalp-Sphenoidal Ictal EEG. *Neurology*, 40(11), 1670-1677.
- England, M. J., Liverman, C. T., Schultz, A. M., and Strawbridge, L. M. (2012). Epilepsy Across The Spectrum: Promoting Health and Understanding.: A Summary of The Institute of Medicine Report. *Epilepsy & Behavior*, 25(2), 266-276.

- Englot, D. J., Han, S. J., Lawton, M. T., and Chang, E. F. (2011). Predictors of Seizure Freedom in The Surgical Treatment Of Supratentorial Cavernous Malformations. *Journal of Neurosurgery*, 115(6), 1169-1174.
- Esteller, R., Echauz, J., Tcheng, T., Litt, B., and Pless, B. (2001). Line Length: An Efficient Feature for Seizure Onset Detection. *In Engineering in medicine and biology society, 2001. Proceedings of the 23rd annual international conference of the IEEE* (Vol. 2, pp. 1707-1710).
- Esteller, R., Echauz, J., and Tcheng, T. (2004). Comparison of Line Length Feature Before and After Brain Electrical Stimulation In Epileptic Patients. *Conference Proceedings : Annual International Conference of the IEEE Engineering in Medicine and Biology Society. IEEE Engineering in Medicine and Biology Society. Conference*, (Vol. 7, pp. 4710-4713).
- Ester, M., Kriegel, H. P., Sander, J., and Xu, X. (1996). A Density-Based Algorithm for Discovering Clusters in Large Spatial Databases With Noise. *In Proceedings of the 2nd international conference on knowledge discovery and data mining* (pp. 226-231).
- Fisher, R. S., Boas, W. V. E., Blume, W., Elger, C., Genton, P., Lee, P., and Engel, J. (2005). Epileptic Seizures and Epilepsy: Definitions Proposed by The International League Against Epilepsy (Ilae) And The International Bureau for Epilepsy (IBE). *Epilepsia*, 46(4), 470-472.
- Fisher, R. S., Cross, J. H., D'Souza, C., French, J. A., Haut, S. R., Higurashi, N., Hirsch, E., Jansen, F. E., Lagae, L., Moshé, S. L., Peltola, J., Roulet Perez, E., Scheffer, I. E., Schulze-Bonhage, A., Somerville, E., Sperling, M., Yacubian, E. M., and Zuberi, S.

- M. (2017). Instruction Manual for The ILAE 2017 Operational Classification of Seizure Types. *Epilepsia*, 58(4), 531-542.
- Foffani, G., Uzcategui, Y. G., Gal, B., and Menendez de la Prida, L. (2007). Reduced Spike-Timing Reliability Correlates With The Emergence of Fast Ripples in The Rat Epileptic Hippocampus. *Neuron*, 55(6), 930-941.
- Frauscher, B., von Ellenrieder, N., Ferrari-Marinho, T., Avoli, M., Dubeau, F., and Gotman, J. (2015). Facilitation of Epileptic Activity During Sleep Is Mediated By High Amplitude Slow Waves. *Brain : A Journal of Neurology*, 138(Pt 6), 1629-1641.
- Freeman, W. J., Rogers, L. J., Holmes, M. D., and Silbergeld, D. L. (2000). Spatial Spectral Analysis of Human Electroconvulsions Including The Alpha and Gamma Bands. *Journal of Neuroscience Methods*, 95(2), 111-121.
- Geertsema, E. E., Visser, G. H., Velis, D. N., Claus, S. P., Zijlmans, M., and Kalitzin, S. N. (2015). Automated Seizure Onset Zone Approximation Based on Nonharmonic High-Frequency Oscillations in Human Interictal Intracranial EEGs. *International Journal of Neural Systems*, 25(5), 1550015.
- Girardeau, G., and Zugaro, M. (2011). Hippocampal Ripples and Memory Consolidation. *Current opinion in neurobiology*, 21(3), 452-459.
- Gotman, J., and Koffler, D. J. (1989). Interictal Spiking Increases After Seizures But Does Not After Decrease in Medication. *Electroencephalography and Clinical Neurophysiology*, 72(1), 7-15.

- Gotman, J., and Marciani, M. G. (1985). Electroencephalographic Spiking Activity, Drug Levels, and Seizure Occurrence in Epileptic Patients. *Annals of Neurology*, 17(6), 597-603.
- Grenier, F., Timofeev, I., and Steriade, M. (2003). Neocortical Very Fast Oscillations (Ripples, 80-200 Hz) During Seizures: Intracellular Correlates. *Journal of Neurophysiology*, 89(2), 841-852.
- Gulyás, A. I., and Freund, T. T. (2014). Generation of Physiological And Pathological High Frequency Oscillations: The Role of Perisomatic Inhibition in Sharp-Wave Ripple And Interictal Spike Generation. *Current Opinion in Neurobiology*, 31C, 26-32.
- Guo, L., Rivero, D., Dorado, J., Rabuñal, J. R., and Pazos, A. (2010). Automatic Epileptic Seizure Detection In Eegs Based on Line Length Feature and Artificial Neural Networks. *Journal of Neuroscience Methods*, 191(1), 101-109.
- Hader, W. J., Tellez-Zenteno, J., Metcalfe, A., Hernandez-Ronquillo, L., Wiebe, S., Kwon, C. S., and Jette, N. (2013). Complications of Epilepsy Surgery: A Systematic Review of Focal Surgical Resections and Invasive EEG Monitoring. *Epilepsia*, 54(5),
- Hamer, H. M., Morris, H. H., Mascha, E. J., Karafa, M. T., Bingaman, W. E., Bej, M. D., Burgess, R. C., Dinner, D. S., Foldvary, N. R., Hahn, J. F., Kotagal, P., Najm, I., Wyllie, E., and Lüders, H. O. (2002). Complications of Invasive Video-Eeg Monitoring With Subdural Grid Electrodes. *Neurology*, 58(1), 97-103.

- Henry, T. R., Ross, D. A., Schuh, L. A., and Drury, I. (1999). Indications and Outcome of Ictal Recording With Intracerebral and Subdural Electrodes in Refractory Complex Partial Seizures. *Journal of Clinical Neurophysiology*, 16(5), 426-438.
- Holden, E. W., Thanh Nguyen, H., Grossman, E., Robinson, S., Nelson, L. S., Gunter, M. J., Von Worley, A., and Thurman, D. J. (2005). Estimating Prevalence, Incidence, and Disease-Related Mortality for Patients With Epilepsy in Managed Care Organizations. *Epilepsia*, 46(2), 311-319.
- Jacobs, J., LeVan, P., Chander, R., Hall, J., Dubeau, F., and Gotman, J. (2008b). Interictal High-Frequency Oscillations (80-500 Hz) Are An Indicator of Seizure Onset Areas Independent of Spikes in The Human Epileptic Brain. *Epilepsia*, 49(11), 1893-1907.
- Jacobs, J., Levan, P., Châtillon, C. E., Olivier, A., Dubeau, F., and Gotman, J. (2009). High Frequency Oscillations in Intracranial EEGs Mark Epileptogenicity Rather Than Lesion Type. *Brain : A Journal of Neurology*, 132(Pt 4), 1022-1037.
- Jacobs, J., Staba, R., Asano, E., Otsubo, H., Wu, J. Y., Zijlmans, M., Mohamed, I., Kahane, P., Dubeau, F., Navarro, V., and Gotman, J. (2012). High-frequency Oscillations (HFOs) in Clinical Epilepsy. *Progress in Neurobiology*, 98(3), 302-315.
- Jacobs, J., Zelmann, R., Jirsch, J., Chander, R., Dubeau, C. E., and Gotman, J. (2009). High frequency Oscillations (80-500 Hz) In The Preictal Period in Patients With Focal Seizures. *Epilepsia*, 50(7), 1780-1792.
- Jacobs, J., Zijlmans, M., Zelmann, R., Chatillon, C. E., Hall, J., Olivier, A., Dubeau, F., and Gotman, J. (2010). High-frequency Electroencephalographic Oscillations Correlate With Outcome of Epilepsy Surgery. *Annals of Neurology*, 67(2), 209-220.

- Jefferys, J. G. R., de la Prida, L., Wendling, F., Bragin, A., Avoli, M., Timofeev, I., and da Silva, F. H. (2012). Mechanisms of Physiological and Epileptic HFO Generation. *Progress in Neurobiology*, 98(3), 250-264.
- Jiang, Y., and Zhang, J. (2014). Parallel K-Medoids Clustering Algorithm Based on Hadoop. In *Software engineering and service science (ICSESS), 2014 5th IEEE international conference* (pp. 649-652).
- Jirsch, J. D., Urrestarazu, E., LeVan, P., Olivier, A., Dubeau, F., and Gotman, J. (2006). High-frequency Oscillations During Human Focal Seizures. *Brain : A Journal of Neurology*, 129(6), 1593-1608.
- Jiruska, P., Alvarado-Rojas, C., Schevon, C. A., Staba, R., Stacey, W., Wendling, F., and Avoli, M. (2017). Update on The Mechanisms and Roles of High-Frequency Oscillations in Seizures and Epileptic Disorders. *Epilepsia*. doi: 10.1111/epi.13830
- Jiruska, P., Finnerty, G. T., Powell, A. D., Lofti, N., Cmejla, R., and Jefferys, J. G. R. (2010). Epileptic High-frequency Network Activity in A Model of Non-Lesional Temporal Lobe Epilepsy. *Brain : A Journal of Neurology*, 133(5), 1380-1390.
- Jooma, R., Yeh, H. S., Privitera, M. D., and Gartner, M. (1995). Lesionectomy Versus Electrophysiologically Guided Resection for Temporal Lobe Tumors Manifesting With Complex Partial Seizures. *Journal of Neurosurgery*, 83(2), 231-236.
- Kaufman, L., and Rousseeuw, P. J. (1987). Clustering by Means Of Medoids. Statistical Data Analysis Based on The L 1-Norm and Related Methods. *First international conference* (pp. 405-416).

- Kerber, K., Dümpelmann, M., Schelter, B., Le Van, P., Korinthenberg, R., Schulze-Bonhage, A., and Jacobs, J. (2014). Differentiation of Specific Ripple Patterns Helps To Identify Epileptogenic Areas For Surgical Procedures. *Clinical Neurophysiology : Official Journal of the International Federation of Clinical Neurophysiology*, 125(7), 1339-1345.
- Kerber, K., LeVan, P., Dümpelmann, M., Fauser, S., Korinthenberg, R., Schulze-Bonhage, A., and Jacobs, J. (2013). High Frequency Oscillations Mirror Disease Activity in Patients With Focal Cortical Dysplasia. *Epilepsia*, 54(8), 1428-1436.
- Ketchen, D., and Shook, C. (1996). The Application of Cluster Analysis in Strategic Management Research: An Analysis and Critique. *Strategic Management Journal*, 17(6), 441-458.
- Khosravani, H., Altier, C., Zamponi, G. W., and Colicos, M. A. (2005). The Arg473cys-neuroigin-1 Mutation Modulates NMDA Mediated Synaptic Transmission and Receptor Distribution in Hippocampal Neurons. *FEBS Letters*, 579(29), 6587-6594.
- Khosravani, H., Mehrotra, N., Rigby, M., Hader, W. J., Pinnegar, R., Pillay, N., Wiebe, S., and Federico, P. (2009). Spatial Localization and Time-Dependent Changes of Electrographic High Frequency Oscillations in Human Temporal Lobe Epilepsy. *Epilepsia*, 50(4), 605-616.
- Koolen, N., Jansen, K., Vervisch, J., Matic, V., De Vos, M., Naulaers, G., and Van Huffel, S. (2014). Line Length As A Robust Method To Detect High-Activity Events: Automated Burst Detection in Premature EEG Recordings. *Clinical*

- Neurophysiology : Official Journal of the International Federation of Clinical Neurophysiology*, 125(10), 1985-1994.
- Korzeniewska, A., Cervenka, M. C., Jouny, C. C., Perilla, J. R., Harezlak, J., Bergey, G. K., Franaszczuk, P. J., and Crone, N. E. (2014). Ictal Propagation of High Frequency Activity Is Recapitulated in Interictal Recordings: Effective Connectivity of Epileptogenic Networks Recorded With Intracranial EEG. *NeuroImage*, 1(101), 96-113.
- Kotagal, P., and Yardi, N. (2008). The Relationship Between Sleep and Epilepsy. *Seminars in pediatric neurology*, 15(2), 42-49.
- Köhling, R., and Staley, K. (2011). Network Mechanisms for Fast Ripple Activity in Epileptic Tissue. *Epilepsy Research*, 97(3), 318-323.
- Kucewicz, M. T., Cimbalnik, J., Matsumoto, J. Y., Brinkmann, B. H., Bower, M. R., Vasoli, V., Sulc, V., Meyer, F., Marsh, W. R., Stead, S. M., and Worrell, G. A. (2014). High Frequency Oscillations Are Associated With Cognitive Processing in Human Recognition Memory. *Brain : A Journal of Neurology*, 137(Pt 8), 2231-2244.
- Kwan, P., and Brodie, M. J. (2000). Early Identification of Refractory Epilepsy. *New England Journal of Medicine*, 342(5), 314-319.
- Le Van Quyen, M., Staba, R., Bragin, A., Dickson, C., Valderrama, M., Fried, I., and Engel, J. (2010). Large-Scale Microelectrode Recordings of High-Frequency Gamma Oscillations in Human Cortex During Sleep. *Journal of Neuroscience*, 30(23), 7770-7782.

- Liu, S., Ince, N. F., Abosch, A., Henry, T. R., and Sha, Z. (2015). Investigation of Automatically Detected High Frequency Oscillations (HFOs) As An Early Predictor of Seizure Onset Zone. *Conference Proceedings : Annual International Conference of the IEEE Engineering in Medicine and Biology Society. IEEE Engineering in Medicine and Biology Society Conference, 2015*, pp. 6602-6605.
- Liu, S., Sha, Z., Sencer, A., Aydoseli, A., Bebek, N., Abosch, A., Henry, T., Gurses, C., and Ince, N. F. (2016). Exploring The Time-frequency Content of High Frequency Oscillations for Automated Identification of Seizure Onset Zone in Epilepsy. *Journal of Neural Engineering*, 13(2), 026026.
- López-Cuevas, A., Castillo-Toledo, B., Medina-Ceja, L., Ventura-Mejía, C., and Pardo-Peña, K. (2013). An Algorithm for On-Line Detection of High Frequency Oscillations Related To Epilepsy. *Computer Methods and Programs in Biomedicine*, 110(3), 354-360.
- Matsumoto, A., Brinkmann, B. H., Matthew Stead, S., Matsumoto, J., Kucewicz, M. T., Marsh, W. R., Meyer, F., and Worrell, G. (2013). Pathological and Physiological High-frequency Oscillations in Focal Human Epilepsy. *Journal of Neurophysiology*, 110(8), 1958-1964.
- Matthews, B. W. (1975). Comparison of The Predicted and Observed Secondary Structure of T4 Phage Lysozyme. *Biochimica Et Biophysica Acta (BBA)-Protein Structure*, 405(2), 442-451.

- Melani, F., Zelman, R., Mari, F., and Gotman, J. (2013). Continuous High Frequency Activity: A Peculiar SEEG Pattern Related To Specific Brain Regions. *Clinical Neurophysiology*, 124(8), 1507-1516.
- Menendez de la Prida, L., Staba, R. J., and Dian, J. A. (2015). Conundrums Of High-frequency Oscillations (80-800 Hz) In The Epileptic Brain. *Journal of Clinical Neurophysiology : Official Publication of the American Electroencephalographic Society*, 32(3), 207-219.
- Mina Amiri, Jean-Marc Lina, Francesca Pizzo, and Jean Gotman. (2016). High Frequency Oscillations and Spikes: Separating Real HFOs From False Oscillations. *Clinical Neurophysiology*, 127(1), 187-196.
- Moshé, S. L., Perucca, E., Ryvlin, P., and Tomson, T. (2015). Epilepsy: New Advances. *The Lancet*, 385, 884-898.
- Nagarajan, L., Lee, M., Palumbo, L., Lee, S., Shah, S., Walsh, P., Cannell, P., and Ghosh, S. (2015). Seizure Outcomes in Children With Epilepsy After Resective Brain Surgery. *European Journal of Paediatric Neurology*, 19(5), 577-583.
- Nagasawa, T., Juhsz, C., Rothermel, R., Hoechstetter, K., Sood, S., and Asano, E. (2012). Spontaneous and Visually Driven High-frequency Oscillations in The Occipital Cortex: Intracranial Recording in Epileptic Patients. *Human Brain Mapping*, 33(3), 569-583.
- Nonoda, Y., Miyakoshi, M., Ojeda, A., Makeig, S., Juhsz, C., Sood, S., and Asano, E. (2016). Interictal High-frequency Oscillations Generated By Seizure Onset and

- Eloquent Areas May Be Differentially Coupled With Different Slow Waves. *Clinical Neurophysiology*, 127(6), 2489-2499.
- Ochi, A., Otsubo, H., Donner, E. J., Elliott, I., Iwata, R., Funaki, T., Akizuki, Y., Akiyama, T., Imai, K., Rutka, J. T., and Snead, O. C. (2007). Dynamic Changes Of Ictal High-Frequency Oscillations in Neocortical Epilepsy: Using Multiple Band Frequency Analysis. *Epilepsia*, 48(2), 286-296.
- Ogren, J. A., Wilson, C. L., Bragin, A., Lin, J. J., Salamon, N., Dutton, R. A., Luders, E., Fields, T. A., Fried, I., Toga, A. W., Thompson, P. M., Engel, J., and Staba, R. J. (2009). Three-Dimensional Surface Maps Link Local Atrophy and Fast Ripples in Human Epileptic Hippocampus. *Annals of Neurology*, 66(6), 783-791.
- Park, S. C., Lee, S. K., and Chung, C. K. (2014). Peri-Ictal Broadband Electrographic Activities Between 1 and 700 Hz and Seizure Onset Zones in 18 Patients. *Clinical Neurophysiology : Official Journal of the International Federation of Clinical Neurophysiology*, 125(9), 1731-1743.
- Paz, J. T., Davidson, T. J., Frechette, E. S., Delord, B., Parada, I., Peng, K., Deisseroth, K., and Huguenard, J. R. (2013). Closed-Loop Optogenetic Control of Thalamus As A Tool For Interrupting Seizures After Cortical Injury. *Nature Neuroscience*, 16(1), 64-70.
- Pearce, A., Wulsin, D., Blanco, J. A., Krieger, A., Litt, B., and Stacey, W. C. (2013). Temporal Changes of Neocortical High-frequency Oscillations in Epilepsy. *Journal of Neurophysiology*, 110(5), 1167-1179.

- Powers, D. M. (2011). Evaluation: From Precision, Recall And F-Measure To Roc, Informedness, Markedness and Correlation. *Journal Of Machine Learning Technologies*, 2(1), 37-63.
- Rigamonti, D., Hadley, M. N., Drayer, B. P., Johnson, P. C., Hoenig-Rigamonti, K., Knight, J. T., and Spetzler, R. F. (1988). Cerebral Cavernous Malformations. Incidence and Familial Occurrence. *The New England Journal of Medicine*, 319(6), 343-347.
- Ritaccio, A., Brunner, P., Crone, N. E., Gunduz, A., Hirsch, L. J., Kanwisher, N., Litt, B., Miller, K., Moran, D., Parvizi, J., Ramsey, N., Richner, T. J., Tandon, N., Williams, J., and Schalk, G. (2013). Proceedings of The Fourth International Workshop on Advances in Electrocorticography. *Epilepsy & Behavior : E&B*, 29(2), 259-268.
- Rosenow, F., and Lüders, H. (2001). Presurgical Evaluation of Epilepsy. *Brain : A Journal of Neurology*, 124(9), 1683-1700.
- Ross, D. A., Brunberg, J. A., Drury, I., and Henry, T. R. (1996). Intracerebral Depth Electrode Monitoring in Partial Epilepsy: The Morbidity and Efficacy of Placement Using Magnetic Resonance Image-Guided Stereotactic Surgery. *Neurosurgery*, 39(2), 327-333; discussion 333-334.
- Roth, J., Carlson, C., Devinsky, O., Harter, D. H., Macallister, W. S., and Weiner, H. L. (2014). Safety of Staged Epilepsy Surgery in Children. *Neurosurgery*, 74(2), 154-62.
- Rousseuw, P. J. (1987). Silhouettes: A Graphical Aid To The Interpretation and Validation of Cluster Analysis. *Journal of Computational and Applied Mathematics*, 20(C), 53-65.

- Schevon, C. A., Trevelyan, A. J., Schroeder, C. E., Goodman, R. R., McKhann, G., and Emerson, R. G. (2009b). Spatial Characterization of Interictal High Frequency Oscillations in Epileptic Neocortex. *Brain : A Journal of Neurology*, 132(Pt 11), 3047-3059.
- Schwartz, T. H. (2010). Epilepsy Surgeons, Rather Than Vascular Neurosurgeons, Should Operate On Cavernous Malformations That Cause Seizures-A Modest Proposal. *Epilepsy Currents / American Epilepsy Society*, 10(3), 59-60.
- Sevy, A., Gavaret, M., Trebuchon, A., Vaugier, L., Wendling, F., Carron, R., Regis, J., Chauvel, P., Mc Gonigal, A., and Bartolomei, F. (2014). Beyond The Lesion: The Epileptogenic Networks Around Cavernous Angiomas. *Epilepsy Research*, 108(4), 701-708.
- Shah, A. K., and Mittal, S. (2014). Invasive Electroencephalography Monitoring: Indications and Presurgical Planning. *Annals of Indian Academy of Neurology*, 17(Suppl 1), S89-94.
- Sinai, A., Bowers, C. W., Crainiceanu, C. M., Boatman, D., Gordon, B., Lesser, R. P., Lenz, F. A., and Crone, N. E. (2005). Electrocorticographic High Gamma Activity Versus Electrical Cortical Stimulation Mapping of Naming. *Brain : A Journal of Neurology*, 128(Pt 7), 1556-1570.
- Sirin, N. G., Gurses, C., Bebek, N., Dirican, A., Baykan, B., and Gokyigit, A. (2013). A Quadruple Examination of Ictal Eeg Patterns in Mesial Temporal Lobe Epilepsy with Hippocampal Sclerosis: Onset, Propagation, Later Significant Pattern, and

- Termination. *Journal of Clinical Neurophysiology : Official Publication of the American Electroencephalographic Society*, 30(4), 329-338.
- So, N., Gloor, P., Quesney, L. F., Jones-Gotman, M., Olivier, A., and Andermann, F. (1989). Depth Electrode Investigations in Patients With Bitemporal Epileptiform Abnormalities. *Annals of Neurology*, 25(5), 423-431.
- So, N. K., and Blume, W. T. (2010). The Postictal EEG. *Epilepsy & Behavior*, 19(2), 121-126.
- Staba, R. J., Wilson, C. L., Bragin, A., Fried, I., and Engel, J. (2002). Quantitative Analysis of High-frequency Oscillations (80-500 Hz) Recorded in Human Epileptic Hippocampus and Entorhinal Cortex. *Journal of Neurophysiology*, 88(4), 1743-1752.
- Staba, R. J., Wilson, C. L., Bragin, A., Jung, D., Fried, I., and Engel, J. (2004). High-frequency Oscillations Recorded in Human Medial Temporal Lobe During Sleep. *Annals of Neurology*, 56(1), 108-115.
- Stacey, W. C., Krieger, A., and Litt, B. (2011). Network Recruitment To Coherent Oscillations in A Hippocampal Computer Model. *Journal of Neurophysiology*, 105(4), 1464-1481.
- Sullivan, D., Csicsvari, J., Mizuseki, K., Montgomery, S., Diba, K., and Buzsáki, G. (2011). Relationships Between Hippocampal Sharp Waves, Ripples, and Fast Gamma Oscillation: Influence of Dentate and Entorhinal Cortical Activity. *The Journal of Neuroscience : The Official Journal of the Society for Neuroscience*, 31(23), 8605-8616.

- Sun, P. Y., Wyatt, K., Nickels, K. C., Wong-Kisiel, L. C., Mandrekar, J., and Wirrell, E. (2015). Predictors of Length of Stay in Children Admitted for Presurgical Evaluation for Epilepsy Surgery. *Pediatric Neurology*, 53(3), 207-210.
- Troester, M., Haine-Schlagel, R., Ng, Y. T., Chapman, K., Chung, S., Drees, C., Prenger, E., Rekate, H., and Kerrigan, J. F. (2011). EEG and Video-EEG Seizure Monitoring Has Limited Utility in Patients With Hypothalamic Hamartoma And Epilepsy. *Epilepsia*, 52(6), 1137-1143.
- Tzallas, A. T., Tsipouras, M. G., and Fotiadis, D. I. (2009). Epileptic Seizure Detection in EEGs Using Time-frequency Analysis. *IEEE Transactions on Information Technology in Biomedicine : A Publication of the IEEE Engineering in Medicine and Biology Society*, 13(5), 703-710.
- Uematsu, S., Lesser, R., Fisher, R. S., Gordon, B., Hara, K., Krauss, G. L., Vining, E. P., and Webber, R. W. (1992). Motor and Sensory Cortex in Humans: Topography Studied With Chronic Subdural Stimulation. *Neurosurgery*, 31(1), 52-59.
- Urrestarazu, E., Jirsch, J. D., LeVan, P., and Hall, J. (2006). High-frequency Intracerebral EEG Activity (100-500 Hz) Following Interictal Spikes. *Epilepsia*, 47(9), 1465-1476.
- von der Brellie, C., Kuczaty, S., and von Lehe, M. (2014). Surgical Management and Long-Term Outcome of Pediatric Patients with Different Subtypes of Epilepsy Associated with Cerebral Cavernous Malformations. *Journal of Neurosurgery Pediatrics*, 13(6), 699-705.

- Von Ellenrieder, N., Frauscher, B., Dubeau, F., and Gotman, J. (2016). Interaction with Slow Waves During Sleep Improves Discrimination of Physiologic and Pathologic High-frequency Oscillations (80-500 Hz). *Epilepsia*, 57(6), 869-878.
- Worrell, G., and Gotman, J. (2011). High-frequency Oscillations and Other Electrophysiological Biomarkers of Epilepsy: Clinical Studies. *Biomarkers in Medicine*, 5(5), 557-566.
- Worrell, G. A., Gardner, A. B., Stead, S. M., Hu, S., Goerss, S., Cascino, G. J., Meyer, F. B., Marsh, R., and Litt, B. (2008b). High-frequency Oscillations in Human Temporal Lobe: Simultaneous Microwire and Clinical Macroelectrode Recordings. *Brain : A Journal of Neurology*, 131(Pt 4), 928-937.
- Worrell, G. A., Jerbi, K., Kobayashi, K., Lina, J. M., Zelmann, R., and Le Van Quyen, M. (2012). Recording and Analysis Techniques for High-frequency Oscillations. *Progress in Neurobiology*, 98(3), 265-278.
- Worrell, G. A., Parish, L., Cranstoun, S. D., Jonas, R., Baltuch, G., and Litt, B. (2004b). High-frequency Oscillations and Seizure Generation in Neocortical Epilepsy. *Brain : A Journal of Neurology*, 127(Pt 7), 1496-1506.
- Wu, J. Y., Sankar, R., Lerner, J. T., Matsumoto, J. H., Vinters, H. V., and Mathern, G. W. (2010). Removing Interictal Fast Ripples on Electroconvulsive Therapy Linked with Seizure Freedom In Children. *Neurology*, 75(19), 1686-1694.
- Yang, T., Hakimian, S., and Schwartz, T. H. (2014). Intraoperative Electroconvulsive Therapy (ECoG): Indications, Techniques, and Utility in Epilepsy Surgery. *Epileptic Disorders : International Epilepsy Journal with Videotape*, 16(3), 271-279.

- Zelmann, R., Mari, F., Jacobs, J., Zijlmans, M., Dubeau, F., and Gotman, J. (2012). A Comparison Between Detectors of High Frequency Oscillations. *Clinical Neurophysiology*, 123(1), 106-116.
- Zijlmans, M., Jacobs, J., Kahn, Y. U., Zelmann, R., Dubeau, F., and Gotman, J. (2011). Ictal and Interictal High Frequency Oscillations in Patients with Focal Epilepsy. *Clinical Neurophysiology : Official Journal of the International Federation of Clinical Neurophysiology*, 122(4), 664-671.
- Zijlmans, M., Jacobs, J., Zelmann, R., Dubeau, F., and Gotman, J. (2009a). High Frequency Oscillations And Seizure Frequency In Patients With Focal Epilepsy. *Epilepsy Research*, 85(2), 287-292.
- Zijlmans, M., Jacobs, J., Zelmann, R., Dubeau, F., and Gotman, J. (2009b). High-frequency Oscillations Mirror Disease Activity in Patients with Epilepsy. *Neurology*, 72(11), 979-986.
- Zijlmans, M., Jiruska, P., Zelmann, R., Leijten, F. S. S., Jefferys, J. G. R., and Gotman, J. (2012). High-frequency Oscillations As A New Biomarker in Epilepsy. *Annals of Neurology*, 71(2), 169-178.
- Zijlmans, M., Worrell, G. A., Dümpelmann, M., Stieglitz, T., Barborica, A., Heers, M., Ikeda, A., Usui, N., and Le Van Quyen, M. (2017). How To Record High-frequency Oscillations in Epilepsy: A Practical Guideline. *Epilepsia*. doi: 10.1111/epi.13814

